

# **WATER VAPOR AND GAS TRANSPORT THROUGH POLYMERIC MEMBRANES**



# **WATER VAPOR AND GAS TRANSPORT THROUGH POLYMERIC MEMBRANES**

PROEFSCHRIFT

ter verkrijging van  
de graad van doctor aan de Universiteit Twente,  
op gezag van de rector magnificus,  
prof. dr. F.A. van Vught,  
volgens besluit van het College voor Promoties  
in het openbaar te verdedigen  
op vrijdag 21 november 2003 om 16.45 uur

door

Sybrandus Jacob Metz

geboren op 14 januari 1975

te Pietersbierum

Dit proefschrift is goedgekeurd door de promotor

Prof. Dr.-Ing. M. Wessling

en de assistant promoter

Dr. Ir. N.F.A. van der Vegt

ISBN ?

© by S.J.Metz, Enschede, The Netherlands, 2003.

All rights reserved.

Printed by PrintPartners Ipskamp B.V., Enschede, The Netherlands.



# Contents

<b>1</b>	<b>Introduction</b>	<b>1</b>
1.1	Water vapor and gas transport through polymeric membranes	1
1.2	Scope of this thesis	7
1.3	References	9
<b>2</b>	<b>Measurement of Water Vapor and Gas Permeation through Polymers</b>	<b>11</b>
2.1	Introduction	12
2.2	Background	12
2.2.1	Measurement of water vapor permeation	12
2.2.2	Mass transfer limitations	14
2.3	Experimental	16
2.3.1	Mixed gas water vapor permeation set-up	16
2.3.2	Permeation cell	18
2.3.3	Determination of the permeability values	19
2.3.4	Materials	20
2.3.5	PEO-PBT block copolymers	20
2.3.6	Film preparation	21
2.4	Results and Discussion	21
2.4.1	Effects of concentration polarization	21
2.4.2	Boundary layer resistance	24
2.4.3	Validation permeability values	27
2.4.4	Highly permeable, highly selective materials	29
2.5	Conclusions	30
2.6	Acknowledgements	30
2.7	References	31
<b>3</b>	<b>Performance of Polyethersulfone/Polyimide Hollow Fiber Membranes in the Separation of Wet CO<sub>2</sub>/N<sub>2</sub> Gaseous Mixtures</b>	<b>33</b>
3.1	Introduction	34
3.2	Background	35
3.2.1	Resistances towards mass transfer	35
3.3	Experimental	39
3.3.1	Materials	39
3.3.2	Module preparation and post treatment	40
3.3.3	Mixed gas/water vapor permeation set-up	40

3.3.4	Determination of the transport rates	41
3.3.5	Sorption experiments	43
3.4	Results and Discussion	44
3.4.1	Effect of water vapor activity on gas permeance	44
3.4.2	Influence of total pressure	47
3.4.3	Resistance towards mass transfer	50
3.5	Conclusions	53
3.6	Acknowledgements	54
3.7	List of Symbols	54
3.8	References	55
<b>4</b>	<b>Gas Permeation Properties of Poly(Ethylene Oxide) Poly(Butylene Terephthalate) Block Copolymers</b>	<b>57</b>
4.1	Introduction	58
4.2	Background	59
4.2.1	Permeability	59
4.3	Experimental section	62
4.3.1	Materials	62
4.3.2	Film preparation	62
4.3.3	Proton-NMR	62
4.3.4	Differential Scanning Calometry (DSC)	62
4.3.5	Gas permeation	63
4.3.6	Equilibrium sorption	63
4.4	Results and Discussion	64
4.4.1	Thermal properties of PEO-PBT block copolymers	64
4.4.2	Selectivity	65
4.4.3	Effect of the amount of PBT on permeation properties	66
4.4.4	Effect of the PEO segment length on permeation properties	72
4.4.5	Effect of temperature on permeation properties	75
4.5	Conclusions	76
4.6	Acknowledgements	76
4.7	References	77
<b>5</b>	<b>Thermodynamics of Water Vapor Sorption in Poly(Ethylene Oxide) Poly(Butylene Terephthalate) Block copolymers</b>	<b>79</b>
5.1	Introduction	80
5.2	Experimental section	80
5.2.1	Materials	80
5.2.2	PEO-PBT block copolymers	81
5.2.3	Film preparation	81
5.2.4	Proton NMR	81



---

5.2.5	Differential Scanning Calometry (DSC)	81
5.2.6	Sorption isotherms	82
5.3	Theory	82
5.3.1	Flory-Huggins sorption model	82
5.3.2	Solvation thermodynamics	83
5.4	Results and discussion	85
5.4.1	Solubility	85
5.4.2	Flory-Huggins sorption model	86
5.4.3	Solvation thermodynamics	89
5.5	Conclusions	95
5.6	References	95
<b>6</b>	<b>Mixed gas water vapor/N<sub>2</sub> transport in Poly(Ethylene Oxide) Poly(Butylene Terephthalate) Block copolymers</b>	<b>97</b>
6.1	Introduction	98
6.2	Experimental	99
6.2.1	Materials	99
6.2.2	Film preparation	99
6.2.3	Mixed gas water vapor permeation	99
6.2.4	Sorption isotherms	99
6.2.5	Infrared Spectroscopy	100
6.3	Results and Discussion	100
6.3.1	Solubility of water vapor in PEO-PBT block copolymers	100
6.3.2	Permeability	102
6.3.3	State of water in PEO-PBT block copolymers	107
6.3.4	Concentration-dependent diffusion coefficient	112
6.3.5	Effect of temperature	114
6.3.6	Effect of block copolymer composition	118
6.4	Conclusions	121
6.5	Acknowledgements	121
6.6	References	121
	<b>Summary</b>	<b>125</b>
	<b>Samenvatting</b> (voor niet-membraantecnologen)	<b>129</b>
	<b>Dankwoord</b>	<b>132</b>

---

# Chapter 1

## Introduction

### 1.1 Water vapor and gas transport through polymeric membranes

The selective transport of water vapor through polymeric membranes is used in various applications. Examples can be found in the drying of compressed air<sup>1</sup>, drying of natural gas<sup>2,3</sup>, breathable apparel<sup>4</sup>, removal of water vapor from flue gases, packaging materials<sup>5</sup>, roofing membranes<sup>6</sup>, diapers, and the humidity control in closed spaces (air conditioning in buildings<sup>7</sup>, aviation, and space flight<sup>8</sup>). This selective transport is possible due to the higher permeation rate of water compared to the other components. An example is presented below for the permeation of various gases through silicone rubber (polydimethylsiloxane, PDMS).

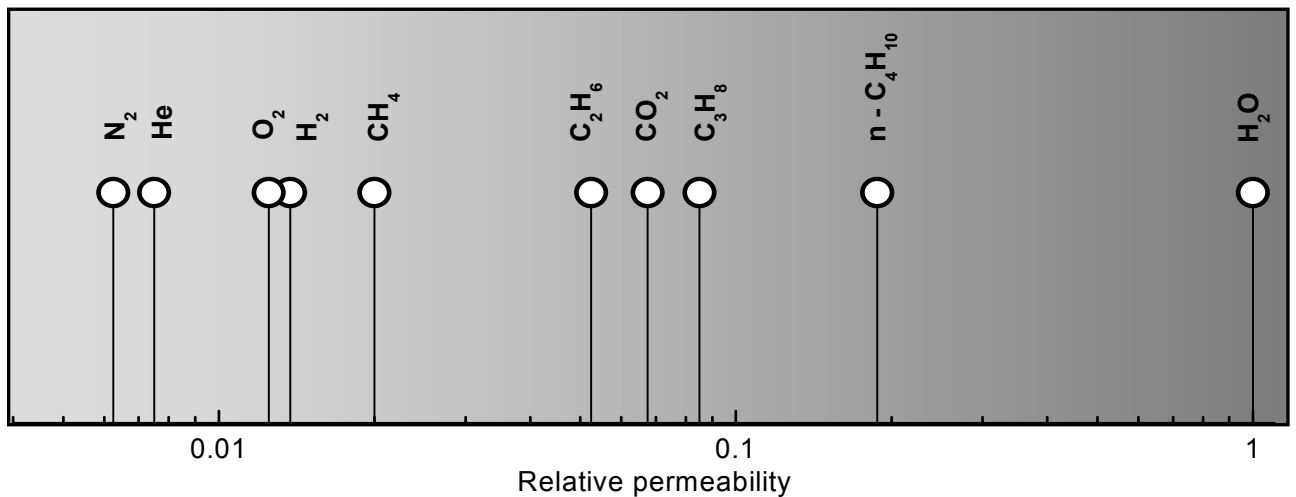


**Figure 1:** Relative permeability of various penetrants compared to water in PDMS. Data reproduced from Baker<sup>9</sup> and for water from Allen<sup>10</sup>.

Figure 1 shows the relative transport rate of various penetrants compared to water. The transport rate for water is much faster compared to the other components even though PDMS is a hydrophobic material. The permeability coefficient of a material is an intrinsic material property, since it gives a measure for the amount of gas permeating per second through a material with a surface area of 1 cm<sup>2</sup> and a thickness of 1 cm normalized for the driving force in cmHg. The total amount of gas permeating is expressed as a flux of gas at standard temperature and pressure (cm<sup>3</sup>(STP)/(cm<sup>2</sup> s)):

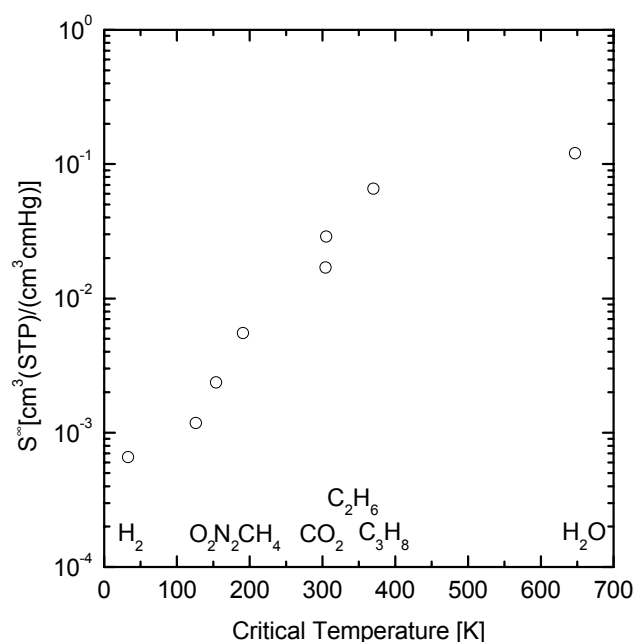
$$J = \frac{P}{l} (f_{i,\text{feed}} - f_{i,\text{permeate}}) \quad (1)$$

with P the permeability (Barrer = 1 10<sup>-10</sup> cm<sup>3</sup> cm/(cm<sup>2</sup> s cmHg)), l the membrane thickness (cm),  $f_{i,\text{feed}}$  and  $f_{i,\text{permeate}}$  the fugacities of component i on the high pressure side (feed) and low pressure side (permeate) (cmHg), respectively. For low pressure applications the fugacities equal the partial pressure.

The permeability of a gas, vapor or liquid through a dense polymeric membrane can be described by the solution-diffusion model<sup>11,12</sup>, equating the permeability P to the product of the diffusivity and solubility:

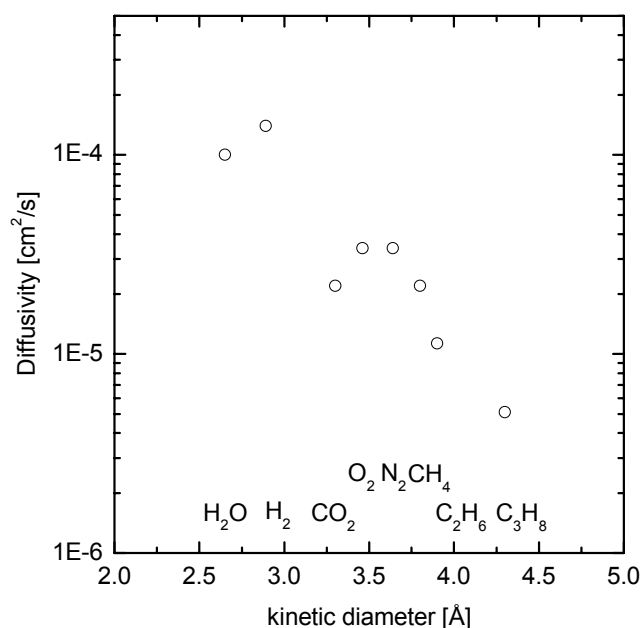
$$P = D \cdot S \quad (2)$$

where D is the diffusion coefficient (cm<sup>2</sup>/s) and S the solubility coefficient (cm<sup>3</sup>(STP)/(cm<sup>3</sup> cmHg)). The magnitude of the permeability is determined by the diffusion rate (D), which is a kinetic parameter, and the solubility, a thermodynamic parameter accounting for the amount sorbed by the membrane. The combination of a high mobility for water (diffusivity) and a high solubility causes a high permeability for water compared to other penetrants. Figure 2 and Figure 3 will visualize this for PDMS.



**Figure 2:** Solubility coefficient at infinite dilution at 35°C versus the critical temperature of various penetrants in PDMS. Data reproduced from Merkel et. al.<sup>13</sup> and water from Barrie<sup>14</sup>.

Figure 2 shows the solubility coefficient for various penetrants in PDMS at 35°C reproduced from literature<sup>13,14</sup> as a function of the critical temperature<sup>15</sup>, which can be interpreted as a measure for the condensability of the penetrant. The solubility coefficient increases with an increase of the critical temperature. The solubility coefficient depicted in Figure 2 is determined at infinite dilution and represents the solubility of a penetrant, which does not change the environment into which it absorbs macroscopically. However, in reality the solubility may depend on the penetrant concentration and various sorption isotherms (deviations from ideal dissolution following Henry's law) can be observed.



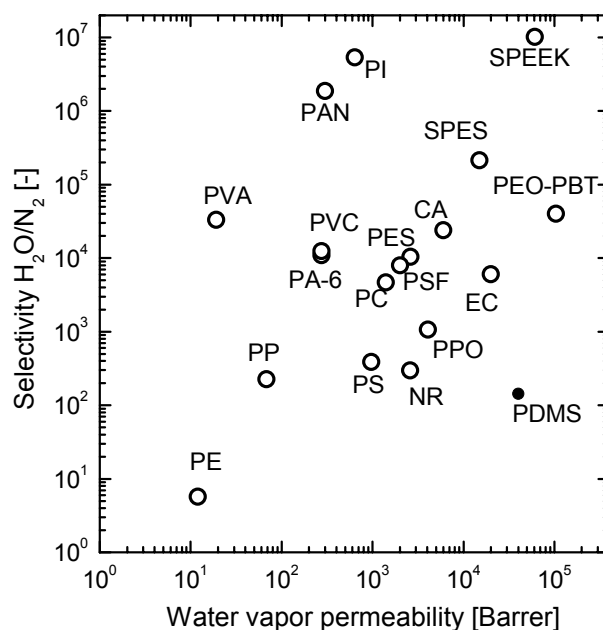
**Figure 3:** The effect of penetrant size on the diffusion coefficient at infinite dilution. Data reproduced from Merkel et. al.<sup>13</sup> and for H<sub>2</sub>O from Barrie<sup>14</sup>.

Figure 3 shows the effect of penetrant size on the diffusivity, which decreases with an increase of penetrant size<sup>16</sup>. The diffusivity of the penetrant depicted in Figure 3 is determined at infinite dilution as well. The diffusion coefficient of a penetrant may depend on its concentration and can increase with the amount of penetrant due to plasticization of the polymeric matrix<sup>17-20</sup> or decreases due to the formation of penetrant clusters in the polymeric matrix<sup>14,21-23</sup> or a combination of both effects<sup>24</sup>.

The smallest penetrant (H<sub>2</sub>O) possesses the highest solubility and diffusivity even in a hydrophobic polymer like PDMS. This causes a remarkable high water vapor permeability (Figure 1). However, the chemical structure of a polymer determines the actual permeability for water vapor as well as for other gases. The water vapor/N<sub>2</sub> selectivity and water vapor permeability for various polymers are listed in Table.1. Figure 4 shows the cross plot of the selectivity, calculated from single gas experiments, as a function of the water vapor permeability. The permeance values are extrapolated to a water vapor activity of 0, since the water vapor permeability strongly depends on the water vapor activity.

**Table.1:** Water vapor permeability and water vapor/N<sub>2</sub> selectivity for various polymers at 30°C extrapolated to water vapor activity 0.

Polymer	Abbreviation	H <sub>2</sub> O Permeability	Selectivity	Reference	
		[Barrer]	[H <sub>2</sub> O/N <sub>2</sub> ]	H <sub>2</sub> O	N <sub>2</sub>
Polyethylene	(PE)	12	5.71	14	12
Polyvinylalcohol	(PVA)	19	33,300	14	12
Polypropylene	(PP)	68	230	14	12
Polyamide 6 (Nylon 6)(PA-6)		275	11,000	10	12
Polyvinylchloride	(PVC)	275	12,500	25	12
Polyacrylonitril	(PAN)	300	1,875,000	10	10
Polyimide (Kapton)	(PI)	640	5,333,300	25	12
Polystyrene	(PS)	970	400	14	12
Polycarbonate	(PC)	1,400	4,700	10	12
Polysulfone	(PSF)	2,000	8,000	10	26
Natural rubber	(NR)	2,600	300	10	26
Polyethersulfone	(PES)	2,620	10,480	10	27
Polyphenyleneoxide	(PPO)	4,060	1,070	25	12
Cellulose acetate	(CA)	6,000	24,000	14	12
Sulfonated polyethersulofon	(SPES)	15,000	214,300	27	27
Ethyl cellulose	(EC)	20,000	6,060	25	26
Polydimethylsiloxane	(PDMS)	40,000	140	10	12
Sulfonated polyetheretherketon	(SPEEK)	61,000	10,166,700	28	28
1000PEO40PBT60	(PEO-PBT)	104,000	40,000	29	



**Figure 4:** Water vapor permeability and water vapor/N<sub>2</sub> selectivity for various polymers at 30°C.

For binary gas mixtures of permanent gases it is well known that a high selectivity is accompanied by a low permeability and vice versa. This trade-off relationship between selectivity and permeability is often visualized in a so called Robeson plot<sup>30</sup>. However, such a relation does not hold for the permeance of water vapor in a mixture with a permanent gas. Most of the highly selective polymers also have a very high water permeability<sup>31</sup>. The water vapor/nitrogen selectivity differs up to 7 orders of magnitude and the water vapor permeability differs 4 orders of magnitude between the various polymers. However, many of the permeability and selectivity values depicted in Figure 4 and Table.1 are obtained from pure gas permeabilities by calculating the ratio of the permeabilities for each species. In real gas mixtures, water will swell the membrane and may affect the transport rate of the other permeating species. This effect on the transport of the slower species often remains unknown. In gas mixtures the extraction of intrinsic polymer properties from the overall transport rate is difficult, due to the rapid and selective transport of water, and as a result the occurrence of concentration polarization.

Poly(ethylene oxide) (PEO) poly(butylene terephthalate) (PBT) block copolymers, and sulphonated glassy polymers, such as sulphonated PEEK materials, are interesting materials for the removal of water vapor from gas streams since they possess a high selectivity and permeability for water vapor.



PEO-PBT block copolymers allow for a structural modification by the amount of PEO and the PEO segment length. Moreover, these materials are also interesting for the separation of polar (quadrupolar) components from gas streams (e.g. CO<sub>2</sub>, H<sub>2</sub>S), since PEO containing block copolymers have a high solubility for these gases<sup>32-34</sup>. Little is known on the water and simultaneous inert gas transport for highly permeable polymers. Frequently, additional mass transport resistances at the feed and permeate side of the membrane develop due to the high permeability and selectivity, and leave the extraction of intrinsic material properties a challenging task.

## 1.2 Scope of this thesis

Until today, no systematic study on the influence of block length and block weight ratio of block copolymers on its permeation properties is published. The major part of this thesis deals with the kinetics and thermodynamics of mass transport through PEO-PBT block copolymers.

However, before elucidating the transport properties of the highly selective and highly permeable PEO-PBT based block copolymer, a thorough investigation of the hydrodynamic resistances during water vapor transport is presented for flat sheet as well as for hollow fiber membranes.

**Chapter 2** describes a new experimental set-up, for the simultaneous measurement of the transport rate of water vapor and permanent gases with a sweep gas, in the temperature range of 20 – 80°C and the pressure range 1 – 80 bars. This chapter describes in detail the set-up and deals with concentration polarization phenomena encountered in the measurement of humidified single and binary gas mixtures. The water vapor permeation rates measured for ethyl cellulose and polysulfone are verified with literature values.

**Chapter 3** presents the permeance of N<sub>2</sub>/H<sub>2</sub>O, CO<sub>2</sub>/H<sub>2</sub>O, and N<sub>2</sub>/CO<sub>2</sub>/H<sub>2</sub>O gaseous mixtures through high flux PES/PI blend hollow fibers, which were recently developed in our lab<sup>19</sup>. The effect of concentration polarization on the water vapor transport rate is quantified and the influence of water vapor on the transport rate of CO<sub>2</sub>, N<sub>2</sub>, and a CO<sub>2</sub>/N<sub>2</sub> mixture is treated.

The remainder of this thesis focuses on the transport through PEO-PBT block copolymers. The pure gas permeabilities of various PEO-PBT block copolymers are presented in **Chapter 4**. These block copolymers allow for a structural modification in the amount of PEO and its PEO segment length. The block copolymer structure is varied systematically and its effect on the permeability and selectivity of CO<sub>2</sub>, N<sub>2</sub>, and He in the temperature range of 10 – 80°C is investigated.

The PEO-PBT block copolymers have a high solubility for water vapor compared to other polymers (**Chapter 5**). This solubility can be tailored by changing the

amount of PEO as well as the PEO segment length. The sorption isotherms are analyzed with the Flory-Huggins model and with a thermodynamic analysis. The latter reveals increased water uptake to be entropy driven.

The permeation of water vapor and N<sub>2</sub> through a series of PEO-PBT block copolymers is covered in **Chapter 6**. The sorption isotherms are analyzed with the Zimm and Lundberg cluster model<sup>35,36</sup>. Diffusivities are extracted from the sorption and permeation isotherms and decrease with an increase of the amount of water in the polymer. The state of water in the polymer is analyzed with Attenuated Total Reflection Fourier Transformed Infrared Spectroscopy (ATR-FTIR). Chapter 6 reflects on the physical reason for increasing and decreasing diffusivities with increasing penetrant concentration and degree of swelling, respectively.

Ultimately, this thesis aims to establish a thorough analysis for water transport through polymeric membranes. Particularly, the transport behavior of systematically tailored PEO-PBT block copolymers is investigated. Due to their superior properties, they are viable candidates for applications such as drying and natural gas dehydration.

### 1.3 References

- (1) Wu, Y. L.; Peng, X.; Liu, J. Z.; Kong, Q. Y.; Shi, B. L.; Tong, M. S. J. *Membr. Sci.* 2002, 196, 179-183.
- (2) Tabe-Mohammadi, A. *Sep. Sci. Technol.* 1999, 34, 2095-2111.
- (3) Liu, L.; Chen, Y.; Kang, Y. X.; Deng, M. *Chem. Eng. Technol.* 2001, 24, 1045-1048.
- (4) Gebben, B. J. *Membr. Sci.* 1996, 113, 323-329.
- (5) George, S. C.; Thomas, S. *Prog. Polym. Sci.* 2001, 26, 985-1017.
- (6) Dutt, O.; Lavallee, C.; Ashton, H. E. *J. Test. Eval.* 1993, 21, 199-210.
- (7) El-Dessouky, H. T.; Ettouney, H. M.; Bouhamra, W. *Chem. Eng. Res. Des.* 2000, 78, 999-1009.
- (8) Scovazzo, P.; Burgos, J.; Hoehn, A.; Todd, P. J. *Membr. Sci.* 1998, 149, 69-81.
- (9) Baker, R. W. *Membrane Technology and Applications*; McGraw-Hill Professional Publishing, 1999.
- (10) Allen, S. M.; Fujii, M.; Stannett, V.; Hopfenberg, H. B.; Williams, J. L. *J. Membr. Sci.* 1977, 2, 153-164.
- (11) Wijmans, J. G.; Baker, R. W. *J. Membr. Sci.* 1995, 107, 1-21.
- (12) Mulder, M. H. V. *Basic principles of membrane technology*, second ed.; Kluwer: Dordrecht, 1996.
- (13) Merkel, T. C.; Bondar, V. I.; Nagai, K.; Freeman, B. D.; Pinnau, I. *J. Polym. Sci., Polym. Phys. Ed.* 2000, 38, 415-434.

- (14) Barrie, J. A. In *Diffusion in Polymers*; Crank, J.; Park, G. S., Eds.; Academic Press, 1968.
- (15) Poling, B. E.; Prausnitz, J. M.; O'Connell, J. P. *The properties of gases and liquids*; McGraw-Hill: New York, 2001.
- (16) Breck, D. W. *Zeolite molecular sieves: structure, chemistry, and use*; Wiley: New York, 1974.
- (17) Bos, A., Punt, I.G.M., Wessling, M., Strathmann, H. J. *Membr. Sci.* 1999, 155, 67-78.
- (18) Wessling, M.; Lopez, M. L.; Strathmann, H. *Sep. Purif. Technol.* 2001, 24, 223-233.
- (19) Kapantaidakis, G. C.; Koops, G. H.; Kaldis, S. P.; Sakelaropoulos, G. P.; Wessling, M. *AIChE J.* 2003, 49, 1702-1711.
- (20) Bos, A.; Punt, I. G. M.; Wessling, M.; Strathmann, H. J. *Polym. Sci., Polym. Phys. Ed.* 1998, 36, 1547-1556.
- (21) Nguyen, Q. T.; Favre, E.; Ping, Z. H.; Neel, J. J. *Membr. Sci.* 1996, 113, 137-150.
- (22) Strathmann, H.; Michaels, A. S. *Desalination* 1977, 21, 195-202.
- (23) Koros, W. J.; Hellums, M. W. In *Encyclopedia of polymer science and engineering*; Kroschwitz, J. I., Ed.; Wiley: New York, 1990; pp 724-802.
- (24) Beck, M. I.; Tomka, I. J. *Macromol. Sci., Phys.* 1997, B36, 19-39.
- (25) Barrie, J. A. *Proceeding of the fourth BOC Priestly Conference* 1986, 89-113.
- (26) Ho, W. S. W.; Sirkar, K. K. *Membrane Handbook*; Van Nostrand Reinhold: New York, 1992.
- (27) Jia, L.; Xu, X. F.; Zhang, H. J.; Xu, J. P. *Polym. Sci., Polym. Phys. Ed.* 1997, 35, 2133-2140.
- (28) Liu, S.; Wang, F.; Chen, T. *Macromol. Rapid. Commun.* 2001, 22, 579-582.
- (29) Metz, S. J.; Ven, W. J. C. v. d.; Mulder, M. H. V.; Wessling, M. Chapter 6.
- (30) Robeson, L. M. *Membr. Sci.* 1991, 62, 165-185.
- (31) Nunes, S. P.; Peinemann, K.-V. *Membrane technology in the chemical industry*; Wiley-VCH: Weinheim, 2001.
- (32) Bondar, V. I.; Freeman, B. D.; Pinnau, I. J. *Polym. Sci., Polym. Phys. Ed.* 1999, 37, 2463-2475.
- (33) Bondar, V. I.; Freeman, B. D.; Pinnau, I. J. *Polym. Sci., Polym. Phys. Ed.* 2000, 38, 2051-2062.
- (34) Okamoto, K.; Fujii, M.; Okamoto, S.; Suzuki, H.; Tanaka, K.; Kita, H. *Macromolecules* 1995, 28, 6950-6956.
- (35) Zimm, B. H. *J. Chem. Phys.* 1953, 21, 934.
- (36) Zimm, B. H.; Lundberg, J. L. *J. Phys. Chem.* 1956, 60, 425.



# Chapter 2

## Measurement of Water Vapor and Gas Permeation through Polymers

### Abstract

This chapter describes in detail the measurement of the permeation properties of a water vapor/N<sub>2</sub> gas mixture for highly permeable polymers. The measurements are complicated by the presence of stagnant boundary layers at feed and permeate side. Its resistance can be extracted from the measurement of the overall resistance of polymeric films having various thicknesses. Water vapor permeabilities of ethyl cellulose and polysulfone films are determined and corrected for the resistance in the stagnant boundary layer and correspond to those in literature.

Permeability values of a highly permeable PEO-PBT block copolymer (1000PEO56PBT44) are presented to illustrate the contribution of the stagnant boundary layer at various process conditions. The water vapor permeability shows a strong dependence on the total pressure. An increase of the total pressure results in a larger resistance in the stagnant feed boundary layer, thereby lowering the total water vapor flux.

## 2.1 Introduction

Water vapor transport through polymeric barrier materials or membranes is of major industrial importance. Applications can be found in the drying of natural gas<sup>1</sup>, drying of compressed air<sup>2</sup>, protective apparel<sup>3</sup>, packaging materials, roofing membranes, diapers, and the humidity control in closed spaces (air conditioning in buildings, aviation and space flight). Various polymers can be used as a selective membrane or barrier material for the transport of water vapor. Depending on the application, a high or low permeability or selectivity for water vapor is preferred. Generally, water permeates to a larger extent than permanent gases due to a larger solubility of water vapor. However, many of the permeability and selectivity values are obtained from pure gas permeabilities by calculating the ratio of the permeabilities for each species. In real gas mixtures water may swell the membrane and its effect on the transport of the slower species often remains unknown. In gas mixtures the extraction of intrinsic polymer properties from the overall transport rate is also difficult, due to the rapid transport of water resulting in concentration polarization.

This chapter describes in detail the measurement of the permeability of a water vapor in a water/N<sub>2</sub> mixture through polymers in a newly developed experimental set-up. Permeability values are compared with literature data. Furthermore, the effect of water vapor activity, temperature, total pressure, membrane thickness and feed flow rate are investigated for a highly selective and highly permeable block copolymer, composed of hydrophilic PEO blocks and impermeable PBT blocks.

## 2.2 Background

### 2.2.1 Measurement of water vapor permeation

The "cup method" is probably the most used technique to determine the transport rate of water vapor through a polymeric material. This method is based on a polymeric film, covering a container containing water or a desiccant. This container is placed in a humidity-controlled environment, and the permeability of water vapor through a polymeric film is determined by the rate of weight change of the container. The permeability determined by the cup method is affected by the presence of stagnant boundary layers on both sides of the polymeric film<sup>4</sup>. Moreover, the sealing of the film can give rise to errors, especially for low permeable films<sup>5</sup>.

More accurate results can be obtained with the variable pressure constant volume method, where a vacuum is applied at the permeate side of the membrane and a

water vapor is presented on the feed side at the membrane. The water vapor permeability is determined from the pressure increase in the calibrated volume. However, corrections have to be made for adsorption of the permeated water vapor on the equipment <sup>6</sup>. In the aforementioned techniques only the pure water vapor permeability can be determined and the simultaneous measurement of the permeability of both a gas as well as vapor is not possible.

When both vapor and gas permeabilities have to be measured other methods can be used as well. The methods described below use a vapor/gas mixture flowing over the membrane. A vacuum in combination with a cold trap can be used to collect the permeated vapor<sup>7,8</sup>. This method has the disadvantage that only the vapor permeability is measured and not the gas permeability. This is circumvented by measuring the flow rate and the composition of the permeate stream at a certain permeate pressure<sup>9</sup>. However, the flux through membrane has to be high enough to be able to determine a flow rate of the permeate stream. The mixed gas vapor permeability can also be measured, without the use of a vacuum, if the vapor pressure is higher than the atmospheric permeate pressure<sup>10</sup>. The permeability values can be calculated from the composition and the flow rate of the permeate stream.

This chapter describes a further sophistication of the last methods. We feel this to be necessary in particular for highly selective and highly permeable materials. Instead of a vacuum we use a sweep gas to remove the water vapor and nitrogen at the permeate side of the membrane as depicted in Figure 1:

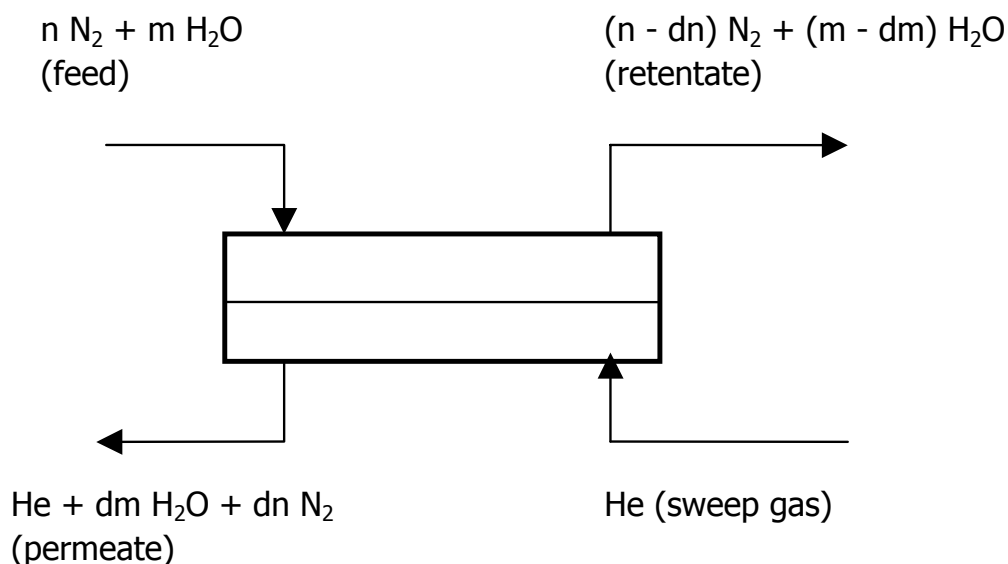


**Figure 1:** Schematic representation of the newly developed permeation equipment.

The permeability of water vapor and  $N_2$  is measured simultaneously using dew-pointing mirrors measuring the water content and gas chromatography for  $N_2$ . A detailed description of the experimental method is presented in the experimental section.

### 2.2.2 Mass transfer limitations

For many polymers, the highly selective transport of water vapor, in contrast to mixtures of permanent gases, can cause concentration polarization phenomena<sup>11</sup>. This is schematically depicted in Figure 2. Concentration polarization occurs in gas/vapor mixtures if the flux of water vapor through a selective polymer is larger than the flux of water vapor from the bulk of the feed to the gas/polymer surface. This flux imbalance causes a stagnant concentration boundary layer near the membrane surface to develop. Similar phenomena can occur on the permeate side of the membrane, but instead of boundary layer depletion as observed at the feed, mass accumulation of the permeate side may occur. Measuring the overall mass transfer rate only can give reliable values for intrinsic membrane properties when the boundary resistances are known.

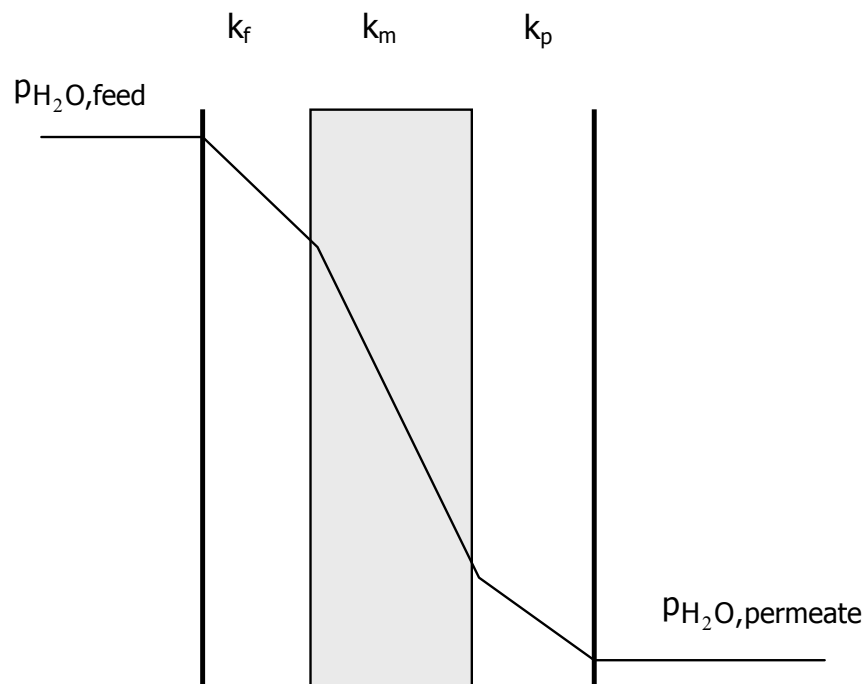


**Figure 2:** Schematic representation of the partial pressure profiles for water vapor in the stagnant boundary layers and the membrane for a water vapor/ $N_2$  mixture.



In Figure 2  $k_f$ ,  $k_m$ , and  $k_p$  are the mass transfer coefficients in the feed boundary layer, the membrane, and the permeate boundary layer, respectively. The stagnant boundary layers on the feed and permeate side of the membrane represent an extra resistance through the membrane. These resistances can be represented with the resistance in series model:

$$\frac{1}{k_{ov}} = \frac{1}{k_f} + \frac{1}{k_m} + \frac{1}{k_p} \quad (1)$$

where  $1/k_{ov}$  is the overall resistance for water vapor permeation (s/m) and  $k_{ov}$  the overall mass transfer coefficient for water vapor (m/s).

The mass transfer coefficients in the feed and permeate depend on the geometry and the hydrodynamic conditions of the system and are often described with Sherwood relations<sup>12</sup>:

$$Sh = aRe^b Sc^c \left(\frac{L}{d_h}\right)^d$$

where

$$Sh = \left(\frac{kd_h}{D}\right), Re = \left(\frac{\rho v d_h}{\eta}\right), Sc = \left(\frac{\eta}{\rho D}\right) \quad (2)$$

and  $a$ ,  $b$ ,  $c$  and  $d$  are specific constants depending on the geometry of the system.  $Sh$  is the Sherwood number (-),  $Re$  the Reynolds number (-),  $Sc$  the Schmidt number (-),  $k$  the mass transfer coefficient (m/s),  $d_h$  the hydraulic diameter (m),  $\rho$  the density ( $\text{kg/m}^3$ ),  $\eta$  the viscosity (Pa s),  $L$  the length of the flow path (m) and  $D$  the diffusion coefficient of water vapor in the gas mixture ( $\text{m}^2/\text{s}$ ). The diffusion coefficient of water vapor in nitrogen at various pressures and temperatures can be estimated with the following empirical relation derived by Massman<sup>13</sup>:

$$D = D_0 \left(\frac{p_0}{p}\right) \left(\frac{T}{T_0}\right)^{1.81} \quad (3)$$

where  $D$  is the diffusion coefficient of water in nitrogen ( $\text{cm}^2/\text{s}$ ),  $D_0$  is the diffusion coefficient of water in nitrogen at 1 bar and 273 K ( $0.2190 \text{ cm}^2/\text{s}$ ),  $p_0 = 1.013 \text{ bar}$ ,  $p$  the pressure (bar),  $T$  the absolute temperature (K) and  $T_0 = 273.15 \text{ K}$ .

The amount of nitrogen near the membrane surface is higher than the bulk concentration due to the lower water vapor pressure near the membrane surface. Frequently, this effect is negligible since the amount of water vapor in the feed is

significantly smaller than the amount of nitrogen. Therefore, concentration polarization phenomena will only affect the water vapor permeability.

## 2.3 Experimental

Measuring transport of water/gas mixtures at elevated pressure and temperature is necessary to obtain reliable intrinsic polymer properties. To the best of our knowledge only few studies report such data. In particular, for highly selective and highly permeable membrane materials, this task is represents an experimental challenge. Figure 3 shows the mixed gas water vapor permeation set up designed for the simultaneous measurement of a vapor and mixed gas permeability, in the temperature range 20 – 80°C, and pressure range 1 – 80 bars.

### 2.3.1 Mixed gas water vapor permeation set-up

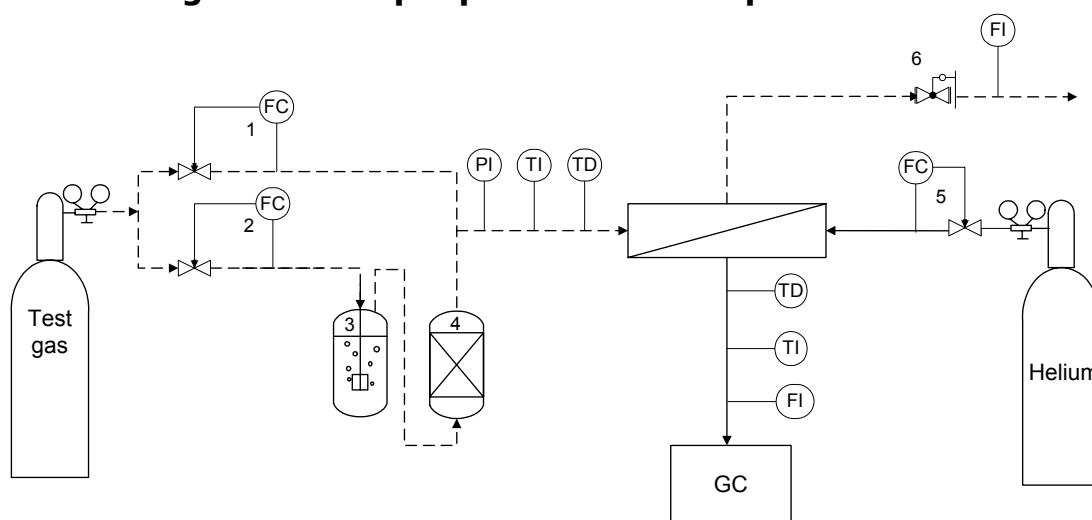


**Figure 3:** Mixed gas vapor permeation set-up for the measurement of gas vapor mixtures in the temperature range 20 – 80°C and pressure range 1 – 80 bars.

A gas/vapor mixture is generated by flowing a gas through a bubble column (3) and a demister (4). The latter separates the entrained liquid droplets from the gas stream. Both the bubble column (0.6 l) and demister (0.5 l), which are tailor-made, are double walled and are thermostated with the use of a heating bath. The wet gas stream is mixed with a dry gas stream to the desired humidity and is sent to the permeation cell. The water vapor concentration in this stream is controlled by adjusting the flow rates of the dry and wet stream with the mass flow controllers 1 and 2 (FC, Brooks 0154) respectively. The following parameters are measured in the feed stream to the membrane test cell: total pressure (PI,

Druck PTX 1400), temperature (TI, thermocouple), and the water vapor dew point (TD, Michel instruments SD). This gas mixture flows over a polymeric film mounted in a membrane test cell and leaves the system via a back pressure (6, Go backpressure regulator), which controls the total pressure in the system. The flow rate of the stream leaving the membrane test cell is measured with a soap bubble meter (FI). Water vapor as well as gas permeate through the membrane material and are removed with a helium sweep gas. The flow rate of this sweep gas can be controlled with a mass flow controller 5 (FC, Brooks 0154). In the sweep gas stream leaving the permeate side of the cell the following parameters are analyzed: water vapor dew point (TD, Michel instruments SD), temperature (TI, thermocouple), flow rate (FI, soap bubble meter), and nitrogen concentration with a gas chromatograph (GS, Varian 3400, column: Porapack Q).

The whole set up is insulated and temperature controlled with the use of a heating bath, via heat exchangers and heating tape (Isopad heating tape and Winkler temperature control unit), which prevent condensation of water vapor in the tubing of the set up.

### 2.3.2 Permeation cell

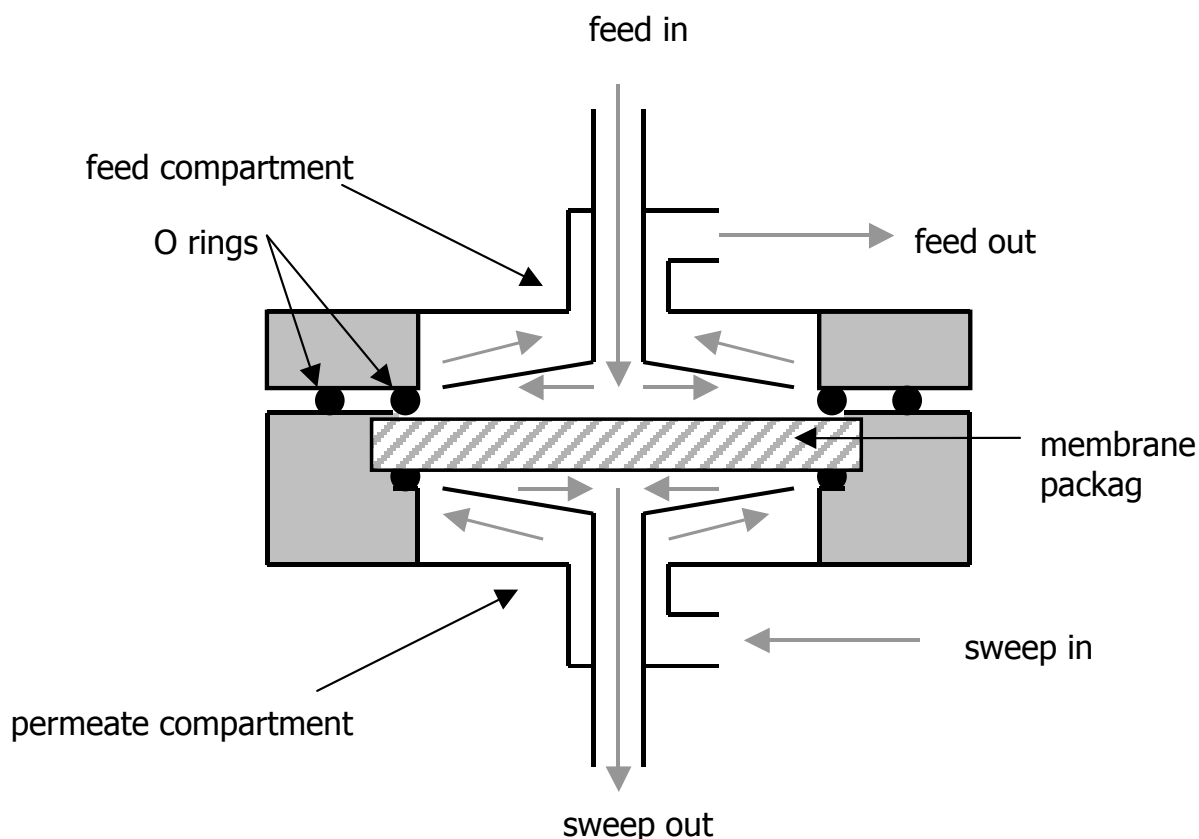


**Figure 4:** Schematic representation of the permeation cell.

Figure 4 shows a schematic representation of the of the permeation cell. The feed gas mixture enters on top and through the centre of the cell and flows radially over the membrane leaving the cell via 12 holes on the outer ring. The sweep gas helium enters the lower part of the permeation cell through the 12 holes and flows radially to the center where it leaves the cell. In this manner the feed and sweep gas establish a counter-current flow pattern. The membrane package comprises of a polymeric film (thickness from 20 to 300  $\mu\text{m}$ ), a filter paper, and a porous metallic support plate supporting the membrane. The effective membrane area is 11.95  $\text{cm}^2$ . The two compartments of the permeation cell are sealed with O-rings (Viton). The cell compartments are double-walled and heated with a heating bath.

### 2.3.3 Determination of the permeability values

Gas or vapor permeate through the membrane material due to a partial pressure difference between the feed and permeate side according to equation 4:

$$J_i = \frac{P}{l} (p_{i,\text{feed}} - p_{i,\text{permeate}}) \quad (4)$$

$J_i$  is the flux through the polymeric film ( $\text{cm}^3$  (STP)/( $\text{cm}^2$  s)),  $P$  the permeability expressed in Barrer ( $1 \text{ Barrer} = 10^{-10} \text{ cm}^3$  (STP)  $\text{cm}/(\text{cm}^2 \text{ s cmHg})$ ),  $l$  the thickness of the material (cm),  $p_{i,\text{feed}}$  and  $p_{i,\text{permeate}}$  the partial pressures on the feed and permeate side of the material (cmHg), respectively.

The partial pressures of water vapor on the feed and permeate side of the material are obtained from the dew point temperature of water vapor, which is measured with dew pointing mirrors. These sensors detect the temperature at which water vapor condenses on a cooled mirror surface. This temperature is related to the vapor pressure of water vapor in the gas mixture. Various relations can be used to relate the dew point temperature with a water vapor pressure. An example is the Antoine equation, which relates the water vapor pressure with the measured dew point temperature<sup>14</sup>:

$$\log_{10} (p_{\text{H}_2\text{O}}) = 5.11564 - \frac{1687.537}{T_{\text{dew}} + 230.17} \quad (5)$$

where  $p_{\text{H}_2\text{O}}$  is the water vapor pressure (bar) and  $T_{\text{dew}}$  the dew point temperature ( $^{\circ}\text{C}$ ).

The water vapor flux permeating through the membrane can be determined from the vapor pressure and the flow rate of the sweep gas:

$$J_{\text{H}_2\text{O}} = \frac{\phi_{v,\text{tot}} p_{\text{H}_2\text{O}} V_m \gamma}{R T A} \quad (6)$$

where  $J_{\text{H}_2\text{O}}$  is the water vapor flux ( $\text{cm}^3$ (STP)/( $\text{cm}^2$  s)),  $\phi_{v,\text{tot}}$  the flow rate of sweep gas ( $\text{m}^3/\text{s}$ ) containing water vapor,  $p_{\text{H}_2\text{O}}$  the water vapor pressure of the permeate stream (Pa),  $R$  the gas constant ( $8.314 \text{ J}/(\text{mol K})$ ),  $T$  the temperature (K),  $A$  the membrane area ( $\text{cm}^2$ ),  $V_m$  the volume of 1 mol penetrant at standard temperature and pressure ( $22414 \text{ cm}^3/\text{mol}$ ) and  $\gamma$  the activity coefficient. The later one is considered to equal unity ( $\gamma = 1$ ), because the sweep gas comprises mainly helium at 1 bar and behaves as an ideal gas mixture.

The nitrogen permeability is determined from the amount of nitrogen present in the sweep gas as detected with the gas chromatograph, and the feed pressure of nitrogen. The flux of can be determined with Eq. (7):

$$J_{N_2} = \frac{\phi_{v,tot} F_{N_2}}{A} \quad (7)$$

where  $J_{N_2}$  is the flux of nitrogen ( $\text{cm}^3$  (STP)/( $\text{cm}^2$  s)),  $\phi_{v,tot}$  the volume flow of the sweep gas ( $\text{cm}^3$ (STP)/s),  $F_{N_2}$  the fraction of nitrogen present in the sweep gas, and  $A$  the effective membrane area ( $\text{cm}^2$ ). The nitrogen permeability can be determined by using Eq. (4), where  $p_{i,feed}$  is the nitrogen pressure in the feed (cmHg) and  $p_{i,permeate}$  the amount of nitrogen in the sweep. The latter partial pressure is negligible compared to the nitrogen pressure in the feed ( $p_{feed} = 2\text{-}5$  bar,  $p_{permeate} = 1 \cdot 10^{-4} - 3 \cdot 10^{-3}$  bar).

### 2.3.4 Materials

Bisphenol A polysulfone (PSf), type Udel<sup>®</sup> P3500 was obtained from Amoco Chemicals (Belgium), and ethyl cellulose (ethoxyl content 49%) was obtained from Acros. Chloroform ( $\text{CHCl}_3$ ), dichloromethane ( $\text{CH}_2\text{Cl}_2$ ) and trifluoroacetic acid (TFA) were both purchased from Merck (analytical grade) and used as solvents. For the gas permeation experiments nitrogen ( $\text{N}_2$ ) and helium (He) were purchased from Hoekloos b.v. (the Netherlands). All the gases have a purity greater than 99.9%. Gas mixtures of helium and nitrogen (1000, 1500 and 2500 ppm), for the calibration of the Thermal Conductive Detector (TCD) of the gas chromatograph (GC), were obtained from Praxair n.v. (Belgium).

### 2.3.5 PEO-PBT block copolymers

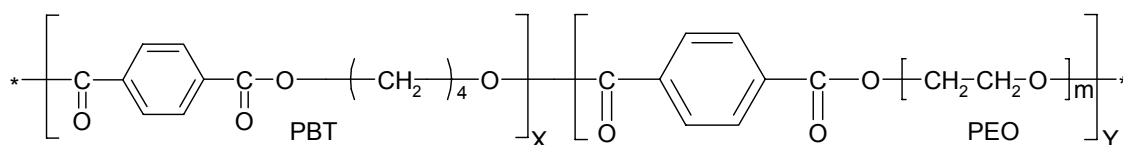


**Figure 5:** Schematic structure of PEO-PBT block copolymers.

PEO-PBT block copolymers were obtained from ISOTIS b.v. (the Netherlands) and were used without further purification. Figure 5 shows the schematic structure of the PEO-PBT block copolymers. These block copolymers consist of two segments: a hard hydrophobic rigid crystalline PBT segment (x) and a soft hydrophilic amorphous rubbery PEO segment (y). The following notation classifies the various block copolymers:  $m\text{PEO}y\text{PBT}x$ , where  $m$  is the molecular weight of the PEO

segment and  $y$  and  $x$  are the weight percentages of PEO and PBT phase respectively. The PEO-PBT block copolymer used in this study is 1000PEO56PBT44.

### 2.3.6 Film preparation

Polymeric solutions (5 – 15 wt. %) were prepared by dissolving 1000PEO56PBT44 in  $\text{CHCl}_3$  and ethyl cellulose and polysulfone in  $\text{CH}_2\text{Cl}_2$ . Thin films of around  $50 \mu\text{m}$  were prepared by solution casting on a glass plate. The cast films were dried in a nitrogen atmosphere at room temperature for 24 hours. The homogeneous dense films were removed from the glass plate with the help of a small amount of water and were further dried and stored in a vacuum oven at  $30^\circ\text{C}$ .

## 2.4 Results and Discussion

### 2.4.1 Effects of concentration polarization

Measuring the overall flux of water and normalizing it to the driving force as well as to membrane thickness (Eq. 4) gives an apparent permeability. Apparent, since it may also contain the transport resistances of the potential boundary layers on the feed and permeate side.

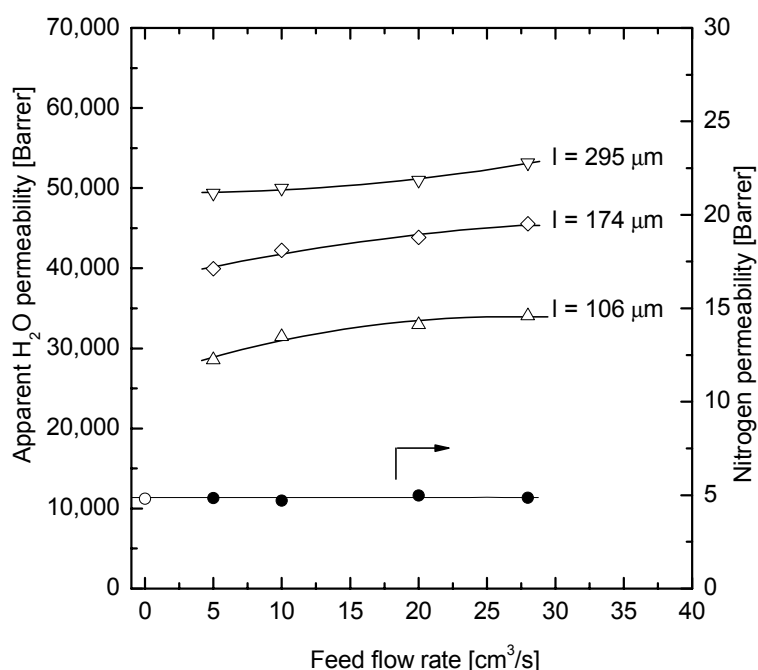


**Figure 6:** Apparent water vapor and nitrogen permeabilities of 1000PEO56PBT44 at various feed flow rates and film thicknesses. (activity 0.41,  $\phi_{V,\text{permeate}}$  0.67  $\text{cm}^3/\text{s}$ , temperature  $50^\circ\text{C}$ ,  $p_{\text{feed}} = 3.5 \text{ bar}$ )

Figure 6 shows the apparent water vapor permeability for 1000PEO56PBT44 with thicknesses of 106, 174 and 295  $\mu\text{m}$  at feed flow rates ranging between 5 and 28  $\text{cm}^3/\text{s}$ . The apparent water vapor permeability is the permeability calculated with Eq. (4) from the water vapor flux through the membrane, the partial pressure difference over the membrane and its thickness. If the membrane resistance only determines the transport of water, one would expect the normalization to result in a single "apparent permeability" value. However, Figure 6 suggests an increasing permeability with increasing thickness. This is only possible if the overall resistance comprises several resistances, only one of them being the membrane resistance. Also, the apparent water vapor permeability increases with an increase of feed flow rate. This increase may stem from: 1) significant depletion of water content in the feed gas mixture at low feed flow rates or, 2) concentration polarization in the feed and permeate side boundary layers. Depletion of the feed gas mixture occurs at low feed flow rates and high fluxes, if the amount of water vapor permeating through the membrane lowers the concentration of water vapor in the bulk phase above the membrane. This reduces the effective driving force at the feed side. An increase in feed flow rate compensates for the water removal, thereby keeping the high driving force, causing a high apparent permeability. At the current experimental conditions the water vapor flux through the membrane is small compared to the amount of water vapor flowing over the membrane (low stage cut). The effect of stage cut results in a 4 % lower partial pressure on the feed side of the membrane with a thickness of 106  $\mu\text{m}$  for a flow rate of 5  $\text{cm}^3/\text{s}$  compared to a flow rate of 27  $\text{cm}^3/\text{s}$ . The increase in permeability is 20 %, indicating that the increase in permeability must be attributed to concentration polarization and an increased mass transfer coefficient at higher flow rates.

The mass transfer of water vapor through the stagnant feed boundary layer ( $k_f$ ) increases due to higher turbulence induced by higher flow rates over the membrane. The stagnant feed boundary layer influences the apparent water vapor permeability, even for very thick membranes (295  $\mu\text{m}$ ) where the permeability also increases at elevated feed flow rate.

Figure 6 also shows the mixed gas nitrogen permeability at feed flow rates between 5 and 28  $\text{cm}^3/\text{s}$ . The nitrogen permeability remains constant with increasing feed flow rate and is equal to the nitrogen permeability determined for pure gas permeation (open circle). A constant nitrogen permeability indicates that the presence of a stagnant boundary layer for water vapor does not affect the nitrogen permeability. This is not surprising since a change in partial nitrogen pressure at the membrane/gas interface due to less concentration polarization is negligible compared to its absolute value.



The permeate flow rate of the sweep gas is varied in order to determine whether concentration polarization on the permeate side may affect the water vapor permeability.

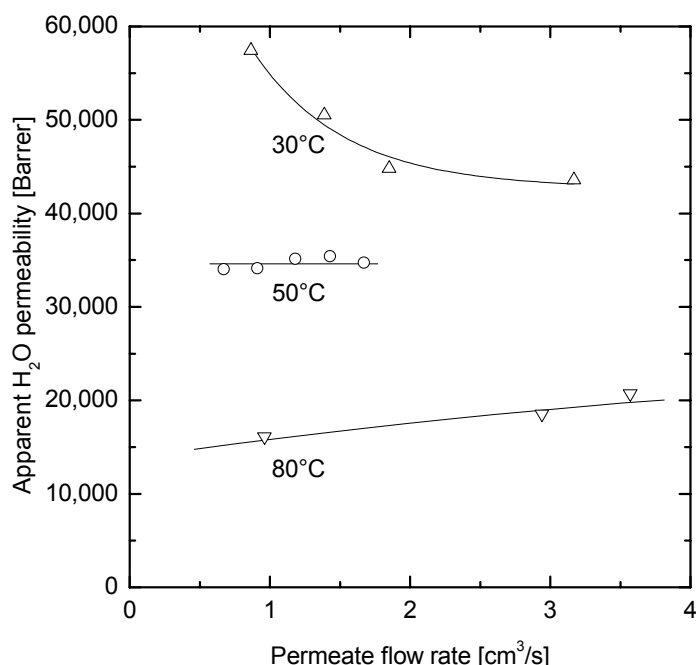


**Figure 7:** Apparent water vapor permeability of 1000PEO56PBT44 at 30°C, 50°C, and 80°C for various permeate flow rates.

Figure 7 shows the apparent water vapor permeability of 1000PEO56PBT44 at 30°C, 50°C, and 80°C for various permeate flow rates. The apparent water vapor permeability decreases at 30°C, remains constant at 50°C, and increases at 80°C with an increase of permeate flow rate. The decrease at 30°C is remarkable since an increase is expected if a stagnant boundary layer would be present at the permeate side of the membrane. In the determination of the apparent water vapor permeability (Eq. 4) it is assumed that the water vapor pressure in the sweep gas leaving the membrane test cell equals the average water vapor pressure on the permeate side of the membrane (ideal mixing). Probably, this assumption of ideal mixing on the permeate side of the membrane is not valid resulting in an erroneous permeate pressure for the calculation of the permeability. The flow pattern of the sweep gas is somewhere between plug flow and ideal mixed, which makes the determination of the exact permeate pressure difficult. This effect is more pronounced at lower temperatures due to the higher

water vapor permeability of this material. The feed- and permeate pressures of water vapor at 30°C, 50°C, and 80°C are presented in Table 1.

**Table 1:** Feed- and permeate pressure at 30°C, 50°C, and 80°C for 1000PEO56PBT44 for  $\phi_{V,feed} = 10 \text{ cm}^3/\text{s}$  and  $\phi_{V,permeate} = 0.67 \text{ cm}^3/\text{s}$ .

Temperature [°C]	$p_{,feed}$ [cmHg]	$p_{,permeate}$ [cmHg]
30	1.08	0.46
50	2.30	0.65
80	6.54	1.51

The permeate pressure at 30°C is lower than at 50°C and 80°C and its relative contribution to the driving force ( $p_{\text{H}_2\text{O},feed} - p_{\text{H}_2\text{O},permeate}$ ) is much larger. A deviation in the permeate pressure will therefore have a larger effect. The apparent water vapor permeability remains constant at 50°C with an increase of sweep gas flow rate, which also indicates that concentration polarization at the permeate side of the membrane is negligible for the flow rates investigated. A stagnant boundary layer on the permeate side of the membrane probably affects the permeability at 80°C, which increases with an increase of permeate flow rate.

The relative contribution of non-ideal mixing and the presence of stagnant boundary layers obviously are less pronounced for thicker polymeric films. An estimate of the contribution of these effects on the total permeability can be determined by plotting the overall resistance for various films versus their thickness.

#### 2.4.2 Boundary layer resistance

The resistance for permeation due to the presence of stagnant boundary layers and non-ideal permeate mixing can be determined by plotting overall resistance for mass transfer ( $1/k_{ov}$ ) versus the film thickness.

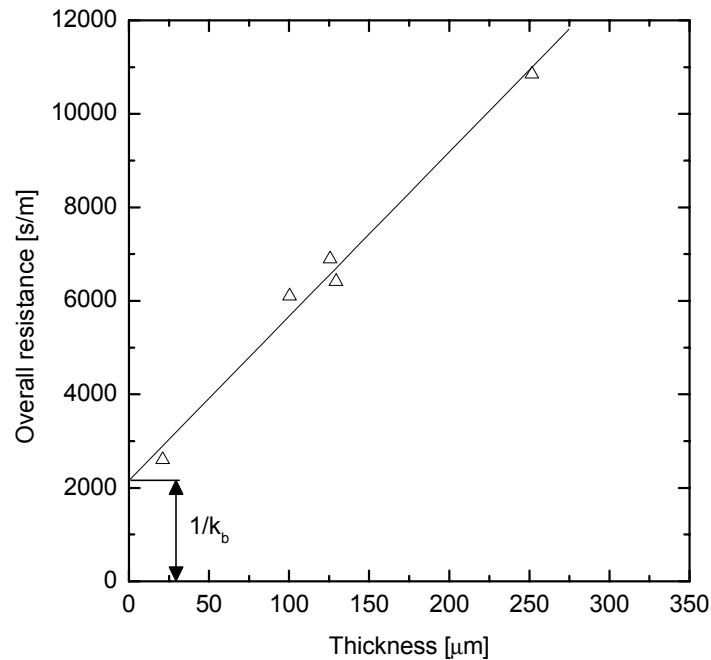


**Figure 8:** Overall resistance towards mass transfer for various film thicknesses. (1000PEO56PBT44, activity 0.20,  $\phi_{v,\text{feed}}$  10 cm<sup>3</sup>/s,  $\phi_{v,\text{permeate}}$  0.67 cm<sup>3</sup>/s, pressure 3.5 bar, activity 0.34 and temperature 80°C).

Figure 8 shows the overall mass transfer resistance for 1000PEO56PBT44 at 80°C versus the film thicknesses. The film thickness is varied and the overall resistance is determined at constant pressure, temperature, and feed- and permeate flow rates and increases with an increase of the polymeric film thickness. The abscissa represents the resistance in the boundary layers and comprises mainly of the resistance in the stagnant permeate boundary layer and non-ideal mixing. The resistance at the permeate side of the polymeric film can stem from resistance for diffusion in the support material (filter paper and porous metallic plate).

The procedure in Figure 8 is repeated at 30°C, 50°C and 80°C to quantify the stagnant boundary layer resistance at different temperatures is. The results are summarized in Table 2.

**Table 2:** Resistances in the stagnant boundary layers at 30°C, 50°C and 80°C.

Temperature [°C]	Resistance boundary layer $1/k_f$ [s/m]	Mass transfer coefficient $k_f$ [m/s]	Diffusion coefficient $D_{H_2O}$ in $N_2$ [m <sup>2</sup> /s]
30	914	1.1E-03	0.27
50	2312	4.3E-04	0.30
80	2155	4.6E-04	0.35

Table 2 shows the resistances in the stagnant boundary layers at 30°C, 50°C, and 80°C, its reciprocal analogues (the mass transfer coefficient), and the diffusion coefficient of water vapor in nitrogen (Eq. (3)). The resistance in the feed boundary layer is only valid at the specific flow conditions at which these resistances were determined ( $\phi_{v,feed} = 10 \text{ cm}^3/\text{s}$ ,  $\phi_{v,permeate} = 0.67 \text{ cm}^3/\text{s}$ , pressure 3.5 bar). The resistance in the stagnant boundary layer decreases from 50°C to 80°C (mass transfer coefficient increases) with an increase of temperature. This result is expected on the basis of the mass transfer coefficient calculated with a Sherwood relation (Eq.(2)), which generally predicts an increasing mass transfer coefficient with an increase of temperature due to an increased diffusivity of water vapor through nitrogen. Only the resistance determined at 30°C deviates in this respect probably due to non-ideal mixed conditions at the permeate side of the membrane. We take the boundary layer resistance as a specific characteristic for the measurement cell. Subtracting this resistance from the overall resistance (Eq. (1)) results in the membrane resistance ( $k_m$ ). The average partial pressure difference over the membrane ( $P_{H_2O,feed} - p_{H_2O,permeate}$ ) in absence of stagnant boundary layers and non-ideal flow conditions can now be determined by using the following equation:

$$J_{H_2O} = k_m (p_{H_2O,feed} - P_{H_2O,permeate}) \quad (8)$$

where  $J_{H_2O}$  is the flux of water vapor through the material determined with eq. 6. The permeability of the material now can be determined from the flux and the average driving force over the membrane (Eq.4).

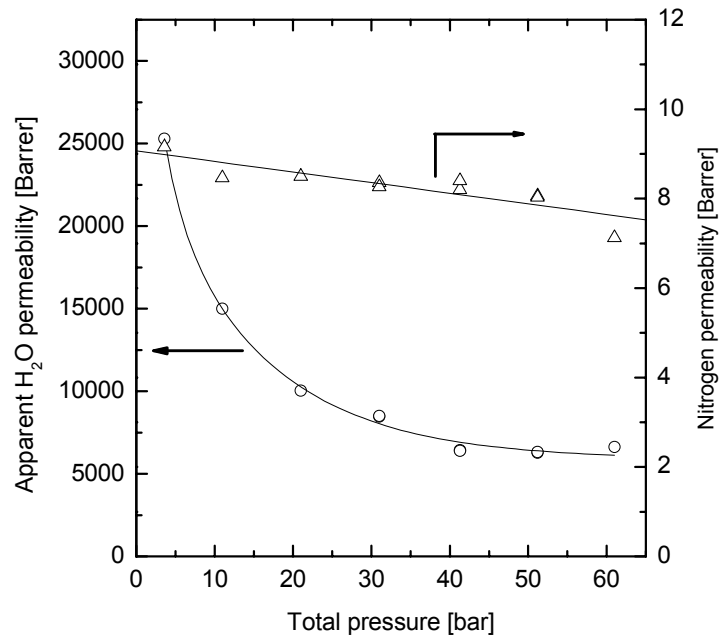
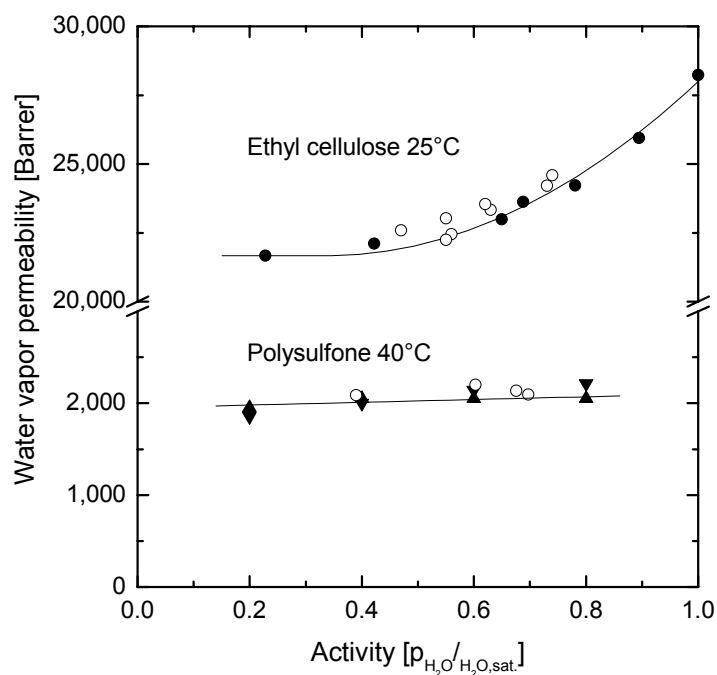


**Figure 9:** Mixed gas water vapor and nitrogen permeability as a function of the feed pressure. (water activity 0.27,  $\phi_{v,feed}$  10 cm<sup>3</sup>/s,  $\phi_{v,permeate}$  0.67 cm<sup>3</sup>/s, temperature 50°C).

Also the feed pressure significantly affects the overall mass transfer as shown in Figure 9. This figure shows the apparent water vapor and nitrogen permeability at 50°C in the pressure range 3.5 – 60 bars. The apparent water vapor permeability decreases 5 times when the feed pressure increase from 3.5 to 60 bars, whereas the nitrogen permeability decreases only slightly. The latter decrease may stem from a compression of the polymer matrix which decreases the free volume, thereby lowering the diffusivity of nitrogen<sup>15,16</sup>. However, the dramatic decrease in water vapor permeability is much larger and cannot be explained by the compression of the material. The decrease of the apparent water vapor permeability stems from an increased resistance in the stagnant feed boundary layer, due to a lower diffusion coefficient of water vapor through nitrogen at higher feed pressures (Eq. (3)).

### 2.4.3 Validation permeability values

Experiments are performed with ethyl cellulose (25°C) and polysulfone (40°C) to validate the results obtained with the new mixed gas water vapor permeation set-up, and the results are compared with literature data. The boundary layer resistance is estimated by extrapolating the values found in Table 2 between 30 and 50°C.



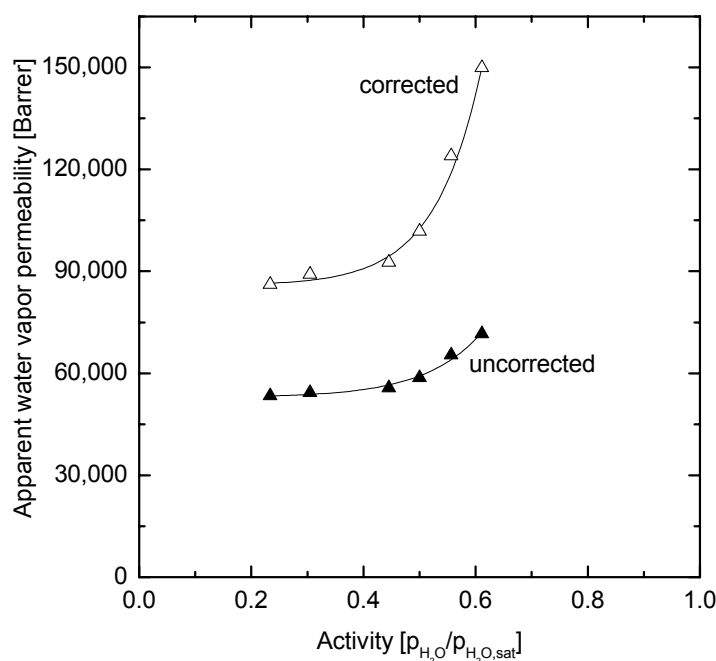
**Figure 10:** Water vapor permeabilities of ethyl cellulose at 25°C and polysulfone films at 40°C, open symbols represent measured values and closed symbols represent literature data. (Literature data: ethyl cellulose 25°C, ● Wellons and Stannet<sup>17</sup>, polysulfone 40°C, ▲ Schult and Paul<sup>6</sup>, ▼ Swinyard et. al.<sup>18</sup>).

Figure 10 shows the water vapor permeabilities of ethyl cellulose at 25°C and polysulfone at  $T = 40^\circ\text{C}$  versus the water vapor activity. The closed symbols represent literature data and the open symbols represent values measured with our equipment. The measured water vapor permeability and activity are corrected for the presence of a stagnant boundary layer. The measured values, which differ one order of magnitude, are in good agreement with literature data, indicating that the experimental set-up and the analysis method gives reliable results. Since the experimental data from literature are obtained for pure water vapor experiments we conclude that the water vapor permeability is not affected by the presence of nitrogen.

The relative contribution of the correction term for the stagnant boundary layer (Table 2) to the overall resistance calculated for a film thickness of 100  $\mu\text{m}$  amounts to 15 % for ethyl cellulose and 3 % for polysulfone at activity 0.5. Using thick films minimizes the influence of the stagnant boundary layer on the total permeability. This correction term has to be taken into account for polymers with a high water vapor permeability ( $>20.000$  Barrer).

#### 2.4.4 Highly permeable, highly selective materials

PEO-PBT block copolymers are investigated for their water vapor permeability, since the PEO block shows a high solubility for water facilitating high water vapor permeability. The high solubility of the block copolymer stems from a high solubility of water vapor in the PEO block, PEO itself as a pure polymer is soluble in water<sup>19</sup>. The addition of a PBT segment in the block copolymer makes the block copolymer insoluble in water, but enables a high solubility of water vapor in the PEO phase.



**Figure 11:** Water vapor permeability of 1000PEO56PBT44 at 30°C. ( $\phi_{v,\text{feed}}$  10  $\text{cm}^3/\text{s}$ ,  $\phi_{v,\text{permeate}}$  0.67  $\text{cm}^3/\text{s}$ , pressure 3.5 bar, film thickness 112  $\mu\text{m}$ )

Figure 11 shows the corrected (open symbols) and uncorrected (closed symbols) water vapor permeability of 1000PEO56PBT44 at 30°C, versus the water vapor activity. The water vapor permeability and activity are corrected for concentration

polarization. The water vapor permeability at 30°C increases with an increase in activity stemming from a higher solubility of water vapor at higher activities. The relative contribution of the correction term for the stagnant boundary layer to the overall resistance calculated for a film thickness of 100  $\mu\text{m}$  is 45 %, which is much higher than for ethyl cellulose and polysulfone due to the higher water vapor permeability of 1000PEO56PBT44. The nitrogen permeability remained constant over the whole activity range and is 1.7 Barrer, which results in a high selectivity of 50,600, compared to other polymers<sup>20</sup>. The selectivity and permeability of 1000PEO56PBT44 classifies the material as highly permeable and selective.

## 2.5 Conclusions

The selectivity and permeability of 1000PEO56PBT44 are relatively high compared to other polymers. However, the measured permeabilities are affected significantly by the presence of a stagnant boundary layer. This resistance is determined by plotting the overall mass transfer coefficient versus the film thickness. The water vapor permeability of ethyl cellulose and polysulfone are corrected for this resistance and identical to literature values.

The water vapor permeability and selectivity of 1000PEO56PBT44 block copolymers are high (86,000 Barrer and  $\text{H}_2\text{O}/\text{N}_2$  selectivity 50,600) compared to other polymers and the permeability increases significantly with the water vapor activity of the feed gas mixture, whereas the nitrogen permeability remains constant. The water vapor permeability shows a strong dependence on the total pressure. An increase of the total pressure results in a larger resistance in the stagnant feed boundary layer, thereby lowering the total water vapor flux. The relative contribution of the resistance of the stagnant boundary layer is larger for materials with a higher permeability due to the lower resistance for permeation in these materials.

## 2.6 Acknowledgements

The European Union is kindly acknowledged for supporting this project: Brite Euram III, Contract no. BRPR-CT 98-0804



## 2.7 References

- (1) Baker, R. W. *Ind. Eng. Chem. Res.* **2002**, *41*, 1393-1411.
- (2) Wang, K. L.; McCray, S. H.; Newbold, D. D.; Cussler, E. L. *J. Membr. Sci.* **1992**, *72*, 231-244.
- (3) Gebben, B. *J. Membr. Sci.* **1996**, *113*, 323-329.
- (4) Stroeks, A. *Polymer* **2001**, *42*, 9903-9908.
- (5) Park, G. S. *Synthetic membranes: science, engineering and applications*; Reidel: Dordrecht, 1986.
- (6) Schult, K. A.; Paul, D. R. *J. Appl. Polym. Sci.* **1996**, *61*, 1865-1876.
- (7) Cha, J. S.; Malik, V.; Bhaumik, D.; Li, R.; Sirkar, K. K. *J. Membr. Sci.* **1997**, *128*, 195-211.
- (8) Yeom, C. K.; Lee, S. H.; Song, H. Y.; Lee, J. M. *J. Membr. Sci.* **2002**, *205*, 155-174.
- (9) Ludtke, O.; Behling, R. D.; Ohlrogge, K. *J. Membr. Sci.* **1998**, *146*, 145-157.
- (10) Dixon-Garrett, S. V.; Nagai, K.; Freeman, B. D. *J. Polym. Sci., Polym. Phys. Ed.* **2000**, *38*, 1078-1089.
- (11) Baker, R. W.; Wijmans, J. G.; Athayde, A. L.; Daniels, R.; Ly, J. H.; Le, M. *J. Membr. Sci.* **1997**, *137*, 159-172.
- (12) Gabelman, A.; Hwang, S. T. *J. Membr. Sci.* **1999**, *159*, 61-106.
- (13) Massman, W. J. *Atmos. Environ.* **1998**, *32*, 1111-1127.
- (14) Poling, B. E.; Prausnitz, J. M.; O'Connell, J. P. *The properties of gases and liquids*; McGraw-Hill: New York, 2001.
- (15) Merkel, T. C.; Bondar, V. I.; Nagai, K.; Freeman, B. D.; Pinnau, I. *J. Polym. Sci., Polym. Phys. Ed.* **2000**, *38*, 415-434.
- (16) Koros, W. J.; Hellums, M. W. In *Encyclopedia of polymer science and engineering*; Kroschwitz, J. I., Ed.; Wiley: New York, 1990; pp 724-802.
- (17) Wellons, J. D.; Stannett, V. *J. Polym. Sci.* **1966**, *4*, 593-602.
- (18) Swinyard, B. T.; Sagoo, P. S.; Barrie, J. A.; Ash, R. *J. Appl. Polym. Sci.* **1990**, *41*, 2479-2485.
- (19) Brandrup, J.; Immergut, E. H.; Abe, A.; Bloch, D. R. *Polymer handbook*, 4 th ed.; Wiley: New York, 1999.
- (20) Barrie, J. A. In *Diffusion in Polymers*; Crank, J.; Park, G. S., Eds.; Academic Press, 1968.



# Chapter 3

## Performance of Polyethersulfone/Polyimide Hollow Fiber Membranes in the Separation of Wet CO<sub>2</sub>/N<sub>2</sub> Gaseous Mixtures

### Abstract

This work presents the permeation properties of PES/PI 80/20 asymmetric hollow fiber membranes in the separation of humidified N<sub>2</sub>, CO<sub>2</sub> and a binary mixture of CO<sub>2</sub>/N<sub>2</sub> 55/45%. The permeance values of CO<sub>2</sub>, N<sub>2</sub> and water vapor were measured by using the variable volume-sweep gas method at various water vapor activities, feed pressures, feed- and permeate flow rates. Increasing feed water vapor activity reduces H<sub>2</sub>O, N<sub>2</sub> and CO<sub>2</sub> permeance values and H<sub>2</sub>O/N<sub>2</sub> and H<sub>2</sub>O/CO<sub>2</sub> selectivity, whereas CO<sub>2</sub>/N<sub>2</sub> selectivity remains constant. The observed reduction in permeance could not be attributed to pore condensation in the porous substructure, since sorption isotherms of a dense PES/PI film and hollow fiber membrane showed the same solubility for water vapor. An increase of the total pressure at constant water vapor activity resulted in a reduction of the water vapor permeance due to a higher diffusivity of water vapor in the stagnant boundary layer on the feed side of the membrane. The nitrogen permeance remained constant with an increase of total pressure whereas the carbon dioxide permeance increased due to plasticization of the membrane. The resistances to mass transport for water vapor were studied at various feed- and permeate flow rates, enabling the derivation of Sherwood relations, which describe the variation of the overall mass transfer coefficient at various process conditions. This analysis of mass transfer reveals that the main resistance for water vapor transport is situated in the stagnant feed boundary layer. This main resistance shifts to the membrane at higher feed flow rates.

### 3.1 Introduction

Asymmetric hollow fiber membranes are used in gas separation applications because they combine a high selectivity (material property) with a high gas flux (membrane property). This high flux is achieved by an ultra-thin dense skin layer supported by a sponge-like substructure. Generally, the main resistance for gas transport is situated in the skin layer and its permeability as well as its thickness controls the flux through the membrane. This dense skin layer performs the actual selective separation of the gas mixture. The sponge-like support membrane is frequently assumed to have a negligible mass transport resistance.

Recently, high flux poly(ethersulfone)-poly(imide) 80/20 wt% (PES-PI) blend hollow fiber membranes were developed in our group<sup>1,2</sup>. These membranes consist of an ultra thin skin layer with a thickness of 0.1  $\mu\text{m}$ , with a  $\text{CO}_2/\text{N}_2$  selectivity higher than existing commercial gas separation membranes<sup>2</sup>.

Numerous papers are devoted to the performance of dense flat polymeric films in pure gases. However, in real gas separation applications hollow fiber membranes are used for the separation of gas mixtures. Very little data are disclosed today in scientific literature, describing the mass transport behavior of such membranes in multi-component mixtures. The PES-PI membranes are already characterized for dry  $\text{CO}_2/\text{N}_2$  gas mixture<sup>2</sup> and this contribution extends the study towards humidified feed gas mixtures.

In particular, we present and interpret separation performance data at different operating conditions (humidity, feed pressure, flow rate). Furthermore, we study the mass transfer resistance for water vapor in boundary layers and relate the mass transfer coefficient to the operating conditions via Sherwood relations.

## 3.2 Background

In contrast to gas transport through homogeneous thick films ( $> 10 \mu\text{m}$ ), hollow fibers show a more complex transport behavior. For membranes with a high selectivity and flux the resistance towards mass transfer is not only situated in the dense skin of the membrane but also in stagnant boundary layers.

### 3.2.1 Resistances towards mass transfer

In particular for the fastest permeating component, water, the resistance towards mass transfer is not only situated in the dense skin layer of the membrane but significant contributions from the stagnant boundary layers on the feed and permeate side of the membrane might be expected<sup>3</sup>. In gas separation this phenomenon is called concentration polarization, which occurs if the transport rate of water vapor through the asymmetric hollow fiber membrane is larger than the transport of water vapor from the bulk of the feed to the membrane surface. This creates a stagnant concentration boundary layer near the membrane surface with a decreasing water vapor concentration towards the membrane gas interface.

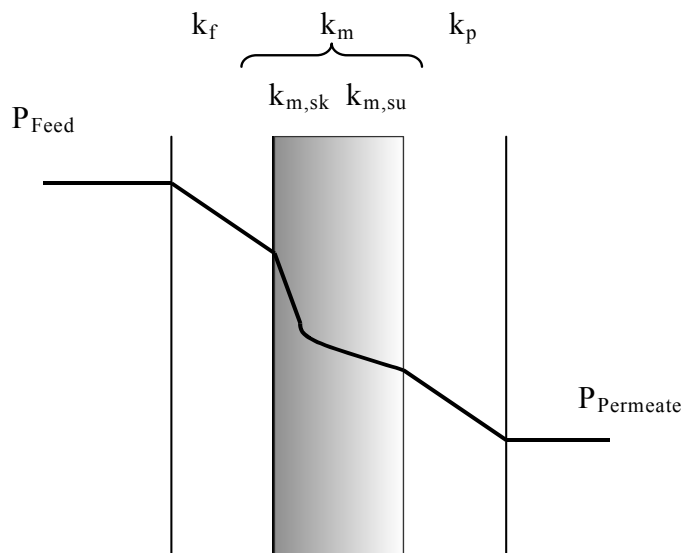


**Figure 1:** Schematic representations of the chemical potential as a function of the position across the membrane indicating the resistances towards mass transfer for water vapor through an asymmetric membrane.

Figure 1 shows schematically the gradient of the chemical potential  $\mu$  of water stemming from resistances towards mass transfer for water vapor through an asymmetric membrane, with  $k_f$  being the mass transfer coefficient through the stagnant boundary layer at the feed side of the membrane,  $k_{m,sk}$  the mass transfer coefficient of the membrane in the skin,  $k_{m,su}$  the mass transfer coefficient of the membrane in the porous support, and  $k_p$  the mass transfer coefficient of water vapor through the stagnant boundary layer at the permeate side of the membrane. The concentration of water vapor at the interface of the membrane is lower than in the bulk of the feed due to the flux imbalance: water vapor permeates to faster through the polymer than diffusive transport from the bulk of the feed to the surface of the membrane. This would result in a higher surface concentration of the other permeating component. However, this effect is negligible for water vapor in  $N_2$  and  $CO_2$  since the water vapor pressure is relatively small compared to the total pressure ( $p_{H_2O} = 31.70$  mbar at  $25^\circ C$  compared to 2 - 5 bar total pressure).

Water vapor permeates through the dense skin of the asymmetric membrane, which establishes the selective separation of water vapor. This resistance is relatively low for water vapor compared to the other gases ( $N_2$ ,  $CO_2$ ). Polyethersulfone e.g. has a water permeability of 2200 Barrer<sup>4</sup> while the  $CO_2$  permeability is only 3.4 Barrer<sup>5</sup>. However, the porous support may contribute considerably to the overall transport resistance for water vapor<sup>6,7</sup>.

The overall resistance for water vapor transport ( $k_{ov}$ ) can be expressed in the following equation:

$$\frac{1}{k_{ov}d_o} = \frac{1}{k_f d_o} + \frac{1}{k_m} + \frac{1}{k_p d_i} \quad (1)$$

where  $d_o$  is the external hollow fiber diameter, and  $d_i$  the internal hollow fiber diameter. The overall mass transfer resistance ( $k_{ov}$ ), is defined with respect to the external hollow fiber diameter.

The mass transfer coefficients of the stagnant feed and permeate boundary layers ( $k_f$ ,  $k_p$ ) are given by the geometry of the membrane module and the hydrodynamic conditions. These mass transfer coefficients are often correlated with Sherwood relations describing these coefficients in a specific system:

$$\text{Sh} = a\text{Re}^b \text{Sc}^c \left(\frac{d_h}{L}\right)^d \quad (2)$$

where  $a$ ,  $b$ ,  $c$  and  $d$  are constants specific for the system,  $d_h$  the hydraulic diameter and  $L$  the length of the flow path.

A specific Sherwood relation for the resistance in the stagnant feed and permeate boundary layer can be obtained via the so-called Wilson plot by plotting  $(1/k_{ov})$  versus  $(1/v^b)^{8,9}$  where  $v$  is the velocity on the feed or permeate side of the membrane. The abscissa of this plot represents the resistance in the membrane and the stagnant permeate boundary layer, and the slope equals  $b$  in Eq. (2).

A number of Sherwood relations are available, which describe the mass transfer coefficient on the shell side of a hollow fiber membrane<sup>8</sup>. Due to the complex flow distributions around the shell side of the hollow fibers these equations are only valid for systems with identical geometry and flow distribution. An example of an equation which correlates this coefficient is the one found by Prasad and Sirkar<sup>9</sup> for liquid-liquid extraction with membranes:

$$\text{Sh} = \beta(1 - \varphi) \text{Re}^{0.60} \text{Sc}^{0.33} \frac{d_h}{L} \quad (3)$$

where  $\varphi$  is the packing fraction of hollow fibers in a module, and  $\beta$  a specific constant which is found to be 5.8 for hydrophobic membranes and 6.1 for hydrophilic membranes<sup>9</sup>.

By combining eq. 2 and 3 the mass transfer coefficient becomes:

$$k = \beta(1 - \varphi) \left(\frac{\rho v d_h}{\eta}\right)^{0.60} \left(\frac{\eta}{\rho D}\right)^{0.33} \left(\frac{d_h}{L}\right) \frac{D}{d_h} \quad (4)$$

where  $\rho$  is the density ( $\text{kg/m}^3$ ),  $\eta$  the viscosity ( $\text{Pa s}$ ),  $v$  the velocity of the gas mixture ( $\text{m/s}$ ), and  $D$  the diffusion coefficient of water vapor ( $\text{m}^2/\text{s}$ ).

For the determination of the mass transfer coefficient in our system we use the density and viscosity of the pure  $\text{N}_2$ ,  $\text{CO}_2$  and  $\text{He}^{10}$ , since the amount of water vapor in the feed is very small ( $< 2$  vol. %). The diffusion coefficients of water vapor in  $\text{N}_2$ ,  $\text{CO}_2$  and  $\text{He}$  can be estimated by using the approach of Fuller<sup>11</sup>:

$$D_{A,B}(\text{cm}^2/\text{s}) = \frac{0.00143T^{1.75}}{\rho M_{A,B}^{1/2} \left( (\Sigma_v)_A^{1/3} + (\Sigma_v)_B^{1/3} \right)^2} \quad (5)$$

where  $D$  is the diffusion coefficient of water vapor in carbon dioxide or helium ( $\text{cm}^2/\text{s}$ ),  $T$  the absolute temperature (K),  $P$  the pressure (bar), and  $\Sigma_v$  the sum of atomic diffusion volumes, which can be found in literature<sup>11</sup>. Eq. (6) is used to calculate the molecular weight ( $M_{ab}$ ):

$$M_{AB} = 2 \left( \frac{1}{M_A} + \frac{1}{M_B} \right)^{-1} \quad (6)$$

where  $M_A$  and  $M_B$  are the molecular weight of both components ( $\text{g/mol}$ ).

The diffusion coefficient of water vapor in nitrogen at various pressures and temperatures needed for the calculation can be estimated with the following empirical relation derived by Massman<sup>12</sup>:

$$D = D_0 \left( \frac{p_0}{p} \right) \left( \frac{T}{T_0} \right)^{1.81} \quad (7)$$

where  $D$  is the diffusion coefficient of water in nitrogen ( $\text{cm}^2/\text{s}$ ),  $D_0$  the diffusion coefficient of water in nitrogen at 1 bar and 273 K ( $0.2190 \text{ cm}^2/\text{s}$ ),  $p_0 = 1.013$  bar,  $p$  the pressure (bar),  $T$  the absolute temperature (K) and  $T_0 = 273.15$  K.



The mass transfer coefficient for the tube side of a hollow fiber can satisfactorily be described with the L ev eque equation (8), since a defined flow pattern exists at the tube side of a hollow fiber <sup>7-9</sup>.

$$Sh = 1.62 \left( Re Sc \frac{d_h}{L} \right)^{0.33} \quad (8)$$

The membrane resistance is calculated with Eq. (1) if the feed and permeate mass transfer coefficients are known. The membrane resistance for water vapor ( $1/k_m$ ) depends on the thickness and material of the skin layer, and the structure of the porous support. First, the overall mass transfer coefficient has to be determined experimentally from the flux of water vapor through the membrane ( $J_{H_2O}$ ):

$$J_{H_2O} = k_{ov} (C_{H_2O,feed} - C_{H_2O,permeate}) \quad (9)$$

where  $C_{H_2O,feed}$  and  $C_{H_2O,permeate}$  ( $\text{mol/m}^3$ ) are the concentrations of water vapor on the feed and permeate side of the membrane. Below, the contributions of the different resistances to the overall resistance are quantified. Unraveling their magnitude allows to develop a molecular picture for the permeation of ternary gas mixtures through the skin of the asymmetric membrane.

### 3.3 Experimental

#### 3.3.1 Materials

PES/PI 80/20 hollow fibers were spun by using the dry-wet phase inversion process as described elsewhere<sup>1</sup>. Polyimide, Matrimid 5218, was purchased from Ciba-Geigy while polyethersulfone, Sumikaexcel, was kindly supplied by Sumitomo. The total polymer concentration in the solution was 35wt%. N-methyl-2-pyrrolidone (NMP, 99%, Acros) was used as the polymer solvent and NMP/H<sub>2</sub>O (80/20 wt%) mixture as the internal coagulant. Finally, polydimethylsiloxane (PDMS), (Sylgard-184, DOW Corning Corp), was used to plug any defects existing on the surface of the hollow fibers. N-hexane was the solvent for Sylgard-184.

Gases used are CO<sub>2</sub>, N<sub>2</sub>, and He, from Hoekloos b.v. (the Netherlands) and had a purity greater than 99.9%. The CO<sub>2</sub>/N<sub>2</sub> mixture (55/45%) mixture was obtained from Praxair n.v. Belgium. For the calibration of the gas chromatograph a He/N<sub>2</sub> mixture containing 2500 ppm N<sub>2</sub>, and a He/CO<sub>2</sub> mixture containing 1000 ppm CO<sub>2</sub> were used and delivered by Praxair n.v. (Belgium).

### 3.3.2 Module preparation and post treatment

About 5 PES/PI 80/20 hollow fibers, 15 cm long, were potted into 3/8" stainless steel holders by using a regular epoxy resin. In order to heal surface defects, the hollow fiber bundle was immersed for 5 minutes in a solution of 3 wt% PDMS in N-hexane and cured in an oven for 4h at 65°C. Then, the coated fibers were placed inside a stainless steel module housing, leaving the fiber mouth open at both ends.

### 3.3.3 Mixed gas/water vapor permeation set-up

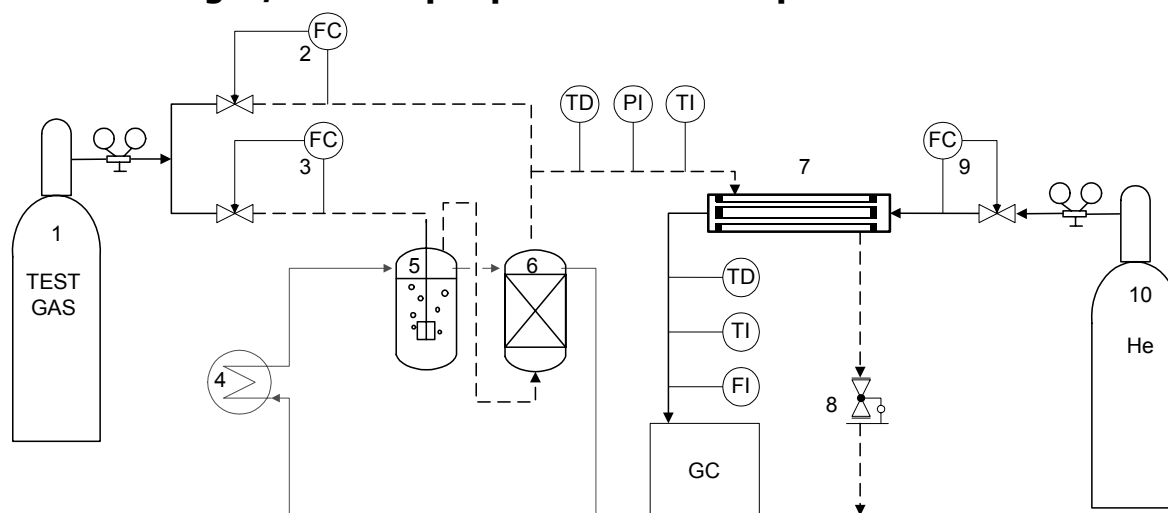


**Figure 2:** Mixed gas vapor permeation set-up with: (1) and (10) gas cylinder, (2), (3) and (9) mass flow controllers, (4) heating bath, (5) water vapor saturator, (6) demister, (7) membrane module, (8) backpressure valve.

Figure 2 presents the flow diagram of the mixed gas/water vapor permeation set-up. In this set-up, the performance of either flat sheet or hollow fiber membranes in the separation of gaseous mixtures at different water activities can be analyzed

as a function of various process parameters (pressure, temperature, feed flow rate). At first, the pure gas or the gaseous mixture stream is saturated in a column filled with water (5), while the entrained liquid droplets are separated in the demister (6). The temperature of both the saturator and the demister is controlled by means of a heating bath (4). Then, the water-saturated stream is mixed with a dry gas stream. The water vapor concentration in the feed stream is controlled by adjusting the flow rates of the two streams, using mass flow controllers (2) and (3), (Brooks 0154). The exact water vapor concentration is measured with a dew-pointing meter, (TD, -Michell Instruments Dewmet SD), the total pressure by a digital pressure indicator (PI, Druck PTX 1400), and the temperature by a thermocouple (TI). The feed stream is directed to the shell side of the hollow fiber module (7), where part of the stream permeates through the membrane. The residue stream leaves the system via a back pressure regulator, which controls the pressure in the system. On the bore side of the hollow fibers, helium is used as a sweep gas to remove the permeating components. A mass flow controller (Brooks 0154) (9) controls the flow rate of the sweep gas. The pressure of the permeate side is maintained at atmospheric level, while the following parameters are analyzed: a) temperature (TI, thermocouple), b) water vapor concentration (TD, dew-pointing meter, Michell Instruments Dewmet SD), c) flow rate (FI, soap bubble meter) and d) the gas concentration by using a gas chromatograph unit (GS, Varian 3400, column: Porapack Q). The gas composition is analyzed with a thermo conductive detector (TCD), which is calibrated with different He/N<sub>2</sub>, and He/CO<sub>2</sub> mixtures.

### 3.3.4 Determination of the transport rates

The performance of a PES/PI 80/20 hollow fiber bundle is tested in the mixed gas/water vapor permeation set-up described in section 3.2. The total molar flow of the water vapor permeating through the hollow fiber bundle ( $\phi_{n,H_2O}$ ) can be calculated by using Eq. (10)

$$\phi_{n,H_2O} = \frac{\phi_{v,tot.} p_{H_2O} Y}{RT} \quad (10)$$

where  $\phi_{n,H_2O}$  is the total mole flow of water vapor (mol/s),  $\gamma$  the activity coefficient correcting for the non ideality of the gas (-),  $T$  the temperature (K) and  $R$  the gas constant (8.314 J/(mol K)). The total permeate flow rate ( $\phi_{v,tot}$ ) is measured by the soap bubble meter, while the vapor pressure ( $p_{H_2O}$ ) of water in the permeate is calculated from the measured dew point temperature using the Antoine equation<sup>11</sup>:

$$\log(p_{H_2O}) = 9.19621 - \frac{1730.63}{T_{dew} + 233.426} \quad (11)$$

where  $p_{H_2O}$  is the water vapor pressure (kPa) and  $T_{dew}$  the dew point temperature (°C).

The permeate stream consists mainly of the sweep gas, which is helium at 1 bar. Hence the water vapor permeance is determined by using Eq. (12):

$$\frac{P}{l} = \frac{\phi_{n,H_2O} V_m}{A \Delta p_{ln}} \quad (12)$$

where  $V_m$  is equal to 22,414 cm<sup>3</sup> (molar volume of 1 mole gas at 1 atm and 0°C),  $P/l$  the thickness normalized permeability, which is given in Gas Permeation Units, GPU (1 GPU = 10<sup>-6</sup> cm<sup>3</sup> (STP) cm<sup>-2</sup>s<sup>-1</sup> cmHg<sup>-1</sup>), and  $A$  the total membrane area (cm<sup>2</sup>) which depends on the number and the geometrical characteristics of the hollow fibers inside the module.  $\Delta p_{ln}$  is an average driving force of water vapor for counter-current operation and can be calculated by using the following logarithmic formula:

$$\Delta p_{ln} = \frac{(p_f - p_{p,out}) - (p_r - p_{p,in})}{\ln\left(\frac{(p_f - p_{p,out})}{(p_r - p_{p,in})}\right)} \quad (13)$$

where  $p_f$  and  $p_r$  are the water vapor pressure entering and leaving the module respectively,  $p_{p,out}$  the water vapor pressure in the sweep gas leaving the module, and  $p_{p,in}$  the water vapor pressure of the sweep gas (He) entering the module,

which equals zero ( $p_{p,in}=0$ ). The water vapor pressure on the residue side ( $p_r$ ) is calculated by a mass balances over the module.

Similarly, the permeance value of a gas component is determined by analyzing its concentration in the permeate stream and by measuring the total permeate flow rate ( $\phi_{v,tot}$ ). Therefore, the flow rate of the permeating gas throughout the hollow fiber membrane is:

$$\phi_{v,gas} = \phi_{v,tot} \cdot x_{gas} \quad (14)$$

where  $x_{gas}$  is the fraction of gas present in the sweep gas leaving the module (-) determined by the gas chromatograph. The gas permeance value is:

$$\frac{P}{l} = \frac{\phi_{v,gas}}{A} (p_f - p_p) \quad (15)$$

where  $p_f$  is the partial pressure of gas in the feed (cmHg) and  $p_p$  the respective value in the permeate stream (cmHg). For the aforementioned calculations only steady state gas and water vapor concentrations are taken into account. This means that the measured values are constant for a time period of half an hour, at least.

### 3.3.5 Sorption experiments

Water vapor sorption experiments were performed with a sorption set-up containing a microbalance described in detail elsewhere<sup>13,14</sup>. The sample is contacted with a N<sub>2</sub> stream containing water vapor. Mixing a dry N<sub>2</sub> stream with a water vapor saturated stream generates this stream. The concentration of water vapor is adjusted by changing the flow rates of both streams. This stream is sent to a microbalance where the polymeric sample is mounted in a microbalance. The whole set-up is temperature controlled.

## 3.4 Results and Discussion

### 3.4.1 Effect of water vapor activity on gas permeance

The presence of water in the feed stream may affect the transport of the co-permeating gases CO<sub>2</sub> and N<sub>2</sub> as observed for dense polyimide films by Chern et al.<sup>15</sup> and Pye et al.<sup>16</sup>. Figure 3 shows the effect of the water vapor activity in the bulk feed on the permeance of N<sub>2</sub> and water vapor.

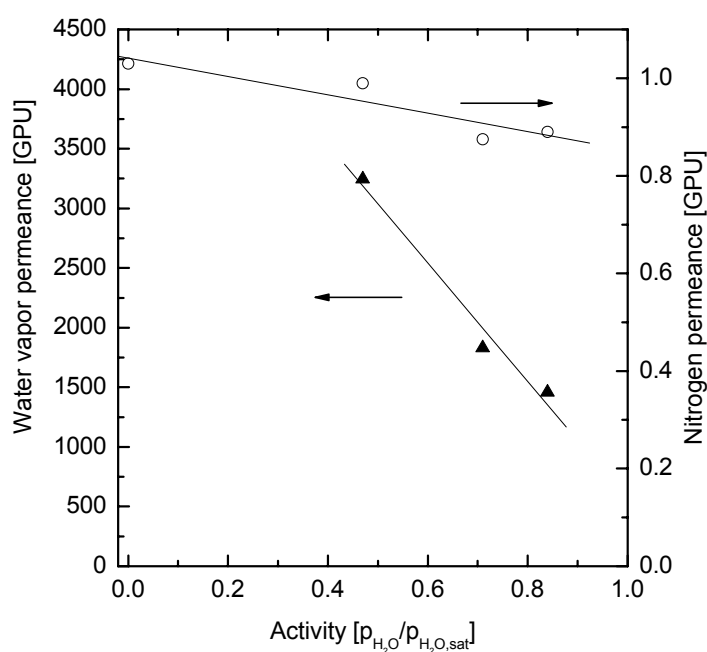


**Figure 3:** Effect of water vapor activity in the feed on N<sub>2</sub> and water vapor permeance. (feed water vapor/N<sub>2</sub>,  $P_{\text{feed}} = 5.1$  bar,  $\phi_{\text{v,feed}} = 5.71$  cm<sup>3</sup>/s,  $\phi_{\text{v,permeate}} = 2.90$  cm<sup>3</sup>/s).

The permeance of dry N<sub>2</sub> (water activity equals 0) is 1.03 GPU and corresponds well to the values obtained for the same PES/PI blend membranes by Kapataidakis et al.<sup>2</sup>. The permeance of N<sub>2</sub> decreases from 1.03 GPU at activity 0 to 0.89 GPU at activity 0.85 (13.5% reduction). The permeance value of water vapor decreases also with increasing activity of the feed gas stream, however to a larger extent

(50 %), going from 3246 GPU at activity 0.47, to 1458 GPU at activity 0.85). The same magnitude in permeance decrease can be observed for H<sub>2</sub>O/CO<sub>2</sub> and H<sub>2</sub>O/N<sub>2</sub>/CO<sub>2</sub> mixtures.

**Table 1:** Decrease in permeance (%) in various gas mixtures at water vapor activity 0.85. (The decrease of N<sub>2</sub> and CO<sub>2</sub> are compared to the dry permeance values, and decrease in H<sub>2</sub>O permeance at activity 0.85 is compared to activity 0.45).

Gas	Decrease in permeance (%) in mixtures of		
	H <sub>2</sub> O/N <sub>2</sub>	H <sub>2</sub> O/CO <sub>2</sub>	H <sub>2</sub> O/N <sub>2</sub> /CO <sub>2</sub>
N <sub>2</sub>	14	-	13
CO <sub>2</sub>	-	14	13
H <sub>2</sub> O	55	50	53

Table 1 summarizes the decrease in permeance for N<sub>2</sub>, CO<sub>2</sub> and H<sub>2</sub>O in three gas mixtures. The decrease in permeance compared to the dry permeance values at feed activity 0.85 is identical for both N<sub>2</sub> and CO<sub>2</sub> (decrease 13-14%). Consequently, the CO<sub>2</sub>/N<sub>2</sub> selectivity remains constant with an increase of water vapor activity due to the same relative permeance decrease of both components. The decrease in water vapor permeance at activity 0.85, compared to permeance values of activity 0.47, is larger (decrease 50-55%) in all the 3 gas mixtures. Vu et al.<sup>17</sup> observed similar behavior in carbon molecular sieves and polyimide membranes in the separation of CO<sub>2</sub> and CH<sub>4</sub> in the presence of toluene and n-heptane traces. The CO<sub>2</sub>/CH<sub>4</sub> selectivity remained constant but the total flux through the membranes decreased. The authors interpret this decrease as “the blocking of non-selective pores, which decrease the flux through the membrane”. However, in the case of hollow fiber membranes one may get water condensation in the cavities or pores just underneath the skin of the asymmetric membrane in

the support structure. This increases the transport resistance through the asymmetric membranes, while the selectivity remains unaffected.

Sorption experiments were performed on asymmetric hollow fibers and dense flat sheet membranes at various water vapor activities to check whether pore condensation in asymmetric membranes occurred.

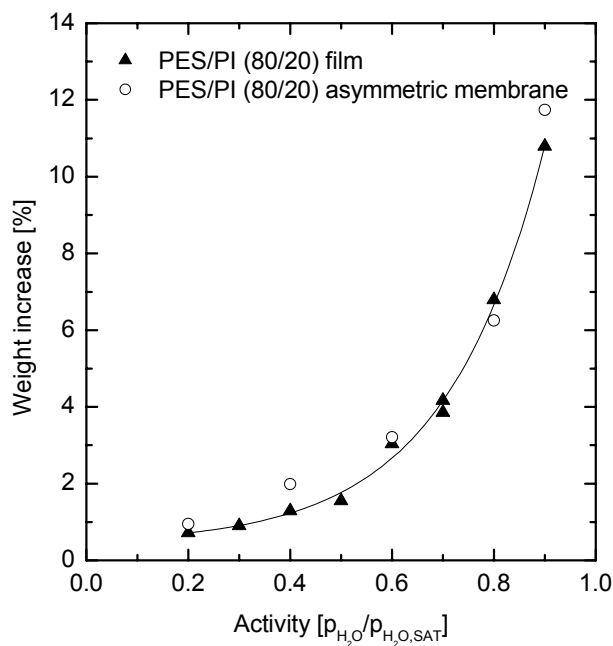


**Figure 4:** Sorption isotherms of water vapor at 25°C for a PES/PI film (▲) and an asymmetric PES/PI hollow fiber (○).

Figure 4 shows the sorption isotherm of water vapor for a dense PES/PI 80/20 film and a PES/PI 80/20 asymmetric hollow fiber. The solubility of water vapor in the PES/PI film and the PES/PI asymmetric hollow fiber increases to the same extent with an increase of water vapor activity. If pore condensation would occur than the values of the asymmetric hollow fiber are believed to show a higher increase than the dense film. Therefore we conclude that pore condensation does not occur for the hollow fibers tested.

A decrease in gas permeance in the presence of water vapor has also been observed for dense glassy polyimide films by Chern et al.<sup>15</sup> and Pye et al.<sup>16</sup>. They



observed a decrease in gas permeance in the presence of water vapor, which they explained to stem from a reduction in diffusivity of the permeating gas in presence of water vapor. Occupation of free volume sites by preferential sorption of water may be the origin of the decrease of free volume available for the transport of the inert component. Such phenomena are also supported by Molecular Dynamic simulations for  $N_2$  diffusivity in polymethylmetacrylate<sup>18</sup>. Similar phenomena might also occur in our situation where the presence of water causes a lower diffusivity of  $N_2$ ,  $CO_2$  and  $H_2O$ . The possible cause of the decrease of the water vapor permeability is most likely attributed to the same phenomena. Due to the high water vapor permeability, may an increase in the resistance of the dense skin layer have a larger impact on the water vapor permeability. It remains an experimental challenge to measure a reduced water mobility explicitly.

The decrease in permeance can not be attributed to an increase in the resistance in the porous support layer, since at high activities one would expect a lower resistance in the porous part of the hollow fiber due to the transition from Knudsen diffusion towards viscous flow<sup>7</sup>, whereas the latter causes a lower resistance.

### **3.4.2 Influence of total pressure**

In gas separation processes, the absolute value of the feed pressure frequently affects the pressure-normalized transport rates. Figure 5 shows the effect of feed pressure on the permeance values of water vapor and  $N_2$ .

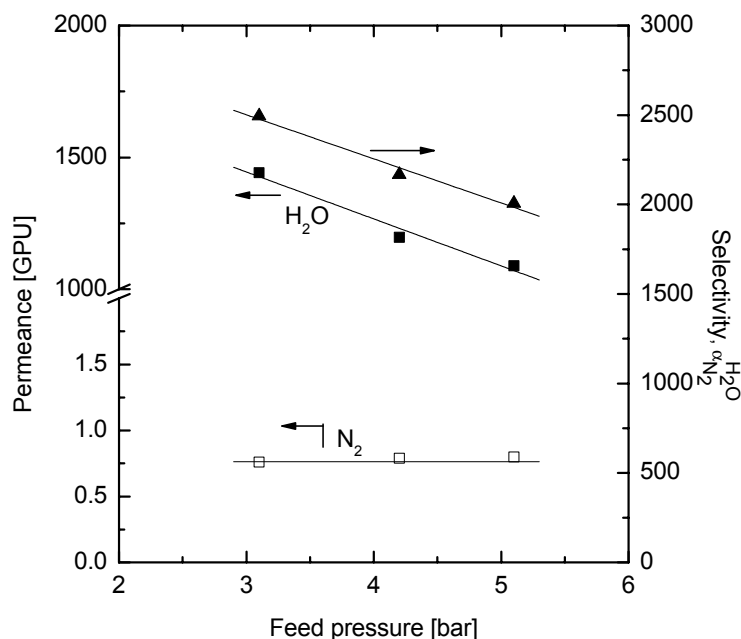


**Figure 5:** Effect of feed pressure on N<sub>2</sub> and water vapor permeance. ( $\phi_{V,\text{feed}} = 13.70 \text{ cm}^3/\text{s}$ ,  $\phi_{V,\text{permeate}} = 2.90 \text{ cm}^3/\text{s}$ ,  $T = 25 \text{ }^\circ\text{C}$ , activity 0.85).

The water vapor permeance decreases with an increase of feed pressure whereas the N<sub>2</sub> permeance remains constant. This decrease of the water vapor permeance stems from the feed side boundary layer of the membrane: an increase of total pressure results in higher resistance for the diffusion of water vapor through the boundary layer (Eq. (7)), which causes the overall water vapor permeance to decrease. Eq. (7) predicts a decrease of 60% if the resistance for permeation would be situated in the stagnant feed boundary layer only. However, the decrease in permeance is less than 60 % because the membrane and the stagnant boundary layer on the permeate side also contribute to the overall resistance, causing a lower decrease as would be expected from Eq. (7).

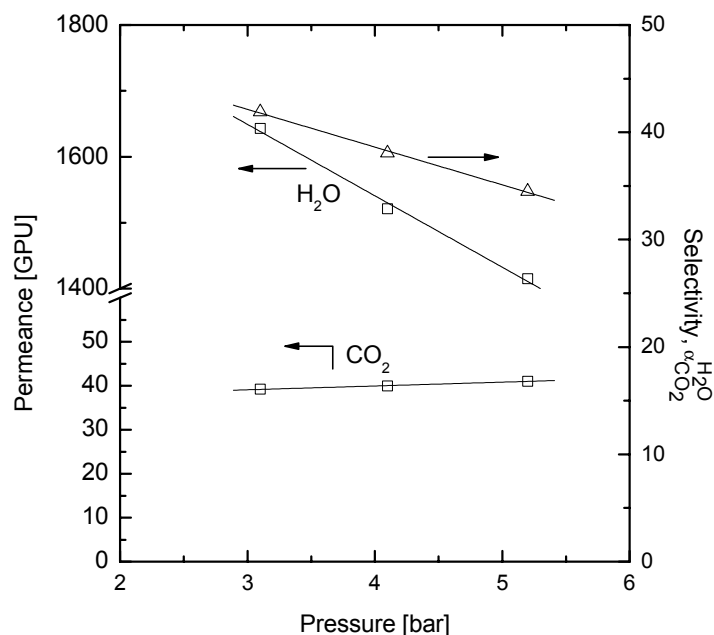


**Figure 6:** Effect of feed pressure on CO<sub>2</sub> and water vapor permeance. ( $\phi_{v,feed} = 13.70 \text{ cm}^3/\text{s}$ ,  $\phi_{v,permeate} = 2.90 \text{ cm}^3/\text{s}$ ,  $T = 25 \text{ }^\circ\text{C}$ , activity 0.85).

Figure 6 shows the effect of feed pressure on the permeance of water vapor and CO<sub>2</sub> as well as their separation factor. Again, the water vapor permeance decreases as the total pressure increases, similar to the case of N<sub>2</sub>/water vapor mixtures. However, the CO<sub>2</sub> permeance increases slightly with feed pressure; one would expect the CO<sub>2</sub> permeance to decrease due to the lower solubility of CO<sub>2</sub> in glassy polymers at higher pressures. The increase of the CO<sub>2</sub> permeance stems from plasticization, by the penetrant itself<sup>2,19-21</sup>.

In pure gas permeation experiments, such behavior can be observed for hollow fiber membranes already at much lower pressures than expected from measurements at thicker films. However, in dry gas mixtures this effect disappears, in fact a decrease with increasing feed pressure can be observed. Now, with a humidified binary CO<sub>2</sub> mixture the plasticization behavior appears again for CO<sub>2</sub>. Apparently, the transport behavior of the skin-layered membranes is complex as one changes the feed gas characteristics. Further detailed mass

transport studies are required to fully comprehend the separation and permeation properties in complex feed gas streams.

### 3.4.3 Resistance towards mass transfer

Experiments at various feed and permeate flow rates are performed in order to determine the resistance towards mass transfer for water vapor caused by the stagnant boundary layers on the feed and permeate side of the membrane.

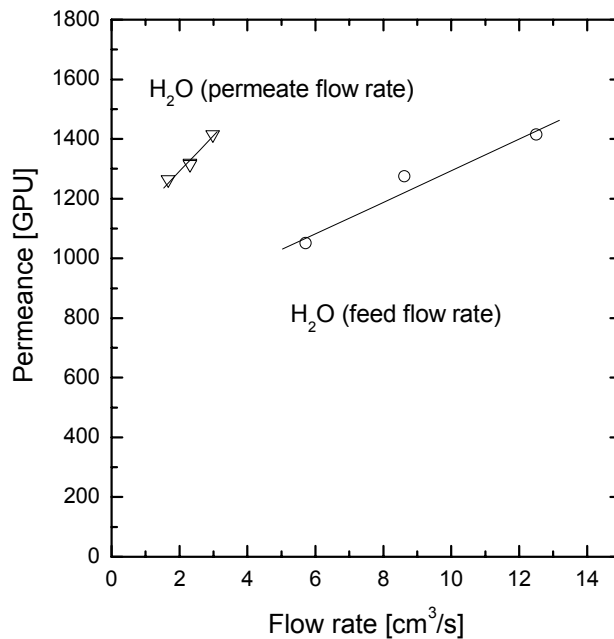


**Figure 7:** Water vapor permeance at various feed ( $\circ$ ) and permeate ( $\nabla$ ) flow rates. ( $P_{\text{feed}} = 5.1$  bar,  $T = 25$  °C, activity 0.85).

Figure 7 shows the water vapor permeance at various feed- and permeate flow rates (total pressure, temperature, water vapor activity and permeate- or feed flow rate are kept constant). The permeance of water vapor increases with flow rate due to a reduction of the laminar boundary layer thickness induced by a higher flow rate. This increases the mass transfer rate, indicating that the stagnant feed- and permeate boundary layers contribute to the overall resistance of water vapor. The  $N_2$  or  $CO_2$  permeance remains constant at various flow rates verifying that the resistance for these components is located in the membrane and

that the permeance is not affected by the amount of water vapor at the membrane surface.

A Sherwood relation is derived by plotting the overall resistance versus  $1/(v_{\text{feed}}^{0.6})$  in a so-called Wilson plot as described by Prasad and Sirkar<sup>9</sup>.

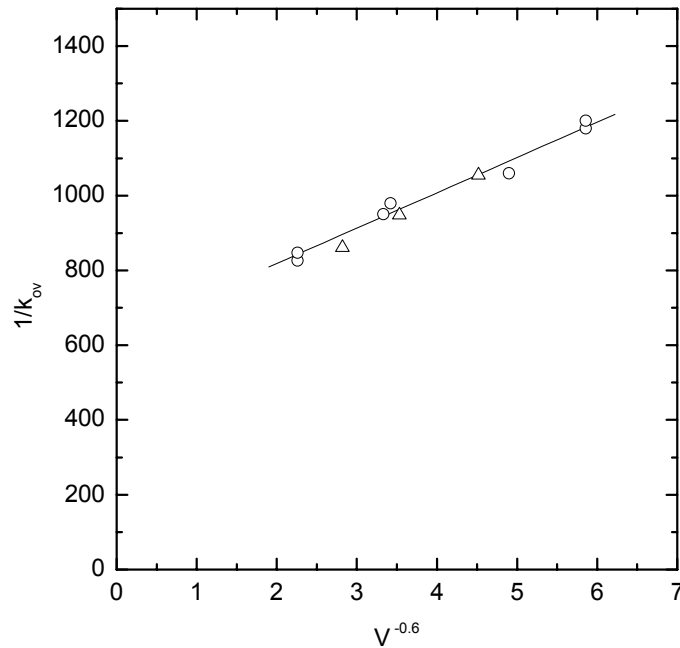


**Figure 8:** Wilson plot for  $N_2$  ( $\circ$ ) and  $CO_2$  ( $\Delta$ ).

By fitting Eq. (4), with  $\beta$  as a variable, to the experimental values we obtain the following relationship, describing the mass transfer coefficient of water vapor on the shell side of the hollow fibers:

$$Sh = 7.21(1 - \phi)Re^{0.60} Sc^{0.33} \left( \frac{d_h}{L} \right) \quad (16)$$

The value of 7.21, found with the Wilson plot, is somewhat higher than the value found by Prasad and Sirkar (Eq. (3))<sup>9</sup> and stems from a different flow distribution in the shell side of the hollow fiber module.

The L ev e equation (Eq. (8)) describes the mass transfer coefficient on the bore side of the hollow fiber. It is difficult to use a Wilson plot to derive this equation, since the permeance increases slightly over a small range of sweep gas flow rate. The theoretical L ev e equation is used to estimate this resistance. Eq. (1) relates the contributions of the asymmetric membrane to the overall resistance. Eq. (16) and Eq. (8) describe the mass transfer coefficient on the feed and permeate side of the membrane, respectively.

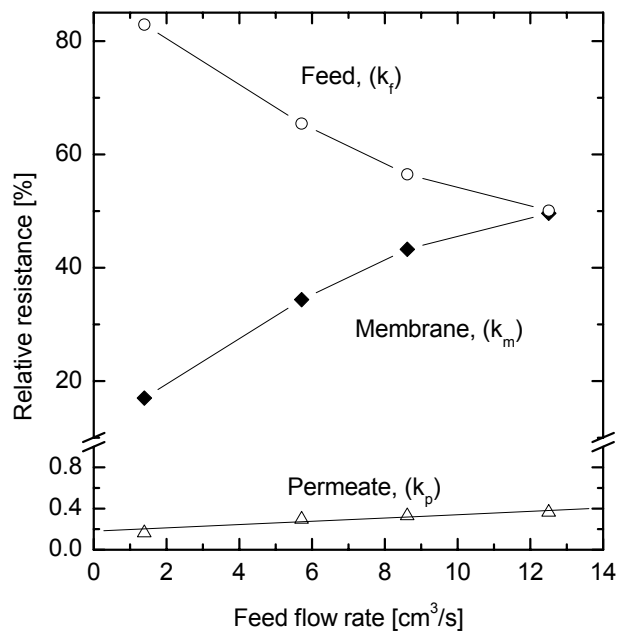


**Figure 9:** Calculated relative contributions of feed, membrane and permeate resistance to the overall resistance for water vapor transport at activity 0.85 ( $P_{\text{feed}} = 5.1 \text{ bar}$ ,  $T = 25 \text{ }^\circ\text{C}$ ).

Figure 9 shows the relative contributions of each resistance to the overall resistance at various feed flow rates. The largest resistance towards mass transfer of water vapor is located in the stagnant boundary layer on the feed side of the membrane and decreases with an increase of feed flow rate. The contributions from the stagnant boundary layer at the permeate side are small ( $\pm 0.3 \%$ ).

Using such hollow fibers in high-pressure applications would require the feed gas to remain on the shell side: the mechanical stability is larger as well as for intrinsic

safety reasons (fiber collapse is preferred over fiber bursting). Due to the high susceptibility of shell-side flow towards concentration polarization, precise packing of the fibers will be of utmost importance.

### 3.5 Conclusions

For glassy hollow fiber membranes based on a blend of PES and polyimide mixed gas permeabilities of water vapor/N<sub>2</sub>, water vapor/CO<sub>2</sub> and water vapor/N<sub>2</sub>/CO<sub>2</sub> are determined at various process conditions. Water vapor activity, total pressure, feed- and permeate flow rate are varied.

The gas and water vapor permeance decrease as the water vapor activity in the feed mixture increases. The relative decrease of the gas permeance, in the presence of water vapor, was independent of the applied gas composition. However, the relative decrease was larger for water vapor compared to N<sub>2</sub> and CO<sub>2</sub>. The decrease in permeance with an increase of water activity was not caused by condensation of water vapor in the pores of the asymmetric membrane: the sorption isotherms of both the asymmetric membrane and a dense PES/PI film showed the same solubility of water vapor. A higher solubility would be expected in the asymmetric hollow fiber if pore condensation would occur. This decrease in permeance stems possibly from a lower diffusivity through the dense skin due to the presence of water, which might lower the free volume thereby increasing the resistance for permeation.

An increase of total feed pressure causes the water vapor permeance to decrease due to a decreased diffusion coefficient of water vapor through the stagnant feed boundary layer. The N<sub>2</sub> permeance remains constant with an increase of pressure whereas the CO<sub>2</sub> permeance increases due to plasticization phenomena.

Sherwood relations are derived, which describe the variation of the overall mass transfer coefficient for water vapor at various feed- and permeate flow rates. This analysis reveals that the main resistance for water vapor transport is located in the stagnant feed boundary layer. At higher flow rates the main resistance shifts towards the membrane.

### 3.6 Acknowledgements

This research was supported through a European Community Marie Curie B-30 Fellowship, (Contract No HPMFCT-2000-0475) and a Brite Euram III Project, (Contract No. BRPR-CT 98-0804).

### 3.7 List of Symbols

A	surface area	[m <sup>2</sup> ]
a, b, c, and d	specific constants in Eq. 2	[-]
D	diffusion coefficient	[m <sup>2</sup> /s]
d <sub>h</sub>	hydraulic diameter (4*wetted area/wetted circumference)	[m]
d <sub>i</sub>	inside diameter	[m]
d <sub>o</sub>	outside diameter	[m]
k	mass transfer coefficient	[m/s]
k <sub>f</sub>	mass transfer coefficient feed	[m/s]
k <sub>m</sub>	mass transfer coefficient membrane	[m/s]
k <sub>ov</sub>	overall mass transfer coefficient feed	[m/s]
k <sub>p</sub>	mass transfer coefficient permeate	[m/s]
L	length of flow path	[m]
l	membrane thickness	[m]
M	molecular weight	[g/mol]
P	permeability	[Barrer]
p	pressure	[bar]
p <sub>f</sub>	feed pressure	[cmHg]
p <sub>feed</sub>	feed pressure	[cmHg]
p <sub>p,in</sub>	permeate pressure e entering the module	[cmHg]
p <sub>p,out</sub>	permeate pressure leaving the module	[cmHg]
p <sub>permeate</sub>	permeate pressure	[cmHg]
p <sub>r</sub>	retentate pressure	[cmHg]



R	gas constant (8.314)	[J/(molK)]
Re	Reynolds number	[-]
Sc	Schmidt number	[-]
Sh	Sherwood number	[-]
T	temperature	[K]
T <sub>dew</sub>	dew point temperature (Eq. 11)	[°C]
v	velocity	[m/s]
V <sub>m</sub>	molar volume	[m <sup>3</sup> /mol]
x	fraction	[-]
Δp <sub>ln</sub>	logarithmic pressure difference	[cmHg]
<i>Greek Symbols</i>		
β	constant in Eq. 3	[-]
φ <sub>n</sub>	molar flow	[mol/s]
φ <sub>v,gas</sub>	flow rate gas	[cm <sup>3</sup> /s]
φ <sub>v,tot</sub>	total flow rate	[cm <sup>3</sup> /s]
γ	activity coefficient	[-]
η	viscosity	[Pa s]
φ	packing fraction	[-]
ρ	density	[kg/m <sup>3</sup> ]

### 3.8 References

- (1) Kapantaidakis, G. C.; Koops, G. H. J. *Membr. Sci.* 2002, 204, 153-171.
- (2) Kapantaidakis, G. C.; Koops, G. H.; Kaldis, S. P.; Sakelaropoulos, G. P.; Wessling, M. *AIChE J.* 2003, 49, 1702-1711.
- (3) Wang, K. L.; McCray, S. H.; Newbold, D. D.; Cussler, E. L. J. *Membr. Sci.* 1992, 72, 231-244.
- (4) Swinyard, B. T.; Sagoo, P. S.; Barrie, J. A.; Ash, R. J. *Appl. Polym. Sci.* 1990, 41, 2479-2485.
- (5) Mulder, M. H. V. *Basic principles of membrane technology*, second ed.; Kluwer: Dordrecht, 1996.
- (6) Liu, L.; Chen, Y.; Li, S. G.; Deng, M. C. *Sep. Sci. Technol.* 2001, 36, 3701-3720.
- (7) Beuscher, U.; Gooding, C. H. J. *Membr. Sci.* 1999, 152, 99-116.
- (8) Gabelman, A.; Hwang, S. T. J. *Membr. Sci.* 1999, 159, 61-106.
- (9) Prasad, R.; Sirkar, K. K. *AIChE J.* 1988, 34, 177-188.

- (10) VDI Heat Atlas: Duesseldorf, 1993.
- (11) Poling, B. E.; Prausnitz, J. M.; O'Connell, J. P. The properties of gases and liquids; McGraw-Hill: New York, 2001.
- (12) Massman, W. J. Atmos. Environ. 1998, 32, 1111-1127.
- (13) Boom, J. P.; Punt, I. G. M.; Zwijnenberg, H.; de Boer, R.; Bargeman, D.; Smolders, C. A.; Strathmann, H. J. Membr. Sci. 1998, 138, 237-258.
- (14) Stamatialis, D.; Wessling, M.; Sanopoulou, M.; Strathmann, H.; Petropoulos, J. J. Membr. Sci. 1997, 125, 165-175.
- (15) Chern, R. T. K., W. J.; Sanders, E. S.; Yui, R. J. Membr. Sci. 1983, 15, 157-169.
- (16) Pye, D. G.; Hoehn, H. H.; Panar, M. J. Appl. Polym. Sci. 1976, 20, 287-301.
- (17) Vu, D. Q.; Koros, W. J.; Miller, S. J. Ind. Eng. Chem. Res. 2003, 42, 1064-1075.
- (18) Bharadwaj, R. K. Macromolecules 2002, 35, 5334-5336.
- (19) Wessling, M.; Lopez, M. L.; Strathmann, H. Sep. Purif. Technol. 2001, 24, 223-233.
- (20) Krol, J. J.; Boerrigter, M.; Koops, G. H. J. Membr. Sci. 2001, 184, 275-286.
- (21) Barsema, J. N.; Kapantaidakis, G. C.; van der Vegt, N. F. A.; Koops, G. H.; Wessling, M. J. Membr. Sci. 2003, 216, 195-205.

# Chapter 4

## Gas Permeation Properties of Poly(Ethylene Oxide) Poly(Butylene Terephthalate) Block Copolymers

### Abstract

This chapter reports the gas permeation properties of poly(ethylene oxide) (PEO) poly(butylene terephthalate) (PBT) segmented block copolymers. These block copolymers allow a structural modification by the amount of PBT and the PEO segment length, enabling a systematic study of the relationship between polymer composition and gas transport properties.

These block copolymers exhibit a high CO<sub>2</sub>/N<sub>2</sub> selectivity ( $\alpha \approx 60$  at T = 35°C) due to the high solubility of CO<sub>2</sub>. However, this selectivity is structure-dependent and is higher for block copolymers with larger amounts of PBT.

The CO<sub>2</sub>/He selectivity shows a different structure dependency since the permeation of CO<sub>2</sub> occurs primarily through the PEO phase and the He permeation occurs through both the PEO and PBT phase. Block copolymers with a better phase separation between the PEO phase and the PBT phase and more PEO therefore have a higher CO<sub>2</sub>/He selectivity. The permeability depends on the amount of PEO and the PEO segment length. The permeabilities are compared with the Maxwell model, and the difference between the experimental values and the Maxwell model are interpreted on the basis of chain flexibility of the PEO phase. The chain flexibility decreases with increasing amounts of PBT due to a less pronounced phase separation between the PEO and PBT phase.

The increase of the permeability with an increasing PEO block length, at the same ratio PEO-PBT, is caused by larger chain flexibility for longer PEO segments. The permeability depends also on the degree of crystallinity and the melting temperature of the PEO phase, which increases with the amount and the PEO segment length.

## 4.1 Introduction

Poly(ethylene oxide) (PEO) based block copolymers are interesting membrane materials for gas separation applications because they combine a high polar/(or quadrupolar)/nonpolar gas selectivity with a high permeability<sup>1</sup>. Applications can be found in the acid gas removal from natural gas<sup>2</sup>, removal of CO<sub>2</sub> from gas mixtures in fuel cells, recovery of CO<sub>2</sub> from flue gases, the drying of natural gas<sup>3</sup> and compressed air.

Various PEO containing block copolymers were studied for their gas transport properties, which differ in the type of hard segment and the amount of PEO<sup>1,4-7</sup>. These block copolymers consist of two different segments: a hard rigid semi-crystalline segment and a soft flexible amorphous PEO segment.

An example of a PEO block copolymer is Pebax<sup>®</sup>, which is a commercial available block copolymer containing hard polyamide domains and soft and poly(tetra methylene oxide) (PTMO) or poly(ethylene oxide) (PEO) segments<sup>1,5,6</sup>. Although the gas permeabilities for Pebax<sup>®</sup> containing PTMO are larger than the ones containing PEO, the polar/nonpolar gas selectivity for the latter is higher, resulting from a strong affinity of the polar ether groups for polar gases<sup>7</sup>.

The gas permeability increases with an increase of the PEO segment length as found for poly(ethylene oxide)-poly(imide) (PEO-PI) block copolymers<sup>4</sup> and polyurethane networks<sup>8</sup>.

Poly(ethylene oxide) poly(butylene terephthalate) (PEO-PBT) block copolymers allow for a structural modification through the variation of the PEO segment length and amount of PEO. This enables a systematic study of the relation between the polymeric structure and the gas transport properties. These polymers are already investigated for the use in medical applications like: protein delivery systems<sup>9</sup>, as a skin substitute<sup>10</sup>, non loading bone replacement<sup>11</sup>, or for the use of breathable clothing in textile applications<sup>12</sup>.

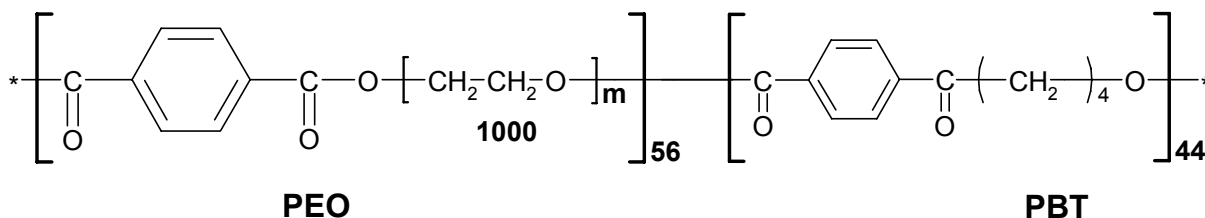


**Figure 1:** Schematic chemical structure of a PEO-PBT block copolymer carrying the abbreviation 1000PEO56PBT44.

Figure 1 shows the chemical structure of a typical PEO-PBT block copolymer. PBT forms the hard hydrophobic rigid crystalline phase: PEO forms the soft hydrophilic amorphous rubbery PEO segment. The mechanical and gas transport properties of these block copolymers can be tailored during polymer synthesis by altering the molecular weight of PEO and the amount of PBT. The following notation classifies the various block copolymers:  $m\text{PEO}_y\text{PBT}_x$ , where  $m$  is the molecular weight of the PEO segment (g/mol) and  $y$  and  $x$  are the weight percentage of PEO and PBT phase. Figure 1 shows an example of  $1000\text{PEO}_{56}\text{PBT}_{44}$ , which has a PEO segment length of 1000 g/mol and contains 44 weight % PBT. Depending on the composition of the block copolymer up to five different phases may be present: 2 amorphous (PEO and PBT), 2 crystalline (PEO and PBT), and an interphase in which amorphous PBT is mixed with amorphous PEO<sup>13</sup>.

In this work we study the gas permeation and thermal properties of PEO-PBT block copolymers. Our aim is to investigate how the permeability of various gases through PEO-PBT block copolymers is affected by the structure of the block copolymer. We want to establish a structure-property relationship for this class of block copolymers and present:

- The permeability and thermal properties of PEO-PBT block copolymers with a constant segment length but with various amounts of PBT. In particular we study the effect of the amount of PBT on the solubility and diffusivity of  $\text{CO}_2$ , and on the tortuosity and chain flexibility of the PEO phase.
- The effects of the PEO segment length on the permeability, at constant PEO-PBT ratio.
- The effect of the melting temperature and the degree of crystallinity of the PEO phase on the permeability.
- Finally, the effect of polymeric composition on the  $\text{CO}_2/\text{N}_2$  and  $\text{CO}_2/\text{He}$  selectivity.

## 4.2 Background

The PEO-PBT block copolymers are semi-crystalline polymers with the amorphous phase being responsible for most of the gas transport. In this part we describe the approaches used in literature to quantify the gas transport in semi crystalline materials and in polymers with impermeable fillers.

### 4.2.1 Permeability

Eq. (1) describes the flux of a gas through a membrane, resulting from a pressure difference over the membrane:

$$J = \frac{P}{l} \Delta p \quad (1)$$

where  $J$  is the gas flux through the membrane ( $\text{cm}^3(\text{STP})/(\text{cm}^2 \text{ s})$ ),  $P$  the permeability coefficient (Barrer,  $1 \text{ Barrer} = 1 \cdot 10^{-10} \text{ cm}^3 (\text{STP})\text{cm}/(\text{cm}^2 \text{ s cmHg})$ ),  $l$  the membrane thickness (cm), and  $\Delta p$  the pressure difference over the membrane (cmHg).

The gas permeability through a dense nonporous polymeric material is given as the product of diffusivity and solubility:

$$P = D S \quad (2)$$

where  $D$  is the diffusivity ( $\text{cm}^2/\text{s}$ ), and  $S$  the solubility coefficient ( $\text{cm}^3(\text{STP})/(\text{cm}^3 \text{ polymer cmHg})$ ) of the solute.

PEO-PBT block copolymers consist of two segments, which can be either amorphous or crystalline. The solubility in semi crystalline materials depends on the fraction of amorphous material present in the polymer <sup>14</sup>:

$$S = \alpha S_0 \quad (3)$$

where  $S$  is the solubility coefficient,  $\alpha$  the fraction of amorphous material and  $S_0$  the solubility coefficient ( $\text{cm}^3(\text{STP})/(\text{cm}^3 \text{ PEO cmHg})$ ) of a completely amorphous material. Eq. (3) implies that the solubility in the crystalline phase can be neglected.

The measured or apparent diffusivity of a solute through a semi crystalline material depends on: 1) the tortuosity in the material ( $\tau$ ), which increases with an increased number of impermeable objects, and 2) the chain mobility, which may be reduced at the surface of crystallites. An increase of the tortuosity and lower chain mobility reduce the diffusivity through the amorphous phase, following <sup>15</sup> :

$$D = \frac{D_0}{\tau\beta} \quad (4)$$

where  $D$  is the apparent diffusivity through the block copolymer,  $D_0$  the diffusivity through a completely amorphous material and  $\beta$  a chain immobilization factor, which increases as the mobility of a chain is reduced. The permeability through semi crystalline materials can be calculated by combining Eq. 2, 3 and 4, resulting in:

$$P = \frac{\alpha S_0 D_0}{\tau \beta} \quad (5)$$

PEO-PBT block copolymers comprise a highly permeable PEO phase and a less permeable PBT phase. This PBT phase can be considered as an impermeable barrier, which influences transport through the PEO phase. The Maxwell model describes the gas transport through polymers with non-interacting barriers and can also be used to describe the gas transport in block copolymers<sup>16-19</sup>:

$$P_{\text{Maxwell}} = P_0 \left( \frac{1 - \phi_b}{1 + \frac{\phi_b}{2}} \right) \quad (6)$$

where  $P_0$  is the permeability through a completely amorphous material, and  $\phi_b$  the volume fraction barrier material. The reduced permeability resulting from the presence of impermeable barriers stems from an increased path length and a reduced cross sectional area for diffusion. The Maxwell model offers an estimate of the increased diffusivity through the continuous phase due to the presence of randomly dispersed barriers. Eq. (6) also states that the presence of an impermeable object does not affect the chain mobility of the permeable phase. Merkel et al. recently have shown that this assumption may not always hold for nanoscale fumed silica particles, which disrupt the chain packing of the polymer thereby increasing its free volume<sup>17</sup>.

The Maxwell model is valid for a randomly mixed dispersion of isometric particles with a uniform interparticle gaps. The size and shape of the isometric particles is unimportant under the condition that the particles are well separated and that the particle size is in the microscopic range<sup>18</sup>. Deviations from the Maxwell model are caused by the nonrandom packing of the impermeable objects. This is not expected in block copolymers and polymer blends since these are considered to be randomly mixed.

## 4.3 Experimental section

### 4.3.1 Materials

PEO-PBT block copolymers were obtained from Isotis b.v. (the Netherlands) and were used without further purification. Chloroform ( $\text{CHCl}_3$ ) and trifluoroacetic acid (TFA) were both purchased from Merck (analytical grade) and used as solvents. For the gas permeation experiments carbon dioxide ( $\text{CO}_2$ ), nitrogen ( $\text{N}_2$ ), and helium (He) were purchased from Hoekloos b.v. (Netherlands), and methane ( $\text{CH}_4$ ), propane ( $\text{C}_3\text{H}_8$ ), and butane ( $\text{C}_4\text{H}_{10}$ ) from Praxair n.v. (Belgium). All the gases had a purity greater than 99.9 %.

### 4.3.2 Film preparation

PEO-PBT block copolymers were dissolved in  $\text{CHCl}_3$  (5 – 10 wt. %), and TFA was added ( $\pm 4$  volume % in  $\text{CHCl}_3$ ) when the weight ratio of PEO in the block copolymer was lower than 50 wt%. Thin films of around 50  $\mu\text{m}$  were prepared by solution casting on a glass plate. The cast films were dried in a  $\text{N}_2$  atmosphere at room temperature for 24 hours. The homogeneous dense films were removed from the glass plate and were further dried and stored in a vacuum oven at 30°C.

### 4.3.3 Proton-NMR

Proton-NMR measurements were performed to determine the exact weight ratio between the soft PEO and the hard PBT phase as described by Fakirov<sup>20</sup>. The PEO-PBT manufacturer (Isotis b.v.) determined the molecular weight of the PEO segment.

### 4.3.4 Differential Scanning Calometry (DSC)

The thermal properties of the PEO-PBT block copolymers were determined using a DSC7 (Perkin Elmer). Indium and cyclohexane were used for calibration. The amount of polymer used was 5 – 10 mg. The samples were dried in a vacuum oven at 30°C and a dry  $\text{N}_2$  atmosphere was used in the DSC experiments, preventing water vapor affecting the measurements. The thermal properties were determined from the second heating scan (heating rate of 10°C/min), in the temperature range from  $-80^\circ\text{C}$  to  $+250^\circ\text{C}$ . The glass transition temperature was determined from the midpoint of the heat capacity change and the melting temperature from the onset of melting.

The degree of crystallinity in both the PEO and PBT phase was calculated by using Eq. 7:

$$X_c = \frac{\Delta H_f}{w \cdot \Delta H_f^0} \quad (7)$$



where  $\Delta H_f$  is the enthalpy of formation of the crystalline PEO or PBT phase (J/g),  $\Delta H_f^0$  the enthalpy of formation of the pure crystal (for PEO 144.5 (J/g)<sup>21</sup> and for PBT 213.4 (J/g)<sup>20</sup>), and  $w$  the weight percent PEO or PBT present in the block copolymer.

#### 4.3.5 Gas permeation

Pure gas permeation properties of the PEO-PBT block copolymer were determined with CO<sub>2</sub>, N<sub>2</sub>, He, CH<sub>4</sub>, C<sub>3</sub>H<sub>8</sub>, and C<sub>4</sub>H<sub>10</sub> in the temperature range from 10 – 80 °C. The experiments were performed following the constant volume variable pressure method, described in detail elsewhere<sup>22-24</sup>. Permeabilities were determined at least 8 hours after contacting the polymeric film with the gas. Experiments performed in duplo yielded values within an experimental error range of 15 %. This falls within the systematic error for the characterization equipment used.

#### 4.3.6 Equilibrium sorption

Equilibrium sorption of CO<sub>2</sub> in various PEO-PBT block copolymers was obtained for pressures up to 50 bar at 25 °C. The equipment used and the experimental procedure of the sorption measurement are described in detail elsewhere<sup>25</sup>. The obtained sorption isotherms increased linear with pressure following Henry's law:

$$C_p = S \cdot p \quad (8)$$

where  $C_p$  is the concentration of CO<sub>2</sub> in the block copolymer (cm<sup>3</sup>(STP)/cm<sup>3</sup> polymer),  $S$  the solubility coefficient (cm<sup>3</sup>(STP)/(cm<sup>3</sup>(polymer) cmHg)), and  $p$  the pressure (cmHg).

## 4.4 Results and Discussion

### 4.4.1 Thermal properties of PEO-PBT block copolymers

The thermal properties as a function of the chemical structure of the PEO-PBT block copolymer composition were investigated with DSC. Table 1 shows the glass transition temperature ( $T_g$ ), melting temperature ( $T_m$ ) and the degree of crystallinity ( $X_c$ ) of both the PEO and PBT phase of the investigated PEO-PBT block copolymers. The amorphous PBT phases are too small to detect a glass transition temperature.

**Table 1:** Thermal properties of the PEO-PBT block copolymers used in this study (- = not detected).

	Polymer		PEO Phase			PBT Phase	
	Mw PEO	Ratio PEO-PBT	$T_g$ (°C)	$T_m$ (°C)	$X_c$ (-)	$T_m$ (°C)	$X_c$ (-)
Table 1a	1000	40-60	-46.2	-	-	190.8	0.23
		52-48	-47.5	-10.5	0.05	163.0	0.12
		56-44	-48.0	-10.2	0.06	150.6	0.15
		64-36	-49.4	-4.0	0.14	-	-
		75-25	-49.5	7.5	0.20	-	-
Table 1b	1000		-47.5	-10.5	0.05	163.0	0.12
	2000	52-48	-52.5	6.9	0.20	182.7	0.15
	3000		-53.0	19.5	0.26	193.5	0.15
Table 1c	1000		-49.5	7.5	0.20	-	-
	2000	75-25	-	29.6	0.23	-	-
	4000		-	38.8	0.42	-	-
Table 1d	600	40-60	-30.7	-	-	178.8	0.18
	1000		-46.2	-	-	190.8	0.23

Up to five different phases can be expected in PEO-PBT block copolymers: two crystalline and two amorphous phases (both PEO and PBT) and an interphase, where amorphous PBT is mixed with amorphous PEO<sup>13</sup>. The latter is demonstrated

in the glass transition temperature of the PEO phase, which increases with increasing amounts of PBT mixed with amorphous PEO<sup>20</sup>. This amorphous PBT present in the amorphous PEO reduces its chain mobility, thereby increasing the glass transition temperature of the PEO phase with increasing amounts of PBT.

An increase of the amount of PEO, at the same PEO segment length (Table 1a), has the following effects on the thermal properties:

- The glass transition temperature of the PEO phase decreases, due to less amorphous PBT present in the amorphous PEO phase.
- The melting temperature and the degree of crystallinity of the PEO phase increase due to larger and more regular PEO crystals.
- The melting temperature and the degree of crystallinity of the PBT phase show an opposite behavior due to less PBT present in the block copolymer.

Increasing the PEO segment length, at constant ratio PEO-PBT, affects the thermal properties in the following way:

- The glass transition temperature of the PEO phase decreases, due to a better phase separation between the PEO and PBT phase<sup>26</sup> (Table 1b and Table 1d).
- The melting temperature and the degree of crystallinity of the PEO phase increase due to larger and more regular PEO crystals (Table 1b and Table 1c).
- The melting temperature and the degree of crystallinity of the PBT phase increase due to longer PBT segments (Table 1b).

These properties must be kept in mind, when the gas transport properties are discussed in the following paragraphs. However, we point out that most of the permeation experiments are carried out well above the melting temperature of the PEO-crystals.

#### **4.4.2 Selectivity**

Figure 2 shows the gas pair selectivities of various gases compared to N<sub>2</sub> for 1000PEO56PBT44 as a function of the kinetic diameter<sup>27</sup>. The selectivity decreases with an increasing kinetic diameter going from He to N<sub>2</sub>. This decrease stems from a lower permeability caused by a reduced diffusivity for larger molecules<sup>28</sup>. An exception is CO<sub>2</sub>, which shows a significant higher selectivity, caused by a higher solubility for CO<sub>2</sub> due to the strong affinity of the polar ether for polar (or quadrupolar) gases<sup>7</sup>. The selectivity increases for molecules larger than N<sub>2</sub> due to a higher solubility for larger gas molecules<sup>29</sup>.

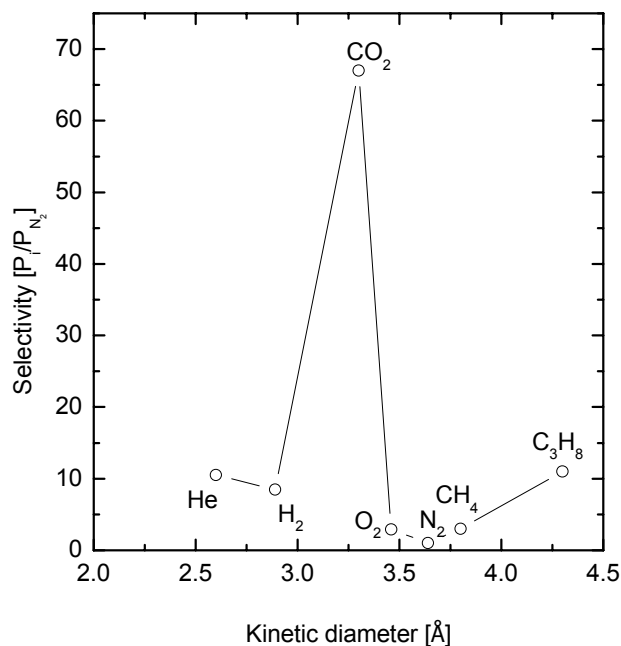


**Figure 2:** Selectivity for various gases compared to nitrogen at  $T=20^\circ\text{C}$  for 1000PEO56PBT44 as a function of the kinetic gas diameter.

The selectivity depicted in Figure 2 is only valid for 1000PEO56PBT44 and depends on the polymeric structure, as we will show later.

#### 4.4.3 Effect of the amount of PBT on permeation properties

This paragraph focuses on the effect of the amount of PBT on the gas permeation properties of PEO-PBT block copolymers with a PEO segment length of 1000 g/mol. The solubility, diffusivity, and permeability of polar components are significantly affected by the amount of PEO present in the block copolymer<sup>30</sup>.

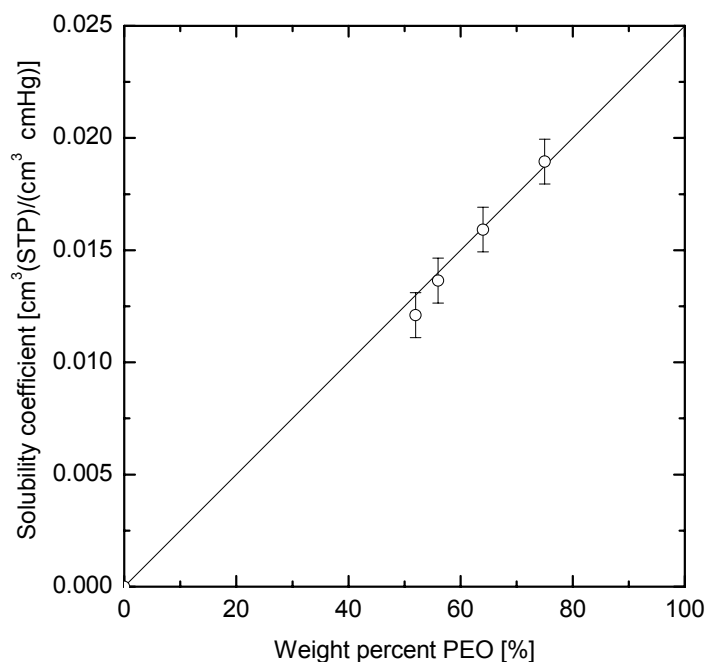


**Figure 3:** Solubility coefficient of CO<sub>2</sub> at 25°C for various PEO-PBT block copolymers with a PEO segment of 1000 g/mol. (Open symbols represent experimental values, the line represents results calculated with Eq. 3 with  $S_0 = 0.025 \text{ cm}^3(\text{STP})/(\text{cm}^3 \text{ PEO cmHg})$ ).

Figure 3 shows the solubility of CO<sub>2</sub> in PEO-PBT block copolymers with a PEO segment length of 1000 g/mol. The error in the solubility coefficient is determined by the least square fit of the solubility coefficient when the concentration of CO<sub>2</sub> is plotted versus the pressure (Eq. 3). (All measured sorption isotherms, concentration as a function of pressure, are linear over the pressure range measured). The slope of the line in Figure 3 represents the weight % normalized solubility coefficient of CO<sub>2</sub> in complete amorphous PEO with a molecular weight of 1000 g/mol. This line is calculated by using Eq. (3) with  $S_0=0.025 \text{ cm}^3(\text{STP})/(\text{cm}^3 \text{ PEO cmHg})$ . Zero gas sorption at zero weight % PEO indicates that the solubility of CO<sub>2</sub> in amorphous PBT phase is negligible compared to the solubility in the amorphous PEO phase. The linear increase of the solubility of CO<sub>2</sub> with the amount of PEO also indicates also that the solubility of CO<sub>2</sub> in the amorphous PEO phase is not affected by the amount or crystallinity of the PBT phase. Such a behavior is also observed for the solubility of various gases in semi-crystalline poly(ethylene)<sup>14</sup>.

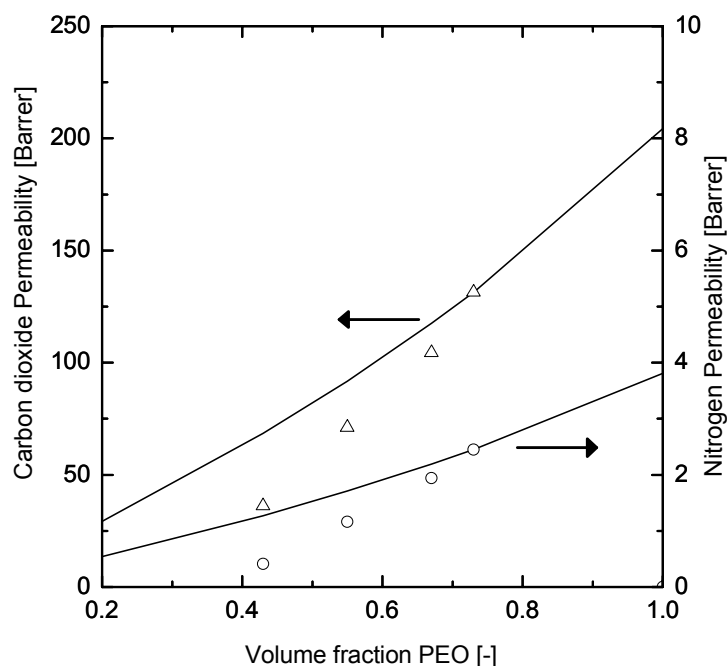


**Figure 4:** CO<sub>2</sub> ( $\Delta$ ) and N<sub>2</sub> ( $\circ$ ) permeability at 25°C for PEO-PBT block copolymers with a PEO segment length of 1000 g/mol, but with various amounts of PEO. (Symbols represent experimental values; lines are calculated with the Maxwell model Eq. 6, with  $P_0 = 204.3$  Barrer for CO<sub>2</sub> and 3.8 Barrer for N<sub>2</sub>)

Figure 4 shows the CO<sub>2</sub> and N<sub>2</sub> permeabilities at 25°C for various PEO-PBT block copolymers with a PEO segment of 1000 g/mol, but with various amounts of PBT as a function of the volume fraction amorphous PEO. The densities of the amorphous PEO, PBT and crystalline PBT<sup>13</sup> are used to convert the weight % to volume fraction. The permeability of both N<sub>2</sub> and CO<sub>2</sub> increase with the amount of PEO present in the block copolymer. The Maxwell model (Eq. 6) is used to fit the experimental values of the CO<sub>2</sub> and N<sub>2</sub> permeability of 1000PEO75PBT25, by adjusting  $P_0$  and the result of this fit is presented as lines in Figure 4. The PBT phase is considered to be impermeable for CO<sub>2</sub> and N<sub>2</sub> since the solubility of CO<sub>2</sub> mainly occurs in the amorphous PEO phase (Figure 3). 1000PEO75PBT25 is used for fitting the Maxwell model since this polymer represents the characteristics of pure PEO (highest amount of PEO). The results of the Maxwell model, with  $P_{0,N_2} = 3.8$  Barrer and  $P_{0,CO_2} = 225.4$  Barrer, are drawn as lines in Figure 4. The Maxwell model deviates, at lower amounts of PEO considerably, from the experimental values.

Deviations between the experimental values and the Maxwell model arise when model assumptions are not completely applicable to the experimental values. The

Maxwell model assumes rigid impermeable objects embedded in a permeable PEO phase. However, intermixing of amorphous PBT in the amorphous PEO phase reduces the chain mobility of the PEO phase<sup>13</sup>. This is reflected in the glass transition temperature of the PEO phase, which increases with an increase of PBT content (Table 1a). It is also observed for Pebax<sup>6</sup> and polyurethane<sup>8</sup> membranes that imperfect phase separation hampers diffusion and lowers the permeability. This occurs probably also in PEO-PBT block copolymers where a higher amount of PEO results in a PEO phase with less intermixed amorphous PBT mixed in this phase. The phase separation between the PEO and PBT phase deteriorates at higher amounts of PBT causing lower chain mobility and larger deviations between the experimental values and the Maxwell model.

The Maxwell model predicts permeabilities when the mobility of the amorphous phase is not reduced by the presence of impermeable barriers. According to Eq. 5, using  $\beta = 1$ , this gives:

$$P_{\text{max well}} = \frac{\alpha S_0 D_0}{\tau} \quad (9)$$

However, the chain mobility of the PEO phase is affected by the presence of an impermeable phase. The chain immobilization factor ( $\beta$ ) is estimated by comparing the measured permeability (Eq. 5) with the permeability calculated with the Maxwell permeability (Eq. 9) in the following way:

$$\frac{P_{\text{Maxwell}}}{P_{\text{measured}}} = \frac{\left( \frac{\alpha S_0 D_0}{\tau} \right)}{\left( \frac{\alpha S_0 D_0}{\tau \beta} \right)} = \beta \quad (10)$$

The diffusivity through complete amorphous PEO ( $D_0$ ) is calculated with Eq. 2 since the permeability and solubility of CO<sub>2</sub> in completely amorphous PEO are known ( $P_0 = 204.3$  (Barrer),  $S_0 = 0.025$  (cm<sup>3</sup>(STP))/(cm<sup>3</sup> PEO cmHg)). This gives  $D_0 = 8.2 \cdot 10^{-7}$  (cm<sup>2</sup>/s).

**Table 2:** Chain immobilization factor ( $\beta$ ) and tortuosity ( $\tau$ ) calculated for various PEO-PBT block copolymers with various amounts of PEO, but with a constant PEO segment length (1000 g/mol).

Mw PEO [g/mol]	Ratio PEO-PBT (-)	$\beta$ (-)	$\tau$ (-)
1000	40-60	1.89	1.29
	52-48	1.29	1.23
	64-36	1.13	1.17
	75-25	1.00	1.14

Table 2 shows the chain immobilization factor ( $\beta$ ), calculated with Eq. (10), and the tortuosity ( $\tau$ ) calculated using Eq. (4). The chain immobilization factor and the tortuosity increase at higher PBT contents, resulting in lower permeability at higher PBT contents as calculated with the Maxwell equation.



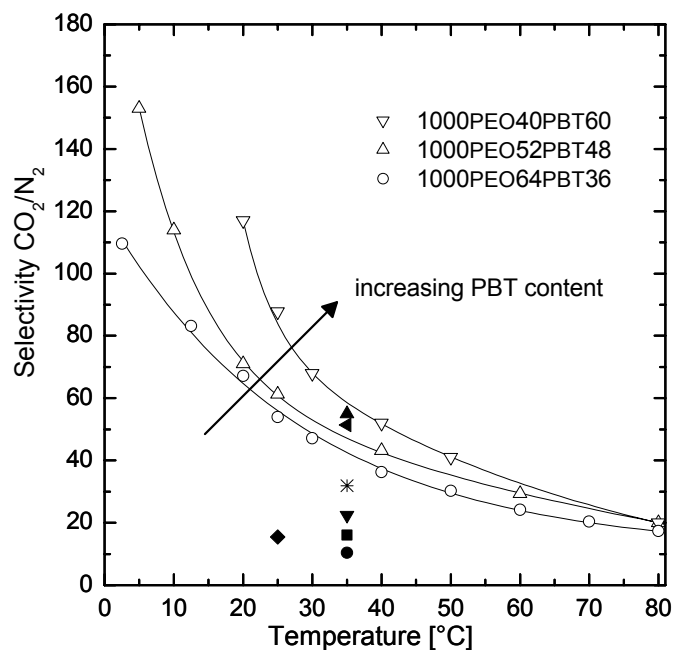


**Figure 5:**  $\text{CO}_2/\text{N}_2$  selectivity for various PEO-PBT block copolymers in the temperature range 0 - 80°C ( $\circ$  1000PEO64PBT36,  $\Delta$  1000PEO52PBT48, and  $\nabla$  1000PEO40PBT60). The closed symbols represent literature values: ( $\bullet$  = PDMS<sup>31</sup>,  $\blacksquare$  = poly(phenylene oxide)<sup>31</sup>,  $\blacktriangledown$  = Poly(sulfone) and poly(carbonate)<sup>31</sup>,  $*$  = Cellulose Acetate<sup>31</sup>,  $\blacklozenge$  = natural rubber<sup>31</sup>,  $\blacktriangleleft$  PEO-polyamide block copolymer (Pebax<sup>®</sup>1074<sup>1</sup>),  $\blacktriangle$  = PEO-PI block copolymer<sup>4</sup>).

Figure 5 shows the  $\text{CO}_2/\text{N}_2$  selectivity for various PEO-PBT block copolymers in the temperature range 0- 80°C and literature values for various polymers (closed symbols). Figure 5 also shows the  $\text{CO}_2/\text{N}_2$  selectivity for various polymers including PEO block copolymers with different types of hard segment. The PEO containing block copolymers shows a significantly higher selectivity, stemming from the high affinity of the PEO segment for polar components<sup>1</sup>. The  $\text{CO}_2/\text{N}_2$  selectivity at 35°C is comparable to other PEO containing block copolymers, indicating that the hard segment contributes to a lesser extent to the selective transport.

The  $\text{CO}_2/\text{N}_2$  selectivity increases with an increase of the amount of PBT, whereas the  $\text{CO}_2$  solubility is not affected by the amount of PBT. This increase in selectivity is most likely caused by differences in diffusion rates of  $\text{CO}_2$  and  $\text{N}_2$  through the various polymers. An increase in the amount of PBT causes a less pronounced phase separation between the PEO and PBT phase. This probably affects the diffusion rate of the larger  $\text{N}_2$  molecule more than  $\text{CO}_2$ , thereby increasing the selectivity for  $\text{CO}_2/\text{N}_2$  at higher amounts of PBT.

The CO<sub>2</sub>/He selectivity shows a different dependence on the polymeric structure.

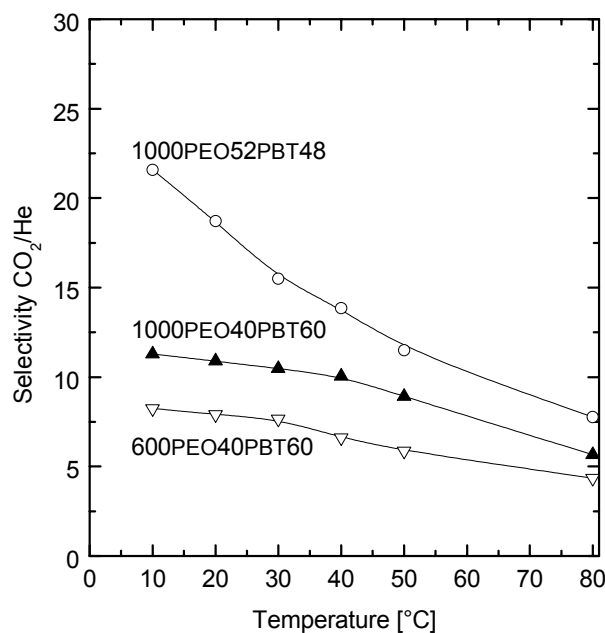


**Figure 6:** CO<sub>2</sub>/He selectivity for 600PEO40PBT60 (▽), 1000PEO40PBT60 (▲) and 1000PEO52PBT48 (○) in the temperature range 10 – 80 °C.

Figure 6 shows the CO<sub>2</sub>/He selectivity for 3 different PEO-PBT block copolymers as a function of temperature. This figure shows an opposite behavior of the selectivity compared to the CO<sub>2</sub>/N<sub>2</sub> selectivity. The block copolymer with the highest amount of PBT (600PEO40PBT60) has the lowest selectivity, whereas an increase of the amount of PEO and the PEO segment length, results in a higher selectivity. An increase of the PEO segment length results in a better phase separation between the PEO and PBT phase (compare 600PEO40PBT60 with 1000PEO40PBT60), which results in a lower glass transition temperature for the amorphous PEO phase (Table 1d). This effect results in higher CO<sub>2</sub> permeability, due to an increased flexibility of the PEO phase which favors the diffusivity of CO<sub>2</sub>. The dependence of the CO<sub>2</sub>/He selectivity on the polymeric structure can be explained by the preferential permeation of CO<sub>2</sub> through the PEO, whereas He diffuses through both the PEO and PBT phase. Therefore results an increase in the amount or PEO segment length in a higher CO<sub>2</sub>/He selectivity.

#### 4.4.4 Effect of the PEO segment length on permeation properties

Not only the amount of PEO, but also the PEO segment length influences the thermal and transport properties of PEO-PBT block copolymers.

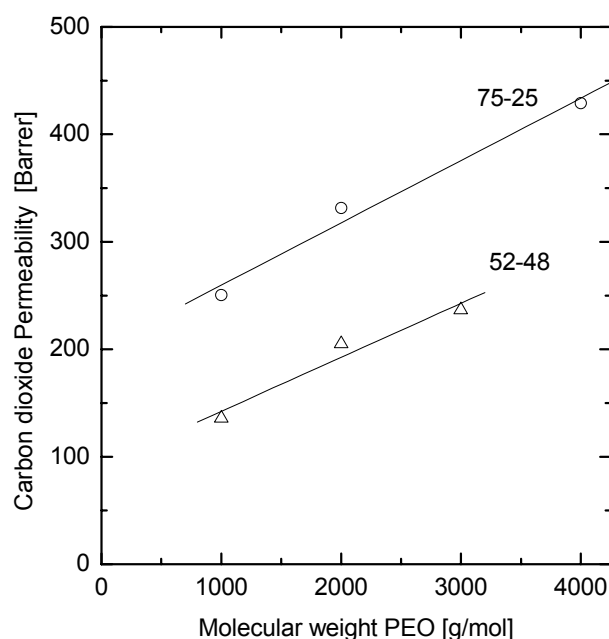


**Figure 7:** CO<sub>2</sub> permeability at 50°C of various PEO-PBT block copolymers with PEO-PBT ratio 52-48 ( $\Delta$ ) and 75-25 ( $\circ$ ) with various PEO segment lengths (lines are drawn to guide the eye).

Figure 7 shows the CO<sub>2</sub> permeability at 50°C for the block copolymers in Table 1b and Table 1c. The PEO segment length does not significantly affect the CO<sub>2</sub>/N<sub>2</sub> selectivity of these polymers. The permeability in Figure 7 is depicted at 50°C, since the PEO phase of all the PEO-PBT block copolymers is amorphous at this temperature. The CO<sub>2</sub> permeability increases with an increase of the PEO segment length, which can be caused by an increased diffusivity, or an increased solubility of CO<sub>2</sub> in the PEO phase.

**Table 3:** Permeability, solubility, diffusivity, and chain immobilization factor ( $\beta$ ) for CO<sub>2</sub> at 25°C for PEO-PBT block copolymers with a ratio PEO-PBT 52-48 and various molecular weights of PEO.

Mw PEO (g/mol)	Ratio PEO PBT (-)	Permeability (Barrer)	Solubility (cm <sup>3</sup> (STP)/(cm <sup>3</sup> cmHg))	Diffusivity (cm <sup>2</sup> /s)	$\beta$ (-)
1000		71.0	0.012 ± 0.001	5.4E-07	1.23
2000	52-48	115.8	0.014 ± 0.001	8.3E-07	0.80
3000		146.0	0.016 ± 0.001	9.1E-07	0.72

Table 3 shows the permeability, solubility, diffusivity, and chain flexibility for CO<sub>2</sub> for a series of PEO-PBT block copolymers with a weight ratio PEO-PBT 52-48 but with various PEO segment lengths. The permeability and solubility of 3000PEO52PBT48 are determined by extrapolation from temperatures > 40°C, since the PEO part is completely amorphous at these temperatures. The chain immobilization factor and tortuosity factor of 1000PEO52PBT48 (Table 2) are used for the calculations of the chain immobilization factor  $\beta$  (Eq. 5) for 2000PEO52PBT48 and 3000PEO52PBT48. Since these block copolymers contain the same amount of PBT (48 wt.%), it is assumed that the tortuosity for diffusion through the materials is equal. The solubility of CO<sub>2</sub> increases with an increase of PEO segment length. This behavior is also observed for the solubility of water in these materials<sup>32,33</sup>. This increased solubility is caused by an increased configurational freedom of the PEO segment, which favors the solubility of water<sup>34</sup>. The diffusivity of CO<sub>2</sub> through these block copolymers also increases with an increase of PEO segment length. This increase is a result of an increased mobility of the PEO segment at longer PEO segments as calculated with Eq. 5. Both effects, increase in solubility and diffusivity, cause the permeability to increase with an increase of PEO segment length.

#### 4.4.5 Effect of temperature on permeation properties

Since the PEO-PBT block copolymers show a rich spectrum of thermal transitions, which may influence the permeation properties the CO<sub>2</sub> permeability is measured in the temperature range 5 – 80 °C for 2000PEO52PBT48, 3000PEO52PBT48, and 4000PEO75PBT25. The results are shown in Figure 8. These block copolymers differ in melting temperature and degree of crystallinity of the PEO phase as can be seen from Table 1. The permeability is measured with increasing temperature, starting from 5 till 80°C and the permeance values are constant for at least 8 hours. The CO<sub>2</sub> permeability increases significantly as the PEO crystals start to melt. The CO<sub>2</sub> permeability below the melting temperature of PEO depends on the amount and the degree of crystallinity of the PEO phase.

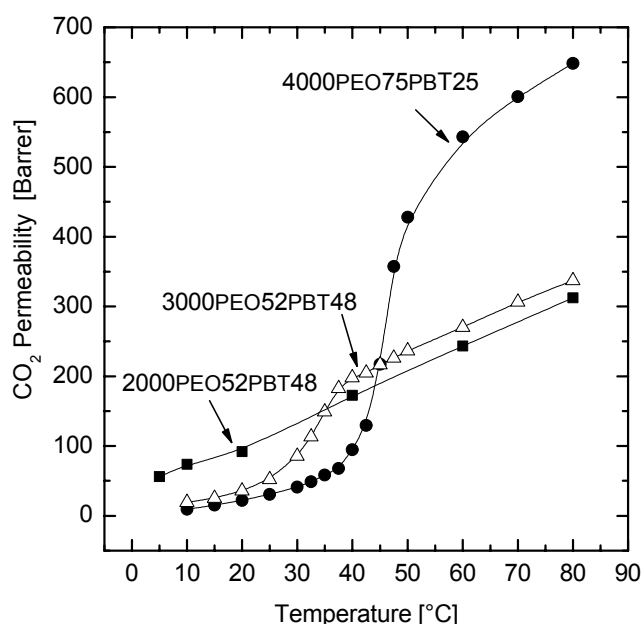


**Figure 8:** CO<sub>2</sub> permeability for 2000PEO52PBT48 (■), 3000PEO52PBT48 (Δ), and 4000PEO75PBT25 (●) in the temperature range 5 – 80 °C.

The permeability at 20°C decreases in the following order  $P_{2000\text{PEO}52\text{PBT}48} > P_{3000\text{PEO}52\text{PBT}48} > P_{4000\text{PEO}75\text{PBT}25}$ . The permeability of 2000PEO52PBT48 at 20°C is higher due to the larger amount of amorphous PEO present at 20°C. The increase in permeance depends on the polymeric structure, which determines the melting temperature and the degree of crystallinity of the PEO phase. 3000PEO52PBT48 and 4000PEO75PBT25 show a gradual increase in permeability when the PEO crystals start to melt. The melting temperature of the PEO phase observed with gas permeation experiments (Figure 8) does not correspond to the melting temperature as determined with DSC (Table 1) (e.g. 3000PEO52PBT48:  $T_{m,\text{DSC}} =$

19.5°C,  $T_{m, \text{gas permeation}} = 35^\circ\text{C}$ ). Deviations between both experiments are caused by (a) different heating rates of the sample, and (b) different thermal history. The heating rate in the gas permeation experiments is much lower ( $< 1^\circ\text{C}/\text{hour}$ ), compared to the heating rate in DSC experiments ( $10^\circ\text{C}/\text{min}$ ). The low heating rate of the gas permeation experiments cause the PEO crystals to melt and recrystallize and thereby increasing the melting temperature of PEO. The thermal history of the samples is also very different. The samples analyzed by DSC have been cooled down to  $T = -80^\circ\text{C}$ . The films used for permeation are prepared at room temperature: any further cooling may stem from solvent evaporation, however the cooling is by no means comparable.

2000PEO52PBT48 does not show a sharp increase in permeability, because the PEO phase is still amorphous due to an insufficient temperature gradient to induce crystallization. Similar phenomena are also observed by Hirayama et. al.<sup>35</sup> who observed hysteresis in the increase in permeance between heating and cooling runs.

### 4.5 Conclusions

The gas transport properties of PEO-PBT block copolymers depend on their structure in the following way:

The transport of  $\text{CO}_2$  and  $\text{N}_2$  occurs mainly through the amorphous PEO phase, whereas He permeates through both the amorphous PBT and PEO phase. This causes the  $\text{CO}_2/\text{He}$  selectivity to decrease with increasing amounts of PBT. The increase of the amount of PBT at constant PEO segment length causes a less pronounced phase separation between the PEO and PBT phase. This lowers the permeability through the amorphous PEO phase more than when the PBT phase is considered as an impermeable barrier, using the Maxwell model, obstructing transport. The  $\text{CO}_2/\text{N}_2$  selectivity increases with the amount of PBT, probably due to a different dependence of the diffusivity on the amount of PBT.

An increase of the PEO segment length, at the same ratio PEO-PBT, elevates the chain flexibility of the PEO phase thereby causing a higher permeance.

The degree of crystallinity and the melting temperature of the amorphous PEO phase, both determined by the amount and PEO segment length, affect the permeance. The melting temperature of the crystalline PEO phase increases with a higher amounts of PEO and larger PEO segments.

### 4.6 Acknowledgements

The European Union is kindly acknowledged for supporting this project: Brite Euram III, Contract no. BRPR-CT 98-0804

## 4.7 References

- (1) Bondar, V. I.; Freeman, B. D.; Pinnau, I. *J. Polym. Sci., Polym. Phys. Ed.* **2000**, *38*, 2051-2062.
- (2) Bhide, B. D.; Voskericyan, A.; Stern, S. A. *J. Membr. Sci.* **1998**, *140*, 27-49.
- (3) Metz, S. J.; Potreck, J.; Mulder, M. H. V.; Wessling, M. *Desalination* **2002**, *148*, 303-307.
- (4) Okamoto, K.; Fujii, M.; Okamoto, S.; Suzuki, H.; Tanaka, K.; Kita, H. *Macromolecules* **1995**, *28*, 6950-6956.
- (5) Kim, J. H.; Ha, S. Y.; Lee, Y. M. *J. Membr. Sci.* **2001**, *190*, 179-193.
- (6) Barbi, V.; Funari, S. S.; Gehrke, R.; Scharnagl, N.; Stribeck, N. *Macromolecules* **2003**, *36*, 749-758.
- (7) Bondar, V. I.; Freeman, B. D.; Pinnau, I. *J. Polym. Sci., Polym. Phys. Ed.* **1999**, *37*, 2463-2475.
- (8) Damain, C. E., E.; Cuney, S.; Pascault, J. P. *J. Appl. Polym. Sci.* **1997**, *65*, 2579-2587.
- (9) Bezemer, J. M. R., R. Grijpma, D.W. Dijkstra, P.J. van Blitterswijk, C.A., Feijen, J. *J. Controlled Release* **2000**, *67*, 249-260.
- (10) Beumer, G. J.; Vanblitterswijk, C. A.; Ponec, M. *J. Biomed. Mater. Res.* **1994**, *28*, 545-552.
- (11) Radder, A. M.; Leenders, H.; vanBlitterswijk, C. A. *J. Biomed. Mater. Res.* **1996**, *30*, 341-351.
- (12) Gebben, B. *J. Membr. Sci.* **1996**, *113*, 323-329.
- (13) Fakirov, S.; Apostolov, A. A.; Boeseke, P.; Zachmann, H. G. *J. Macromol. Sci., Phys.* **1990**, *B29*, 379-395.
- (14) Michaels, A. S.; Bixler, H. J. *J. Polym. Sci.* **1961**, *50*, 393-412.
- (15) Michaels, A. S.; Bixler, H. J. *J. Polym. Sci.* **1961**, *50*, 413-439.
- (16) Barrer, R. M. *Diffusion in polymers*; Academic press: New York, 1968.
- (17) Merkel, T. C.; Freeman, B. D.; Spontak, R. J.; He, Z.; Pinnau, I.; Meakin, P.; Hill, A. J. *Science* **2002**, *296*, 519-522.
- (18) Petropoulos, J. H. *J. Polym. Sci., Polym. Phys. Ed.* **1985**, *23*, 1309-1324.
- (19) Arnold, M. E.; Naga, i. K.; Freeman, B. D.; Spontak, R. J.; Betts, D. E.; DeSimone, J. M.; Pinnau, I. *Macromolecules* **2001**, *34*, 5611-5619.
- (20) Fakirov, S.; Gogeva, T. *Makromol. Chem.* **1990**, *191*, 603-614.
- (21) Tsutsui, K.; Yoshimizu, H.; Tsujita, Y.; Kinoshita, T. *J. Appl. Polym. Sci.* **1999**, *73*, 2733-2738.
- (22) Meuleman, E. E. B.; Willemsen, J. H. A.; Mulder, M. H. V.; Strathmann, H. *J. Membr. Sci.* **2001**, *188*, 235-249.
- (23) Wessling, M.; Lopez, M. L.; Strathmann, H. *Sep. Purif. Technol.* **2001**, *24*, 223-233.

- (24) Bos, A.; Punt, I. G. M.; Wessling, M.; Strathmann, H. *J. Polym. Sci., Polym. Phys. Ed.* **1998**, *36*, 1547-1556.
- (25) Krause, B.; Sijbesma, H. J. P.; Munuklu, P.; van der Vegt, N. F. A.; Wessling, M. *Macromolecules* **2001**, *34*, 8792-8801.
- (26) Fakirov, S.; Gogeva, T. *Makromol. Chem.* **1990**, *191*, 615-624.
- (27) Breck, D. W. *Zeolite molecular sieves: structure, chemistry, and use*; Wiley: New York, 1974.
- (28) Koros, W. J.; Hellums, M. W. In *Encyclopedia of polymer science and engineering*; Kroschwitz, J. I., Ed.; Wiley: New York, 1990; pp 724-802.
- (29) Mulder, M. H. V. *Basic principles of membrane technology*, second ed.; Kluwer: Dordrecht, 1996.
- (30) Bondar, V. I. F., B. D.; Pinnau, I. *J. Polym. Sci., Polym. Phys. Ed.* **2000**, *38*, 2051-2062.
- (31) Ho, W. S. W.; Sirkar, K. K. *Membrane Handbook*; Van Nostrand Reinhold: New York, 1992.
- (32) Bezemer, J. M.; Grijpma, D. W.; Dijkstra, P. J.; van Blitterswijk, C. A.; Feijen, J. *J. Controlled Release* **1999**, *62*, 393-405.
- (33) Deschamps, A. A.; Grijpma, D. W.; Feijen, J. *Polymer* **2001**, *42*, 9335-9345.
- (34) Metz, S. J.; van der Vegt, N. F. A.; Mulder, M. H. V.; Wessling, M. *Chapter 5*.
- (35) Hirayama, Y.; Kase, Y.; Tanihara, R.; Sumiyama, Y.; Kusuki, Y.; Haraya, K. *J. Membr. Sci.* **1999**, *160*, 1.



# Chapter 5

## **Thermodynamics of Water Vapor Sorption in Poly(Ethylene Oxide) Poly(Butylene Terephthalate) Block copolymers**

### **Abstract**

This chapter studies: (a) the influence of the composition of poly(ethylene oxide) (PEO) poly(butylene terephthalate) (PBT) block copolymers on the solubility of water vapor, (b) the thermodynamic quantities governing the solubility of water vapor in these polymers. The block copolymers examined differ with respect to their hydrophilic block length (PEO segment) and the weight ratio between the hard hydrophobic PBT segment and the soft hydrophilic PEO segment.

Water sorption isotherms, determined gravimetrically, are of Flory-Huggins type exhibiting a linear relation between weight uptake and vapor activity at low activities and a sharp increase (convex shape) at higher activities. The Flory-Huggins interaction parameter decreases as the concentration of water inside the polymer increases. Its numerical value strongly depends on the polymeric structure: an increase of the soft hydrophilic PEO block length and PEO content both lead to a decrease of the interaction parameter.

Solvation Gibbs energies, entropies and enthalpies, extracted from temperature dependent sorption data, reveal that: (1) water-polymer interactions are stronger than water-water interactions in liquid water, (2) the water-polymer interactions become weaker at higher water vapor activities, (3) the water sorption entropy increases with increasing vapor activity. The last observation (3) is responsible for the convex nature of the water sorption isotherm. Moreover, this effect depends on the structure of the polymer: the larger the PEO segment length and more PEO weight fraction the higher the solvation entropy and, consequently, the solubility of water vapor in the PEO-PBT block copolymer.

## 5.1 Introduction

Solute transport in polymeric materials, in particular in polymer membranes, occurs via the so-called solution diffusion mechanism: a solute dissolves at the polymer interface, diffuses through the material and desorbs at the opposite side. A specific component can selectively be removed from a molecular mixture when its solubility and/or diffusion coefficient in the polymeric phase is higher than that of the other components. Applications based on this separation mechanism can be found in membrane based gas separation, pervaporation, and vapor permeation. Sorption models are often used to describe the solubility of solutes in polymers. At low solute concentrations Henry's law describes the concentration of a gas or vapor in a rubbery polymer: the solubility coefficient, defined as the concentration of dissolved vapor divided by the equilibrium vapor pressure, is independent of the solute concentration. Rubbery and glassy polymers demonstrate, especially at high gas or vapor concentrations, non-ideal behavior leading to increased solubility coefficients and sorption isotherms that are convex to the relative pressure axis. Such non-ideal sorption behavior can often be described with Flory-Huggins thermodynamics<sup>1-14</sup>, however, often requires researchers to invoke a concentration dependent polymer-solute interaction parameter. The concentration dependence of the interaction parameter, often obtained by fitting or through the use of empirical expressions, hampers physical chemical interpretations of the nature of the sorption process.

We study the solubility of water vapor in a series of poly(ethylene oxide) (PEO) poly(butylene terephthalate) (PBT) block copolymers. These polymers are promising candidates for membrane-based separations targeting the removal of water vapor from gas streams as they demonstrate high water vapor solubility, as we will show below. We report the influence of the polymeric structure on the solubility of water vapor. The data are analyzed using the classical Flory-Huggins sorption model commonly used for fitting sorption isotherms<sup>1-14</sup> as well as an approach based on solvation thermodynamics<sup>15,16</sup>. The latter approach reveals relations between the polymer structure and the free energy, enthalpy and entropy of interaction with water. The Flory-Huggins model cannot adequately account for such contributions, which we will show to be important to adequately interpret trends in the water vapor solubility.

## 5.2 Experimental section

### 5.2.1 Materials

The PEO-PBT block copolymers were obtained from Isotis b.v. (the Netherlands) and were used without further purification. Chloroform ( $\text{CHCl}_3$ ) and trifluoroacetic acid (TFA) were both purchased from Merck (analytical grade) and used as

solvents. Nitrogen (N<sub>2</sub>, 99,9%) was purchased from Hoekloos b.v. Demineralized water was used for the sorption experiments.

### 5.2.2 PEO-PBT block copolymers

PEO-PBT block copolymers belong to the class of multi block copolymers, and their schematic chemical structure of is depicted in Figure 1:

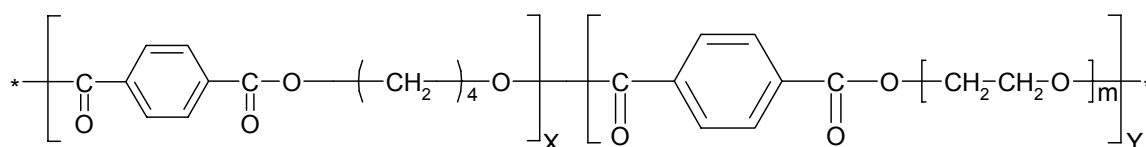


**Figure 1:** Chemical structure of the PEO-PBT block copolymer

The PEO-PBT block copolymer consists of a hard hydrophobic PBT segment (x) and a soft hydrophilic PEO segment (y) with a certain molecular weight of PEO (m). The various block copolymers can be identified with the following notation: mPEOyPBTx, where m is the molecular weight of the PEO segment, y the weight percentage PEO and x the weight percentage PBT present in the block copolymer. PEO-PBT block copolymers used in this work are: 1000PEO52PBT48, 2000PEO52PBT48, 3000PEO52PBT48, and 1000PEO64PBT36 and their thermal properties are described elsewhere<sup>17</sup>.

### 5.2.3 Film preparation

The PEO-PBT block copolymers were dissolved in CHCl<sub>3</sub> and TFA was added ( $\pm$  4 volume % in chloroform) when the weight ratio of PEO in the block copolymer was lower than 50 wt%. Thin films of around 50  $\mu$ m were prepared by solution casting on a glass plate. The cast films were dried in a N<sub>2</sub> atmosphere at room temperature for 24 hours. The homogeneous dense films were removed from the glass plate with the help of a small amount of water and were further dried and stored in a vacuum oven at 30°C for further use.

### 5.2.4 Proton NMR

Proton NMR measurements were performed in order to determine the exact weight ratio between the soft PEO and the hard PBT phase as described by Fakirov<sup>18</sup>. The manufacturer (Isotis b.v.) determined the molecular weight of the PEO segment.

### 5.2.5 Differential Scanning Calometry (DSC)

Thermal properties of the segmented PEO-PBT block copolymers were determined using a DSC7 (Perkin Elmer). Indium and cyclohexane were used for calibration. The amount of polymer used was 5 – 10 mg. The samples were dried in a vacuum

oven at 30°C and a dry N<sub>2</sub> atmosphere was used in the DSC experiments, preventing water vapor affecting the measurements. The thermal properties were determined from the second heating scan (heating rate of 10°C/min), in the temperature range from -80°C to +250°C. The glass transition temperature was determined from the midpoint of the heat capacity change and the melting temperature was determined from the onset of melting.

### 5.2.6 Sorption isotherms

An electro balance (TGA Perkin Elmer) was used to perform the gravimetric sorption experiments and is described also elsewhere<sup>19,20</sup>.

The concentration of water inside the polymeric film was determined from the mass uptake due to sorption and was calculated by using the following equation<sup>21</sup>:

$$c = \frac{(M_{\infty} - M_i) \cdot 22414}{M_w \cdot V_p} \quad (1)$$

where  $c$  is the equilibrium concentration of water inside the polymeric film [ $\text{cm}^3(\text{STP})/\text{cm}^3\text{polymer}$ ],  $M_{\infty}$  and  $M_i$  are the final and initial mass of the polymer, respectively,  $M_w$  is the molecular weight of the penetrant,  $V_p$  the volume of the polymer and 22414 the volume (units  $\text{cm}^3$ ) of 1 mol penetrant at standard temperature and pressure.

Sorption isotherms of water vapor in ethyl cellulose were determined and compared with literature data. The results of the sorption isotherm and the diffusion coefficient calculated from the sorption kinetics were in good comparison with literature data<sup>22</sup>.

## 5.3 Theory

### 5.3.1 Flory-Huggins sorption model

The Flory-Huggins theory<sup>7</sup> is frequently used to fit the sorption isotherms of vapor penetrants in polymers<sup>1-14</sup>. This theory uses a lattice model to account for the entropy effects of mixing and requires the interaction parameter  $\chi$  for the mixing enthalpy. According to this theory the excess chemical potential ( $RT \ln a_s$ ) of a penetrant dissolved in a polymer matrix of infinite molecular weight can be written as:

$$RT \ln(a_s) = RT \left[ \ln(1 - \phi_p) + \phi_p + \chi \phi_p^2 \right] \quad (2)$$

with  $a_s$  being the vapor activity,  $\phi_p$  the polymer volume fraction,  $\chi$  the parameter related to the interaction Helmholtz energy of the first neighbors,  $R$  the universal

gas constant, and  $T$  the temperature. Although  $\chi$  was originally introduced as a system constant, many experimental measurements have shown this parameter to be concentration dependent for a successful fit.

### 5.3.2 Solvation thermodynamics

To characterize the physical-chemical interactions of water with the PEO-PBT block copolymer thermodynamic solvation quantities need to be extracted from the experimental data. These quantities involve the thermodynamic work involved in the process of transferring a water molecule from the vapor phase into the PEO-PBT matrix (i.e. the solvation Gibbs energy) together with its enthalpic and entropic components. These thermodynamic data allow a simple and unambiguous (model independent) interpretation unlike the Flory-Huggings interaction parameter commonly reported in vapor sorption studies<sup>1-14</sup>.

Following Ben-Naim's convention<sup>16</sup>, the solvation Gibbs energy,  $\Delta G_s^*$ , has been defined as the Gibbs energy change for transferring a solute molecule  $S$  (water) from a *fixed* position in the vapor phase to a *fixed* position in the polymer at constant pressure  $P$ , temperature  $T$ , and composition. This quantity, which has been proven to be "the only genuine measure of the average free energy of interaction of a single (solute) molecule with its surrounding"<sup>15</sup>, is directly accessible from equilibrium sorption data according to<sup>16,23</sup>.

$$\begin{aligned}\Delta G_s^* &= -RT \ln \left( \frac{\rho_s}{\rho_s^{ig}} \right)_{eq} \\ &\equiv -RT \ln(L)\end{aligned}\quad (3)$$

In eq. (3)  $\rho_s$  and  $\rho_s^{ig}$  are the solute molar densities [ $\text{mol}/\text{cm}^3$ ] in the polymer and vapor phase, respectively.  $\rho_s$  is determined gravimetrically (cf. experimental section), whereas  $\rho_s^{ig} = p_{\text{H}_2\text{O}}/RT$ , where we assume ideal gas behavior of the vapor phase. The subscript *eq* indicates that both phases are at equilibrium. The ratio of these two equilibrium molar densities is usually referred to as the Ostwald solubility  $L$ .

$\Delta G_s^*$  is the solute free energy of interaction with the environment it is transferred into. Theoretically,  $\Delta G_s^*$  can be broken up into two parts by writing  $\Delta G_s^* = \Delta G_{\text{cavity}}^* + \Delta G_{\text{interactions}}^*$ <sup>23</sup>. The cavity term reflects the work invested to create a molecular sized cavity of suitable size and shape and is always positive. The interaction term reflects the work released due to solute polymer interactions established when introducing the solute and is always negative. When weakly

interacting gases are dissolved in a rubbery polymer (for example poly(ethylene)<sup>23</sup>), cavity formation dominates and  $\Delta G_s^*$  is positive. Stronger interacting gases such as CO<sub>2</sub> give rise to negative values of  $\Delta G_s^*$ <sup>23</sup>. The stronger polar (hydrogen bonding) interactions between water and PEO-PBT give rise to negative values of the solvation Gibbs energy presented later on in this chapter.

The solvation entropy  $\Delta S_s^*$  and solvation enthalpy  $\Delta H_s^*$  can be obtained from the temperature dependence of  $\Delta G_s^*$ . This information is obtained from the temperature dependence of the vapor sorption isotherms in which the solute concentration in the polymer is presented versus the vapor activity  $a = p_{H_2O}/p_{H_2O,sat}$ . The iso-steric heat of water sorption  $\Delta H_c$  is defined as<sup>24</sup>:

$$\left(\frac{\partial \ln a}{\partial 1/T}\right)_{P,c} = \Delta H_c / R \quad (4)$$

and is directly accessible from vapor sorption isotherms obtained at different temperatures. The relation between  $\Delta H_c$  and  $\Delta H_c^*$  is derived below. Again assuming the vapor phase to behave ideal and using the definition of the Ostwald solubility L (eq. 3) we can write:

$$a = \frac{p_{H_2O}}{p_{H_2O,sat}} = \frac{RT\rho_s}{p_{H_2O,sat}L} \quad (5)$$

Substituting the right-hand-side of eq. (5) into eq. (4) yields

$$\left(\frac{\partial \ln a}{\partial 1/T}\right)_{P,c} = \left(\frac{\partial \ln[RT\rho_s / p_{H_2O,sat}]}{\partial 1/T}\right)_{P,c} - \left(\frac{\partial \ln(L)}{\partial 1/T}\right)_{P,c} \quad (6)$$

The first term at the right-hand-side of eq. (6) can be evaluated by employing the Clausius-Clapeyron relation to the temperature dependence of the saturated water vapor pressure and equals  $(\Delta H_{vap} - RT)/R$ . Using  $\ln L = -\Delta G_s^*/RT$  (eq. 3) and invoking the Gibbs-Helmholtz relation, the second term on the rhs of eq. (6) relates to  $\Delta H_s^*/R$ . Hence, we obtain:

$$\left(\frac{\partial \ln a}{\partial 1/T}\right)_{P,c} = \frac{\Delta H_{vap} + \Delta H_s^* - RT}{R} \quad (7)$$

By plotting the logarithm of the vapor activity versus the reciprocal temperature  $\Delta H_s^*$  can be obtained. The solvation entropy  $\Delta S_s^*$  is subsequently obtained from  $T\Delta S_s^* = \Delta H_s^* - \Delta G_s^*$ .

## 5.4 Results and discussion

### 5.4.1 Solubility

The sorption isotherms of water vapor at 20°C in several PEO-PBT materials are represented in Figure 2. At this temperature, the PEO phase is fully amorphous and, with regard to its sorption behavior, compares to a hydrophilic rubbery material. The PEO, however, is embedded in a rigid PBT phase that may affect the water uptake. The isotherms are linear at low vapor activities ( $a < 0.4$ ) while increasing exponentially at higher vapor activities. The propensity of the PBT phase to absorb water is very low as can be inferred from Figure 2 for the PEO-PBT sample with the highest amount of PBT (300PEO32PBT68). Strong localized interactions may develop between water and the PBT hydrogen bond acceptor groups (ester group oxygen's), but the intrinsic rigidity of the semi-crystalline PBT inhibits large water uptake. The PEO block on the other hand, is very flexible and, driven by hydrogen bonding interactions with water, prospers extensive water uptake. PBT determines H<sub>2</sub>O solubility too, as it may restrict swelling or affect the nature of the PEO phase.

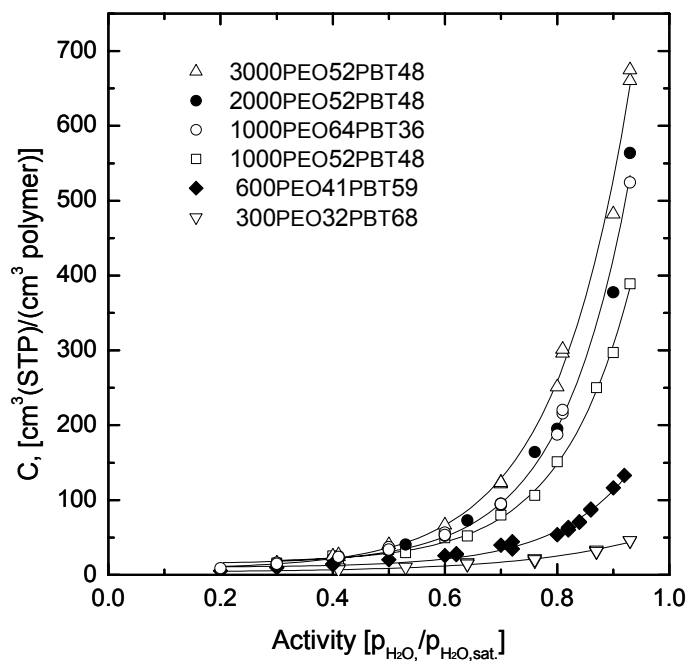


**Figure 2:** Solubility of water vapor in PEO-PBT block copolymers at 20°C.

As can be observed from Figure 2 has the polymeric structure an enormous effect on the solubility of water vapor in PEO-PBT materials. In general, the water concentration increases with an increase of the molecular weight of PEO and the overall weight percentage PEO. The latter can be seen by comparing the sorption isotherms of 1000PEO64PBT36 and 1000PEO52PBT48. Interestingly, the water solubility increases, as the PEO block length gets larger while the PEO-PBT weight ratio remains unchanged. This effect is observed for three different PEO-PBT block copolymers, with the same weight ratios of the PEO and PBT phase (52-48), but with different molecular weights of PEO (1000, 2000 and 3000 g/mol).

The amount of water absorbed in 3000PEO52PBT48 is higher than in 1000PEO64PBT36 over the whole activity range, although the total amount of PEO in the former is lower. This effect must, in some way be caused by differences in the polymeric microstructure. A higher molecular weight of PEO in fact facilitates a better phase separation between the PEO and PBT phase. Consequently, the PEO segment is less restricted in its mobility (lower  $T_{g,PEO}$ ) and can absorb more water<sup>25</sup>. The latter explanation does not apply to 3000PEO52PBT48, which has a higher solubility for water vapor than 2000PEO52PBT48. Both polymers, however, have the same glass transition temperature for the amorphous PEO phase ( $T_{g,PEO}$ ), which is comparable to the glass transition temperature of pure PEO<sup>18</sup>. At higher PEO molecular weight the solubility of water vapor increases probably due to a higher swelling tendency of the polymeric matrix. We will discuss the molecular origin of this behavior later in the section solvation thermodynamics.

#### 5.4.2 Flory-Huggins sorption model

The shape of the sorption isotherms depicted in Figure 2 are of typical Flory-Huggins type as commonly observed for highly interactive vapors in rubbery polymers. The Flory-Huggins theory is commonly used for the description of solutes in rubbery polymers<sup>1-14</sup>. For highly exothermal systems it is known that the interaction parameter is usually concentration dependent and decreases with an increase of the solute concentration in the polymer<sup>4,8</sup>. The original Flory-Huggins model introduces a concentration independent energy parameter ( $\chi$ ), any decrease of  $\chi$  with penetrant loading is therefore difficult to interpret in terms of physical changes in the system. In very general terms one may argue that decreasing  $\chi$  values with increasing penetrant concentration indicate that the environment into which the penetrant molecules are dissolved is becoming more like that of the pure liquid penetrant<sup>4,8</sup>.

The interaction parameter ( $\chi$ ) is calculated by using Eq. 1. The volume fraction of water vapor in the PEO phase in the block copolymer,  $\phi_{s,PEO}$ , is determined from the mass uptake of penetrant by the polymer by using the following equation<sup>4,8</sup>:



$$\phi_{s,PEO} = \frac{C \frac{V}{22414}}{y + C \frac{V}{22414}} \quad (9)$$

where  $C$  is the concentration of water vapor ( $\text{cm}^3$  (STP)/ $\text{cm}^3$  polymer),  $V$  the molar volume of the penetrant (which is taken to be  $18 \text{ cm}^3/\text{mol}$ ) and  $y$  is the volume fraction of PEO present in the block copolymer.

Similar trends in the interaction parameter would be observed if in Eq. 9 the total volume of the polymer was used ( $y=1$ ) instead of the volume fraction of PEO. However, the volume fraction of PEO was used since water primarily absorbs in the PEO phase. This allows a comparison of the interaction parameters of various block copolymers. The interaction parameter decreases with increasing concentration of water in the polymer. Figure 3 shows a typical example for 1000PEO52PBT48.

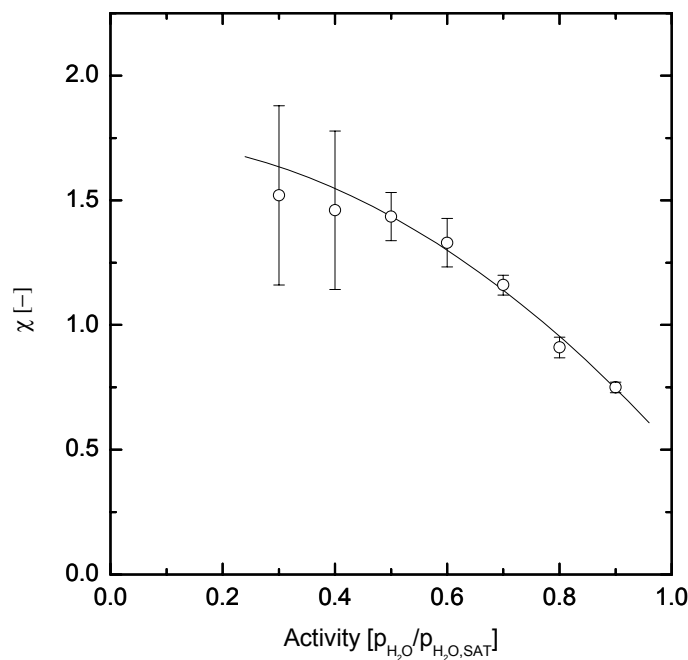


**Figure 3:** Flory-Huggins interaction parameter as a function of the water activity for 1000PEO52PBT48 at 20°C.

The error in the interaction parameter is statistically determined from measurements on 6 different samples and is high at low activities, due to the lower solubility of water vapor at low activities. The interaction parameter decreases with an increase of concentration of water in the block copolymer.

Comparable trends are also observed for other polymer water vapor systems such as: ethyl cellulose water<sup>1,8</sup> cellulose nitrate and cellulose acetate water<sup>6</sup>. Figure 4 shows the interaction parameter ( $\chi$ ) for different PEO-PBT block copolymers differing in molecular weight of the PEO block and ratio between the PEO and PBT phase.

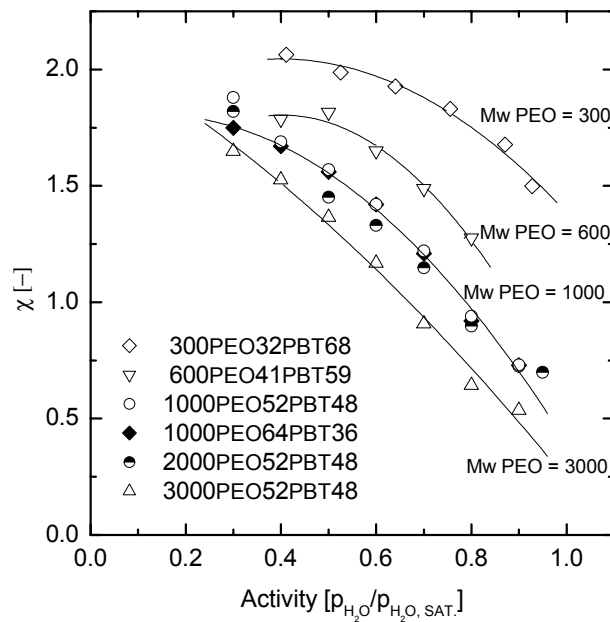
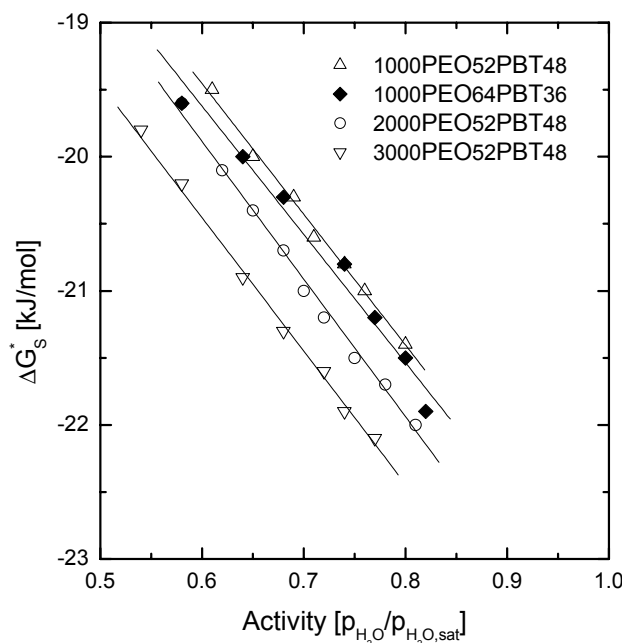


**Figure 4:** Interaction parameter for water vapor in different PEO-PBT block copolymers at 20°C.

Again for all PEO-PBT block copolymers the interaction parameter decreases with activity. The interaction parameter, amounts to  $\chi = 2$  at low activities and decreases at higher activities to a value of 0.5, indicating that sorption becomes energetically more favorable. Furthermore, there is a dependence of the interaction parameter on the molecular weight of the PEO segment. The higher the molecular weight of the PEO part the lower the value for the interaction parameter and the more energetically favorable it is for the water molecule to be in the polymeric matrix. The exact physical background of the decreasing interaction parameter with activity is difficult to explain, in particular since the interaction parameter ( $\chi$ ) contains both enthalpic and entropic contributions<sup>5</sup>. Whether this decrease in interaction parameter with increasing activity is due to an average stronger binding of the water vapor molecule with the swollen polymeric matrix or due to more favorable entropic contributions is still unclear and cannot be directly deduced from the Flory Huggins model.

### 5.4.3 Solvation thermodynamics

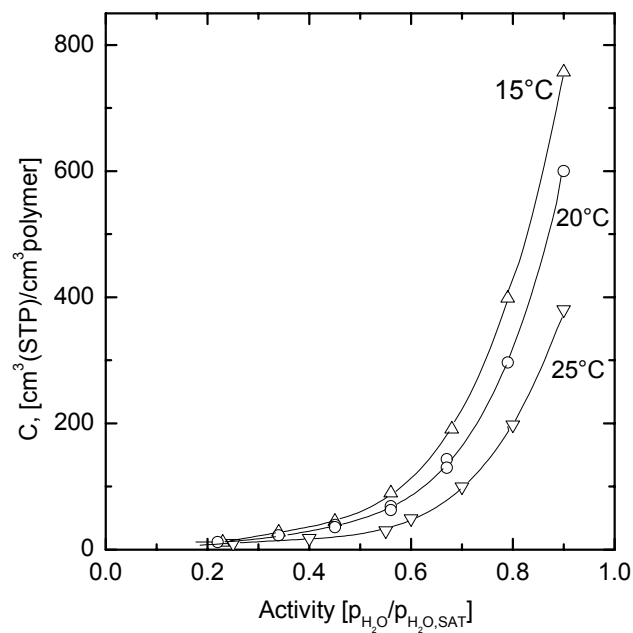
The solvation Gibbs energy, calculated from eq. (3), is presented in Figure 5 as a function of the water vapor activity. Due to high statistical errors at low vapor activities, we present the data for activities larger than 0.5 only.



**Figure 5:** Solvation Gibbs energy versus water vapor activity for various PEO-PBT block copolymers at 25°C.

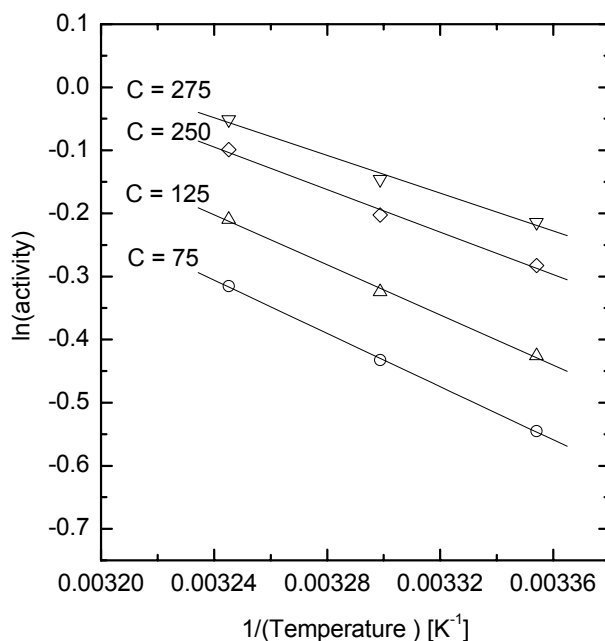
The solvation Gibbs energy decreases monotonically as the water vapor activity increases. Hence, cavity formation becomes less expensive or polymer-penetrant interactions get stronger with increasing water concentration in the polymer. A decrease of  $\Delta G_s^*$  reflects the increase of the water solubility coefficient (eq. 3) with the vapor activity as observed in the isotherms (Figure 2). The solvation Gibbs energy becomes stronger negative when the segment length of the PEO increases (at the same ratio PEO-PBT), which corresponds to an increased solubility observed in the corresponding sorption isotherms (Figure 2). These differences are easier interpreted based on the enthalpic (interaction) and entropic (swelling) contributions discussed below.

Temperature dependent sorption isotherms are required to determine the isosteric heat of solvation from the sorption data. Such experiments are performed for 4 different PEO-PBT block copolymers: 1000PEO52PBT48, 2000PEO52PBT48, 3000PEO52PBT48 and 1000PEO64PBT36 respectively. The first three differ in molecular weight of the PEO block while the last one has a higher amount of PEO with a molecular weight of 1000.



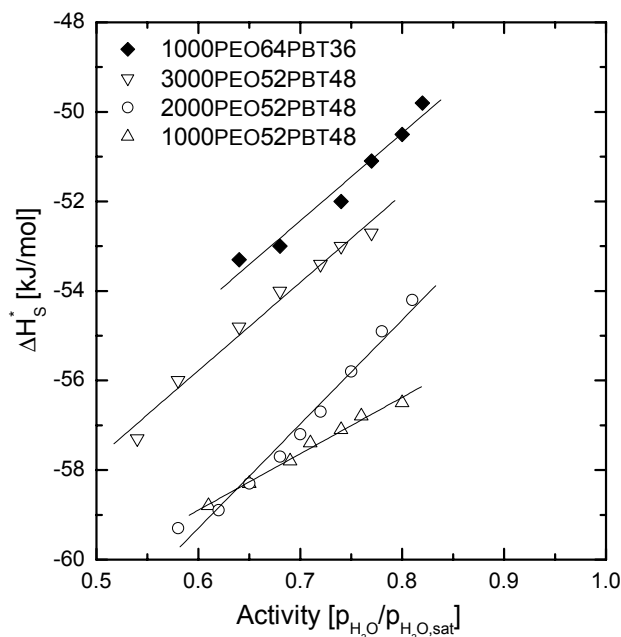
**Figure 6:** Sorption isotherm of 3000PEO52PBT48 at 15, 20 and 25°C.

Figure 6 shows the water sorption isotherm of 3000PEO52PBT48 at various temperatures with a decreasing solubility with increasing temperature, indicating the exothermic nature of water sorption.



**Figure 7:** Determination of the water isosteric heat of solvation in 2000PEO52PBT48. Numbers represent concentrations of water ( $\text{cm}^3(\text{STP})/\text{cm}^3$  polymer) in the polymer

Figure 7 shows the logarithm of the activity, at constant water concentration in the polymer, at various temperatures for 2000PEO52PBT48. The water vapor activity at a fixed concentration of water in the polymer is obtained from an exponential fit of the sorption data. The isosteric heat of solvation is determined from the slope of the lines in Figure 7 and Eq. 4. The slopes increase, from  $-2110$  K at  $75$  ( $\text{cm}^3$  (STP)/ $\text{cm}^3$  polymer) to  $-1500$  K at  $250$  ( $\text{cm}^3$  (STP)/ $\text{cm}^3$  polymer), reflecting a less favorable heat of solvation at higher water contents.



**Figure 8:** Heat of solvation versus water vapor activity for various PEO-PBT block copolymers at 25°C.

The heat of solvation ( $\Delta H_s^*$ ) has been calculated from Eq. (7) and is presented in Figure 8 versus the vapor activity.  $\Delta H_s^*$  has a negative sign and therefore favors the solubility of water. The average heat of solvation increases (less exothermic) for all the four PEO-PBT block copolymers with an increase of activity, indicating that the interactions between the water molecules and the polymer become weaker as the water vapor concentration inside the polymer increases. The heat of solvating a water molecule from the equilibrium vapor phase into pure liquid water amounts to  $-41.96$  [kJ/mol]<sup>16</sup>, which is less favorable than the heat of solvation of water vapor in PEO-PBT block copolymers. This is an indication that polymer-water interactions are stronger than the hydrogen bonding water-water interactions in the bulk liquid. The heat of solvation increases in the order  $1000\text{PEO}64\text{PBT}36 < 3000\text{PEO}52\text{PBT}48 < 2000\text{PEO}52\text{PBT}48 < 1000\text{PEO}52\text{PBT}48$ , indicating that polymer-penetrant interactions are the strongest for the system with the smallest PEO block length and the smallest amount of PEO (1000PEO52PBT48). Apparently, in the latter system, water-polymer interactions are stronger localized restricting the water molecules to positions where its interactions with the polymer is the strongest. Below, we will see that this interpretation is confirmed by the behavior of the solvation entropy in the various systems.

For all four PEO-PBT block copolymers the heat of solvation increases with the vapor activity, possibly due to swelling of the polymer matrix. Solvent swelling renders penetrant-polymer interactions to become weaker localized, while in addition causing the water molecules to interact to an increased extent with other water molecules that are ubiquitous at higher activities. The latter interactions are weaker than the interactions between water and the polymer, hence contributing to the increase of  $\Delta H_s^*$ . Because  $\Delta G_s^*$  decreases with activity (Figure 5) while  $\Delta H_s^*$  increases (Figure 8), the solvation entropy,  $T\Delta S_s^* = \Delta H_s^* - \Delta G_s^*$ , is an increasing function of the vapor activity. The increase of the water solubility coefficient (convex shape of the isotherms) with vapor activity is therefore a result of the entropy change rather than changes of the energetics of polymer-penetrant interaction.

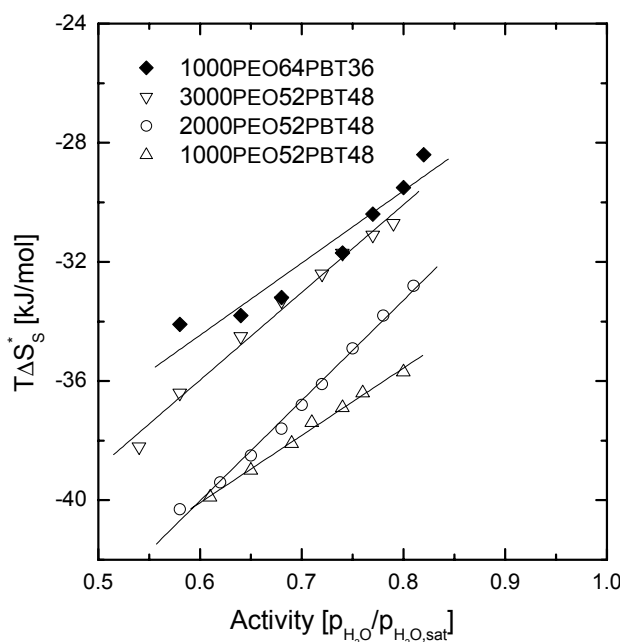


**Figure 9:** Entropy of solvation versus water vapor activity for various PEO-PBT block copolymers at 25°C

The solvation entropy is presented in Figure 9 versus the water vapor activity. The entropies are negative; therefore solvation entropy opposes the solubility of water from the vapor. Increasing PEO segment length or total amount of PEO affects the entropy such that the opposing effect becomes less important. The dependence of  $\Delta S_s^*$  on the polymer block composition is the same as the dependence of  $\Delta H_s^*$  on the polymer structure (Figure 8). Because strong

interactions generally are those that are site specific and localized, the system exhibiting the strongest negative  $\Delta H_s^*$  values (1000PEO52PBT48) exhibits the strongest negative  $\Delta S_s^*$  values too. The dependence of the water solvation entropy on the equilibrium water vapor activity is comparable to the dependence of the solvation enthalpy on vapor activity. (Figure 8). An increase in  $\Delta H_s^*$  with water vapor activity means that at higher water concentrations in the polymer the water molecules interact weaker with their surrounding molecules. As a weaker binding between molecules in the system generally leads to an increased configurational freedom of the molecules, one expects entropy to increase. The Flory-Huggins analysis in the previous section showed that the polymer-water interaction parameter decreases with increasing vapor activity. Based on the data in Figure 8 and Figure 9 it can be concluded that the decrease of the interaction parameter is not a result of a more favorable energetic interaction of the water molecule with its environment. Instead, it results from the strong increase of the water solvation entropy with the water vapor activity. The convex shape of the water vapor isotherms (Figure 2 and Figure 6) thus expresses dissolved water to bind weaker to the polymer at higher vapor activity resulting in a reduced entropic expense of water uptake.



## 5.5 Conclusions

PEO-PBT block copolymers show a high solubility for water vapor, which is completely determined by the PEO segment. The amount of dissolved water vapor depends on the polymeric structure: the more PEO and the higher the molecular weight of the PEO segment the higher the solubility of water vapor.

Based on the Flory-Huggins theory the polymer water interaction parameter has been calculated, which is concentration dependent and decreases with the amount of dissolved water vapor. The absolute value of this interaction parameter depends on the polymeric structure: the larger the PEO content and the higher the PEO segment molecular weight the lower the value for the interaction parameter.

The solvation Gibbs energy, enthalpy and entropy of solvation have been determined from the sorption data as well. These thermodynamic properties give more insight in the structure property relationship. When the concentration of water in the block copolymer increases the interactions between water and the polymer become weaker. The solvation Gibbs energy decreases with an increase of water vapor concentration due to an increase of the solvation entropy. This effect is responsible for the convex shape of the water sorption isotherm. Moreover, this effect is structure dependent: the larger the PEO segment and the more PEO present the higher the solvation entropy and the lower the solvation Gibbs energy of interaction.

## 5.6 References

- (1) Beck, M. I.; Tomka, I. *J. Macromol. Sci., Phys.* **1997**, *B36*, 19-39.
- (2) Dixon-Garrett, S. V.; Nagai, K.; Freeman, B. D. *J. Polym. Sci., Polym. Phys. Ed.* **2000**, *38*, 1078-1089.
- (3) Merkel, T. C.; Bondar, V. I.; Nagai, K.; Freeman, B. D.; Pinnau, I. *J. Polym. Sci., Polym. Phys. Ed.* **2000**, *38*, 415-434.
- (4) Singh, A.; Freeman, B. D.; Pinnau, I. *J. Polym. Sci., Polym. Phys. Ed.* **1998**, *36*, 289-301.
- (5) Favre, A.; Nguyen, Q. T.; Schaezel, P.; Clement, R.; Neel, J. *J. Chem. Soc. Faraday. Trans.* **1993**, *89*, 4339-4346.
- (6) Perrin, L.; Nguyen, Q.; Sacco, D.; Lochon, P. *Polym. Int.* **1997**, *42*, 9-16.
- (7) Flory, P. J. *Principles of polymer chemistry*; Cornell University press, 1953.
- (8) Schuld, N.; Wolf, B. A. *Polymer Handbook*, 4th ed.; Wiley: New York, 1999; Vol. VII.

- (9) Yamaguchi, T. N., S.I.; Kimura, S. *J. Polym. Sci., Polym. Phys. Ed.* **1997**, *35*, 469-477.
- (10) Williams, J. L.; Hophenberg, H. B.; Stannett, V. *J. of Macromol. Sci. Phys.* **1969**, *B3*, 711-725.
- (11) Serad, G. E. F., B.D.; Stewart, M.E.; Hill, A.J. *Polymer* **2001**, *42*, 6299-6943.
- (12) Kamiya, Y. T., K.; Naito, Y.; Wang, J. S. *J. of Polym. Sci. Part B- Polym. Phys.* **1995**, *33*, 1663-1671.
- (13) Wang, P.; Schneider, N. S.; Sung, N. H. *J. of Appl. Polym. Sci.* **1999**, *71*, 1525-1535.
- (14) Russell, S. P. W., D. H. *Polymer* **2001**, *42*, 2827-2836.
- (15) Ben-Naim, A. *Journal of Solution Chem.* **2001**, *30*, 475-487.
- (16) Ben-Naim, A. *Solvation Thermodynamics*; Plenum Press: Jerusalem, 1987.
- (17) Metz, S. J.; Mulder, M. H. V.; Wessling, M. *Chapter 4*.
- (18) Fakirov, S.; Gogeva, T. *Makromol. Chem.* **1990**, *191*, 615-624.
- (19) Boom, J. P.; Punt, I. G. M.; Zwijnenberg, H.; de Boer, R.; Bargeman, D.; Smolders, C. A.; Strathmann, H. *J. Membr. Sci.* **1998**, *138*, 237-258.
- (20) Stamatialis, D.; Wessling, M.; Sanopoulou, M.; Strathmann, H.; Petropoulos, J. *J. Membr. Sci.* **1997**, *125*, 165-175.
- (21) Rezac, M. E.; John, T.; Pfromm, P. H. *J. Appl. Polym. Sci.* **1997**, *65*, 1983-1993.
- (22) Wellons, J. D.; Stannett, V. *J. Polym. Sci.* **1966**, *4*, 593-602.
- (23) van der Vegt, N. F. A. *J. Membr. Sci.* **2002**, *205*, 125-139.
- (24) Skirrow, G.; Young, K. R. *Polymer* **1974**, *15*, 771-776.
- (25) Deschamps, A. A.; Grijpma, D. W.; Feijen, J. *Polymer* **2001**, *42*, 9335-9345.

# Chapter 6

## Mixed gas water vapor/N<sub>2</sub> transport in Poly(Ethylene Oxide) Poly(Butylene Terephthalate) Block copolymers

### Abstract

This chapter studies the mass transport properties for water vapor and nitrogen for a series of poly(ethylene oxide) (PEO) poly(butylene terephthalate) (PBT) block copolymers via: (a) the water vapor sorption, (b) the permeation of water vapor/N<sub>2</sub> mixtures, (c) the diffusion of water vapor, (d) Zimm and Lundberg cluster analysis, and (e) the state of water in these polymers by FTIR-ATR analysis. The studied block copolymers consist of a PEO segment length of 1000 g/mol containing various amounts of PBT.

The water vapor permeability depends strongly on the polymeric structure and increases with an increased amount of PEO due to a higher solubility and diffusivity for water vapor for block copolymers with a larger amount of PEO. The diffusivity of water vapor decreases significantly with an increase of the amount of water vapor sorbed in the block copolymer. This decrease is caused by the clustering of water vapor, as revealed by a Zimm and Lundberg cluster analysis of the sorption isotherm and by FTIR-ATR. The latter technique shows that the interactions between water and the polymer become weaker as the amount of water in the block copolymer increases. This observation suggests that the decrease in interaction energy between water and the polymer must be compensated by an entropy gain, because the amount of water vapor increases with an increase of activity. Water vapor preferably remains in the cluster, which makes diffusion through the polymer energetically less favorable. This causes the diffusion coefficient to decrease with the increase of the amount of water vapor in the polymer.

The mixed gas N<sub>2</sub> permeability remains constant with an increase of water vapor activity but depends strongly on the polymeric structure, whereas the water vapor permeability depends on the solubility in the block copolymer. This causes a higher selectivity for block copolymers containing more PBT.

## 6.1 Introduction

Water vapor transport through polymeric films is often complicated by non-ideal solubility and anomalous diffusivity. Water may interact with the polymer causing plasticization or cluster formation<sup>1-3</sup>.

A trade-off relationship between selectivity and permeability, commonly used for permanent gases in the so called Robeson plot<sup>4</sup>, where a higher selectivity is accompanied by a lower permeability and vice versa. This not valid for water vapor since the selectivity increases with the pure gas permeability<sup>5</sup>. Moreover, there exists hardly any literature on the permeation of a permanent gas in the presence of water vapor.

The aim of this work is study the permeability of water vapor and N<sub>2</sub> in a water vapor/N<sub>2</sub> mixture through PEO-PBT block copolymers with various amounts of PEO but with a constant PEO segment length of 1000 g/mol. The water vapor transport is studied via its diffusivity. The state of water in these polymers, affecting the diffusivity, is analyzed via the Zimm and Lundberg cluster analysis and infrared spectroscopy.

The mixed gas water vapor and N<sub>2</sub> permeability are studied at 30°C, 50°C and 80°C, revealing the temperature and structural dependence of the permeability and selectivity for these block copolymers.

## 6.2 Experimental

### 6.2.1 Materials

PEO-PBT block copolymers were obtained from Isotis b.v. (the Netherlands) and were used without further purification. The structural and thermal properties of these materials are discussed elsewhere<sup>6</sup>. Chloroform (CHCl<sub>3</sub>) and trifluoroacetic acid (TFA) were both purchased from Merck (analytical grade) and used as solvents. For the gas permeation experiments carbon dioxide (CO<sub>2</sub>), nitrogen (N<sub>2</sub>), and helium (He) were used and purchased from Hoekloos b.v. (Netherlands). The purity of the gases was greater than 99.9 %.

### 6.2.2 Film preparation

PEO-PBT block copolymers were dissolved in CHCl<sub>3</sub> (5 – 10 wt%), and TFA was added ( $\pm$  4 vol. % in CHCl<sub>3</sub>) when the weight ratio of PEO in the block copolymer was lower than 50 wt%. Thin films of around 50  $\mu$ m were prepared by solution casting on a glass plate. The cast films were dried in a N<sub>2</sub> atmosphere at room temperature for 24 hours. The homogeneous dense films were removed from the glass plate and were further dried and stored in a vacuum oven at 30°C.

### 6.2.3 Mixed gas water vapor permeation

The mixed gas water vapor and nitrogen permeability were determined in a set up described in detail elsewhere<sup>7</sup>. The determination of the permeance consists in principle of water vapor/N<sub>2</sub> mixture flowing over a polymeric film (membrane) and a sweep gas removing the permeated water vapor and N<sub>2</sub> at the permeate side. The permeability of both components was determined from the flux through the membrane and the partial pressure difference between the feed- and permeate side of the membrane. A correction of a stagnant boundary layer was necessary and performed for water vapor.

### 6.2.4 Sorption isotherms

An electro balance (TGA Perkin Elmer) was used to perform the gravimetric sorption experiments and is also described elsewhere<sup>8,9</sup>.

The concentration of water inside the polymeric film was determined from the mass uptake due to sorption and was calculated by using the following equation<sup>10</sup>:

$$c = \frac{(M_{\infty} - M_i) \cdot 22414}{M_w \cdot V_p} \quad (1)$$

where  $c$  is the equilibrium concentration of water inside the polymeric film [ $\text{cm}^3(\text{STP})/\text{cm}^3\text{polymer}$ ],  $M_{\infty}$  and  $M_i$  are the final and initial mass of the

polymer, respectively,  $M_w$  is the molecular weight of the penetrant,  $V_p$  the volume of the polymer and 22414 the molar volume (units  $\text{cm}^3$ ) of an ideal gas at standard temperature and pressure.

### 6.2.5 Infrared Spectroscopy

A Bio-Rad FS60 was used to perform the infrared experiments. An ATR (Attenuated Total Reflectance) device (Biorad) was used for the ATR measurements. The polymeric sample was put on the ATR crystal and a box tightly pressed the sample on the crystal. This modification of the ATR crystal is shown in Figure 1

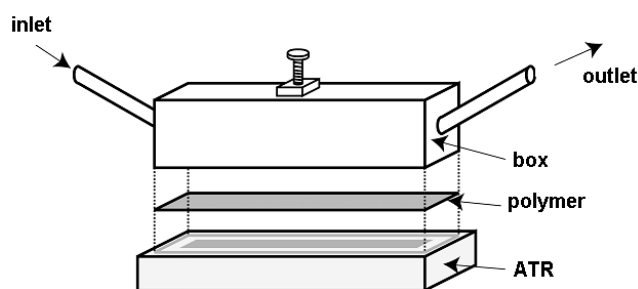


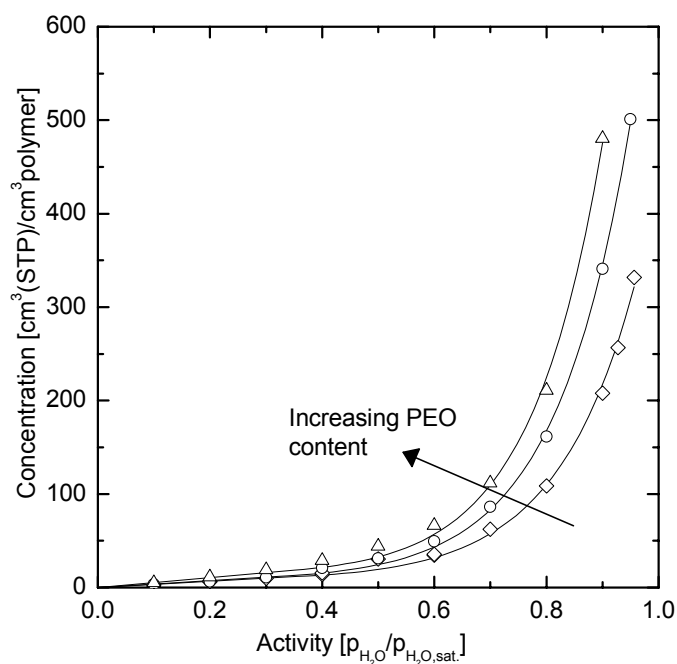
**Figure 1:** Modification ATR device to allow vapor saturation of the polymeric film

The box allows to expose the polymeric film to a controlled water vapor environment by the passage of a  $\text{N}_2$  stream with a controlled amount of water vapor. A  $\text{N}_2$  stream with a controlled water vapor activity is generated by mixing a  $\text{N}_2$  stream saturated with water vapor with a dry  $\text{N}_2$  stream. This configuration prevents direct contact of water vapor with the ATR crystal.

## 6.3 Results and Discussion

### 6.3.1 Solubility of water vapor in PEO-PBT block copolymers

The transport of a gas or vapor through a dense polymeric film can be described with the so-called solution-diffusion model<sup>11</sup>. The penetrant dissolves at the feed interface of the membrane, diffuses through it and desorbs at the permeate side. In rubbery polymers the selective separation of gases and vapors is accomplished by the difference in solubility. This holds also for water/ $\text{N}_2$  separation by the rubbery PEO phase in PEO-PBT block copolymer. Hence it is necessary to know the water sorption behavior of the block copolymer.



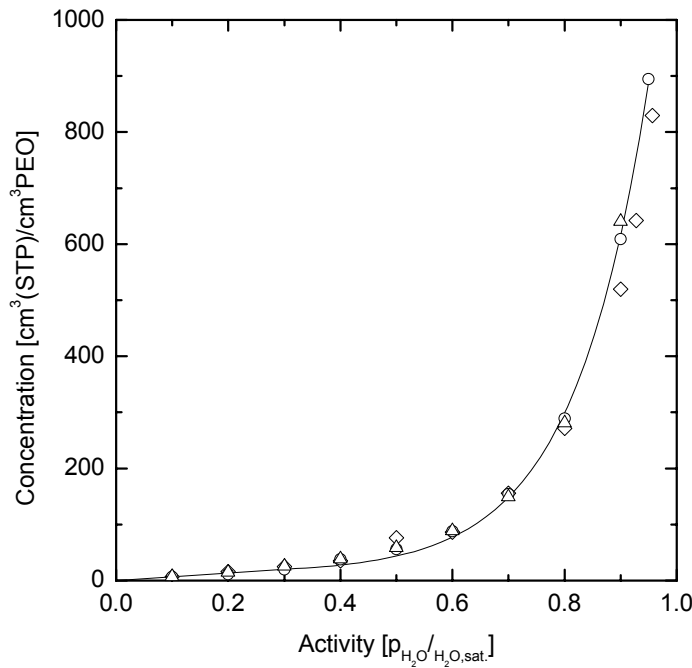
**Figure 2:** Sorption isotherms of 1000PEO40PBT60 (◇), 1000PEO56PBT44 (○), and 1000PEO75PBT25 (△) at 30°C.

Figure 2 shows the water vapor sorption isotherms of 3 different PEO-PBT block copolymers at 30°C as a function of the water vapor activity. The block copolymers contain the same PEO segment length (1000 g/mol), but differ in the amount of PEO (40, 56, or 75 wt% of PEO present in the block copolymers). The sorption isotherms are linear at low activities but increase convex to the activity axis at higher activities. This type of sorption isotherm is often found for the sorption of organic vapor in rubbery polymers like PDMS<sup>12,13</sup> and water vapor in several other polymers<sup>1</sup>.

The exponential increase of the sorption isotherm at higher water vapor activities stems from an energetically more favorable environment into which water vapor dissolves. Solvation Gibbs energies, entropies and enthalpies, extracted from temperature dependent sorption data, reveal that the water-polymer interactions become weaker at higher water vapor activities and that the gain in water sorption entropy at increasing vapor activity predominates the enthalpy loss. This results in an overall decrease of the free enthalpy of sorption with increasing vapor activity and causes the convex nature of the water sorption isotherm<sup>14</sup>.

The amount of water vapor sorbed in the polymer increases with the amount of PEO present in the block copolymer due to the hydrophilic nature of the PEO part, which sorbs significantly more water than the PBT part<sup>14</sup>. This can also be

observed from Figure 3, which shows the water sorption isotherm for the 3 PEO-PBT block copolymers calculated per  $\text{cm}^3$  PEO.



**Figure 3:** Sorption isotherms of 1000PEO40PBT60 (◇), 1000PEO56PBT44 (○), and 1000PEO75PBT25 (△) at 30°C calculated per  $\text{cm}^3$  PEO.

The solubility of water vapor for the 3 block copolymers, in the PEO phase does not depend on the amount of PBT in the block copolymers. Hence, water mainly dissolves in the PEO phase and sorption into the PBT phase can be neglected. However, the solubility of water vapor does depend on the molecular weight of PEO, which increases with the PEO segment length at equal ratio of PEO-PBT<sup>14-16</sup>.

### 6.3.2 Permeability

Due to the strong dependence of the water sorption on the feed activity one expects also a strong non-linear relationship between permeability and feed gas activity.

Figure 4 shows the mixed-gas water vapor permeability of 1000PEO40PBT60, 1000PEO56PBT44, and 1000PEO75PBT25 as a function of the water vapor activity at the feed side of the membrane. The water vapor permeability is determined with a water vapor/nitrogen mixture and the water vapor permeability and activity are corrected for concentration polarization phenomena as described in detail elsewhere<sup>7</sup>. The water vapor permeability increases exponentially with the water vapor activity and is the highest for the block copolymer with the largest amount



of PEO, similar to the trend in the sorption isotherms. The increase of the water vapor permeance with activity is larger for the block copolymer containing more PEO.

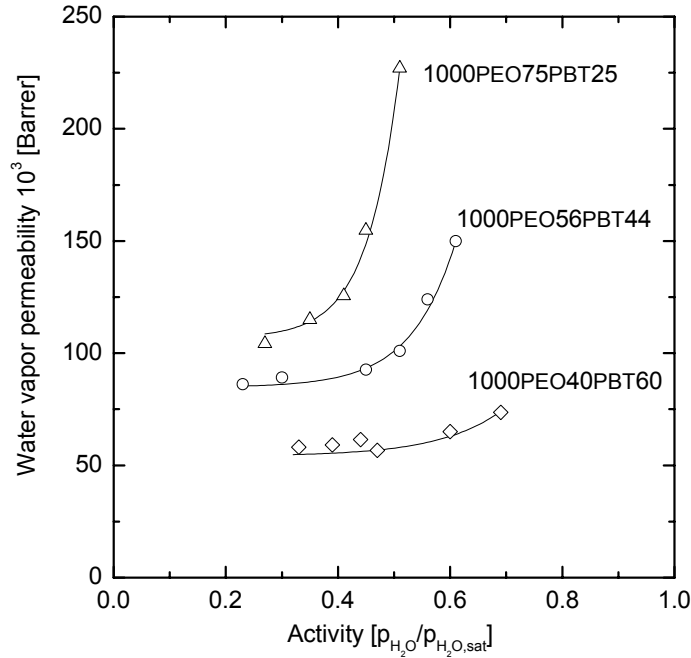


**Figure 4:** Water vapor permeability of 1000PEO40PBT60 (◇), 1000PEO56PBT44 (○), and 1000PEO75PBT25 (Δ) at 30°C.

The increase in permeability may completely stem from an increased solubility with increasing vapor activity as shown in Figure 2. However, the water diffusivity may change as well with higher water vapor activities. The diffusion coefficient can be determined from the permeability- and sorption isotherms, and one can estimate the Fickian film diffusion coefficient as<sup>17,18</sup>:

$$P = \left( \frac{C_2 - C_1}{p_2 - p_1} \right) \bar{D} \quad (2)$$

where  $\bar{D}$  is called the concentration-averaged diffusion coefficient between the concentration at the feed side of the membrane ( $C_2$ ) and the permeate side ( $C_1$ ). For the permeation of pure gases, Eq. 2 becomes  $P = (C_2 D)/p_2$ , since the pressure on the feed side of the membrane ( $p_2$ ) is much higher than the pressure on the permeate side ( $p_1$ ). However, water vapor has a relatively low partial pressure on the feed side of the membrane ( $T = 30^\circ\text{C}$ ,  $a^{\text{H}_2\text{O}} = 0.69$ ,  $p^{\text{H}_2\text{O}} =$

38.49 mbar) and the water vapor pressure on the permeate side of the material cannot be neglected due to the high permeability for water vapor. The permeate activity may range from 0.16 to 0.45 depending on the selectivity of the PEO-PBT membrane used.

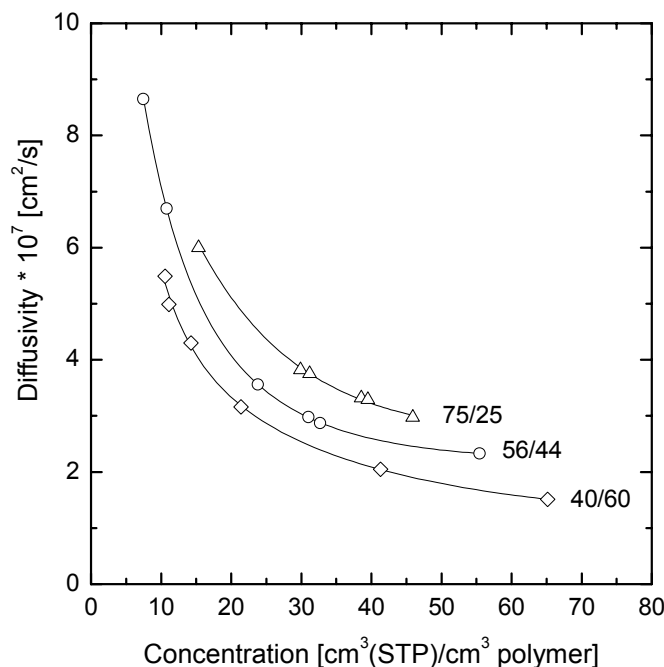


**Figure 5:** Concentration averaged diffusion coefficients for 1000PEO40PBT60 ( $\diamond$ ) 1000PEO56PBT44 ( $\circ$ ) 1000PEO75PBT25 ( $\Delta$ ) at 30°C.

Figure 5 presents the concentration averaged diffusion coefficients calculated according to Eq. 2 from the permeation and sorption data as a function of the concentration of water vapor on the feed side of the membrane. This diffusion coefficient for water is the highest for the block copolymer containing the largest amount of PEO (1000PEO75PBT25), which stems from a larger amount of PEO available for diffusion. The permeability of water vapor is larger for the block copolymer containing the highest amount of PEO due to a higher solubility and diffusivity.

For all polymers the diffusion coefficient decreases with increasing penetrant concentration. This behavior may be considered anomalous since the diffusion coefficient for water increases with an increase of activity for hydrophilic polymers: well established examples are polyvinylalcohol<sup>19,20</sup>, cellulose<sup>1</sup>, Nafion<sup>21</sup> and Nylon<sup>1</sup>. In these systems water causes plasticization of the polymeric matrix, which leads to an increasing diffusion coefficient. However, for a number of other systems the diffusion coefficient decreases with activity e.g.:

polydimethylsiloxane<sup>22</sup>, ethylcellulose<sup>23</sup> and polymethylmethacrylate<sup>22</sup>. This decrease in diffusivity appears to be accompanied by the formation of water clusters, which –as we will show later– represents a less mobile environment than the non-swollen polymer for monomeric water.

To elucidate the significant decrease of water diffusivity with increasing activity, we first compare three different methods to estimate the molecular mobility of water in the PEO phase. Using the lattice based theory of Zimm and Lundberg we then evaluate the formation of clusters using the sorption isotherm. Finally, we use ATR-FTIR to quantify changes of the molecular state of water in the PEO/H<sub>2</sub>O mixture as a function of swelling degree.

The concentration-averaged diffusion coefficient is defined as<sup>18</sup>:

$$\bar{D} = \frac{1}{C_2 - C_1} \int_{C_1}^{C_2} D(C) dC \quad (3)$$

where  $D$  is the local concentration dependent diffusion coefficient,  $C_2 - C_1$  the concentration difference over the membrane, and  $D(C)$  the local effective diffusion coefficient, which is a measure of the ability of a penetrant to migrate through a polymer at a well defined penetrant concentration<sup>17</sup>. The effective diffusion coefficient can be determined from the permeability and solubility by assuming Fickian diffusion:

$$P = \frac{1}{p_2 - p_1} \int_{C_1}^{C_2} D(C) dC \quad (4)$$

which leads to:

$$D(C_2) = (p_2 - p_1) \frac{\partial P}{\partial C_2} + P \left( \frac{\partial p_2}{\partial c_2} - \frac{\partial p_1}{\partial c_2} \right) \quad (5)$$

where  $\partial P/\partial C_2$  is the slope of the permeation isotherm, and  $\partial p_2/\partial c_2$  and  $\partial p_1/\partial c_2$  the reciprocal slope of the sorption isotherm for the feed and permeate side of the membrane. Eq. 5 is often used to describe the diffusivity of gaseous penetrants in polymers where it is assumed that the permeate pressure ( $p_1$ ) is negligible compared to the feed pressure ( $p_2$ ). However, this is not applicable for the permeation water vapor due to the low partial pressure of water vapor on the feed side of the membrane and the existence of a significant water vapor pressure on the permeate side of the membrane due to the high water vapor permeability

of the polymer. Hence, Eq.5 has to be used in its complex form. The term  $\partial p_1/\partial c_2$  in Eq. 5 is the change of the water vapor pressure at the permeate side of the membrane due to a change in concentration at the feed side of the membrane. The concentration on the feed side is known via the sorption isotherm and the change in permeate pressure is measured.

For Eq.3, 4, and 5, diffusion is assumed to occur due to a concentration gradient over the membrane. However, transport occurs because of a chemical potential gradient over the membrane, which depends on the amount of water sorbed. The diffusion coefficients can be corrected for thermodynamic driving force resulting in the mobility (L) of the penetrant in the polymeric matrix<sup>1,13,24,25</sup>

$$L = \frac{D(c)}{\frac{d\ln(a)}{d\ln(c)} RT} \tag{6}$$

The decrease of the diffusion coefficient may reside in either the mobility or the correction for the driving force ( $d \ln(a)/d \ln(c)$ ). The latter term can be obtained from the sorption isotherm and its value depends on its curvature.

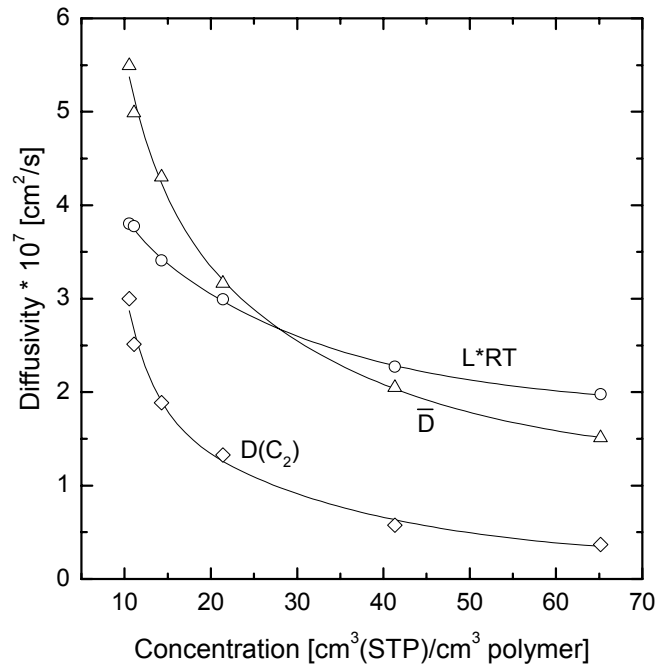


**Figure 6:** Concentration averaged ( $\bar{D}$ , Eq. 2), effective diffusion coefficient ( $D(C_2)$  Eq. 5), and mobility  $L*RT$  (Eq. 6) for 1000PEO40PBT60 as a function the concentration of water vapor on the feed side of the membrane.

Figure 6 shows the concentration-averaged diffusion coefficient ( $\bar{D}$ , Eq. 3), the effective diffusion coefficient ( $D(C_2)$ , Eq. 5) and the mobility (Eq. 6) for 100PEO40PBT60 as a function of the concentration of water vapor on the feed side of the membrane. The concentration-averaged diffusion coefficient has a higher value than the effective diffusion coefficient since the former is averaged over the membrane thickness and plotted as a function of the concentration at the feed side of the membrane. Both diffusion coefficients and the mobility decrease with an increase of concentration of water vapor in the membrane. The same trends are observed for the other block copolymers. However, the relative decrease is much less prominent for the mobility  $L$ . Hence, we conclude that the decrease in molecular mobility with increasing penetrant concentration is real and independent of the calculation method.

### 6.3.3 State of water in PEO-PBT block copolymers

A Zimm and Lundberg cluster analysis can be performed to characterize the tendency of water to associate. The analysis generally results in a quantitative description of the size of a solvent cluster. This information can be obtained from the sorption isotherm by using the cluster function  $G_{aa}/v_a$  for a two component system<sup>26,27</sup>:

$$\frac{G_{aa}}{v_a} = -(1 - \phi_a) \left[ \frac{\partial(a/\phi_a)}{\partial a} \right]_{p,T} - 1 \quad (7)$$

where  $v_a$  is the penetrant molar volume of the penetrant (molecule  $a$ ),  $G_{aa}$  the cluster integral,  $\phi_a$  the volume fraction of penetrant in the polymer and  $a$  the activity of the penetrant in the vapor phase. For ideal solutions (sorption isotherms following Henry's law)  $G_{aa}/v_a = -1$ , which means that a molecule  $a$ , excludes its own volume to molecules but does not affect their distribution. However, the connectivity of polymer segments leads to a non-random distribution of penetrant molecules and polymer segments. Penetrants tend to cluster if the concentration is higher in the neighborhood of a penetrant molecule as would be expected on the basis of non-random mixing<sup>13</sup>.

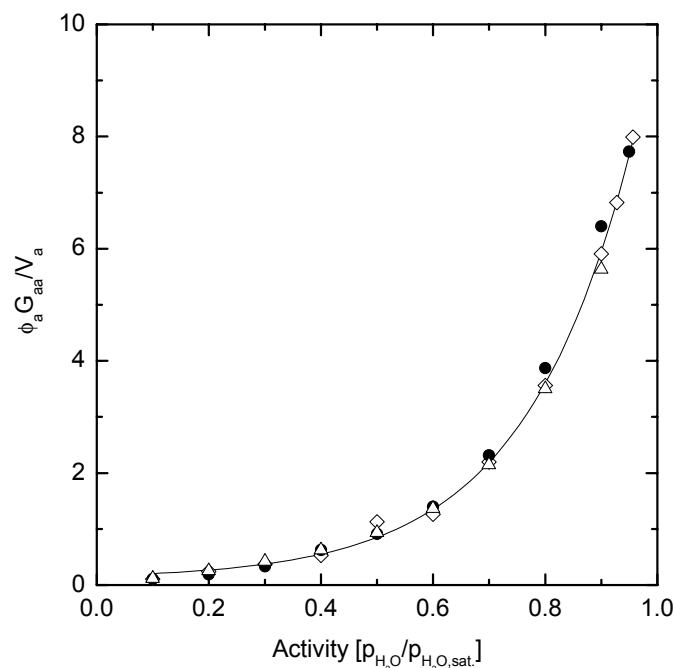


**Figure 7:** Zimm-Lundberg analysis of clustering in: 1000PEO40PBT60 (●), 1000PEO56PBT44 (◇), and 1000PEO75PBT25 (△) at 30°C.

The expression  $\phi_a G_{aa}/v_a$  yields the mean number of penetrant molecules in excess of the mean concentration in the neighborhood of a type a molecule. The quantity  $1+\phi_a G_{aa}/v_a$  is then the average number of molecules which exist in a cluster<sup>28</sup>. The quantity  $\phi_a G_{aa}/v_a$  is plotted as a function of the water vapor activity in Figure 7.

The value of  $\phi_a G_{aa}/v_a$  is positive and increases with an increase of the water vapor activity indicating that substantial clustering occurs at higher activities. The average number of molecules in a cluster increases from 1 at low activities to 9 at high activities. Furthermore, the difference between the different polymers is negligibly small, indicating that the clustering in the PEO phase is similar irrespective of the amount of PBT present in the block copolymer. This means that the cluster size in the PEO phase is equal and not affected by the PBT phase.

FTIR-ATR measurements are performed to study the cluster tendency further. To reveal the interactions between water and the polymer the spectrum of the dry polymer is subtracted from the polymeric spectrum in equilibrium with water vapor. There are two type of vibrations for water the bending vibration band located at ca. 1650 cm<sup>-1</sup> and the stretching vibration, where the symmetrical stretching is located at ca. 3650 cm<sup>-1</sup> and the asymmetric band at ca. 3760 cm<sup>-1</sup>.

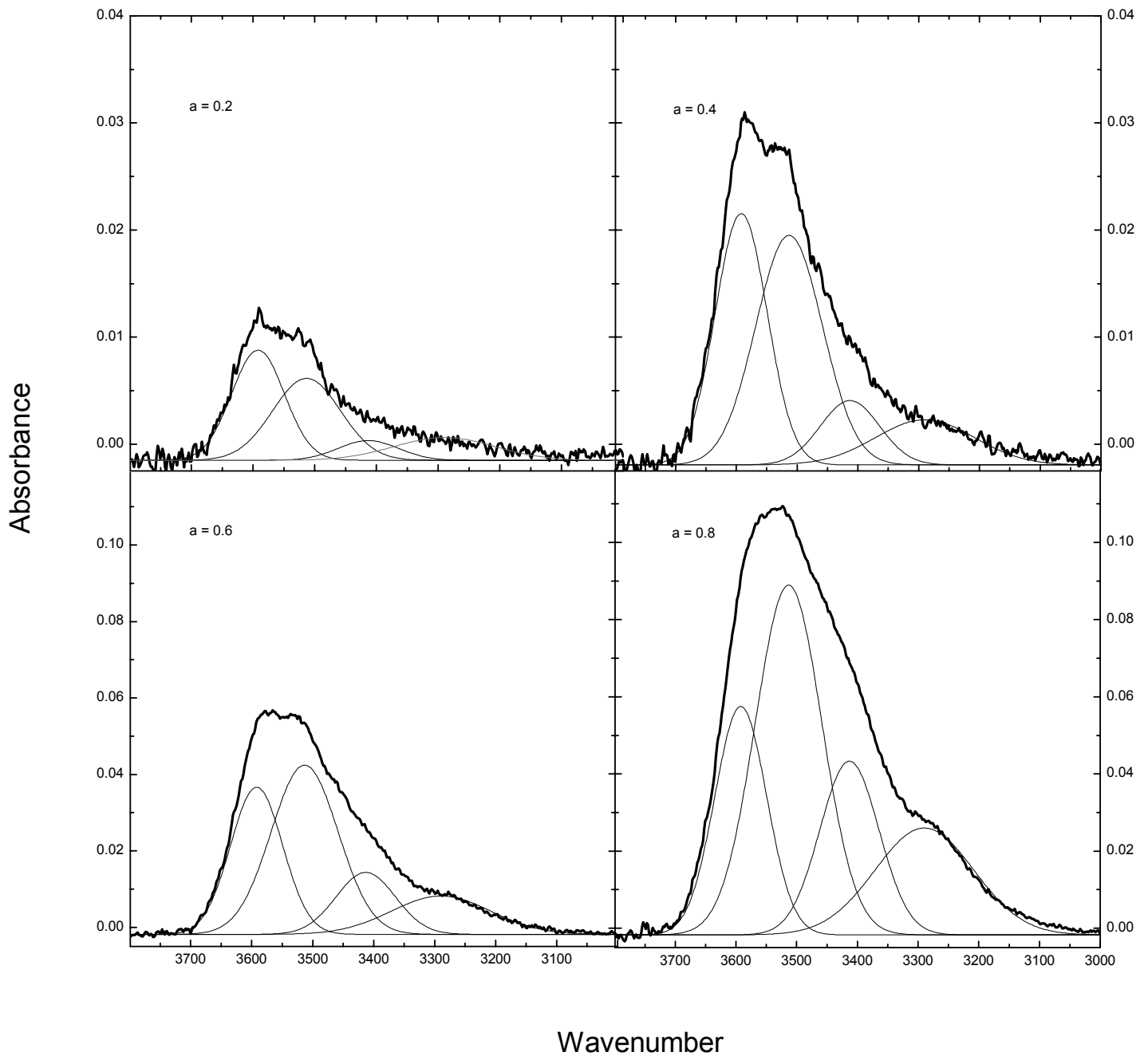


**Figure 8:** Close-up of the stretching region of the ATR spectrum of 1000PEO75PBT25 at various activities.

Figure 8 shows the absorbance (%) as a function of the wave number in the stretching region of water in 1000PEO75PBT25 at water vapor activities of 0.2, 0.4,

0.6 and 0.8. Gaussian curves were fit to the experimental data to quantify the different states of water in the polymer. Only 4 different peaks are assumed to be found in free water. Peak 1 corresponds to the OH stretching of monomeric water, peak 2 corresponds to dimeric and trimeric water, and peak 3 and 4 exist at lower wave numbers due to the OH stretching in hydrogen bounded water clusters<sup>29</sup>. The center of the peaks used for curve fitting are displayed in Table 1.

**Table 1:** Center of peaks for water<sup>30</sup> and water in PEO-PBT at various activities.

peak	center of component [cm <sup>-1</sup> ]		molecular state
	water	polymer	
1	3620	3592	monomeric
2	3520	3513	dimeric/trimeric
3	3411	3413	water clusters
4	3260	3290	

In the fitting of water in PEO-PBT spectra, the wave number of the peak center is adjustable as well as the area belonging to the peaks. The spectrum fit with fixed peak positions for water results in insufficient quality fits. The centers of the peaks are shifted compared to pure water, which is caused by the interaction of water with the polymers<sup>29</sup>. Hence, the peak positions obtained from the data fit are close to the ones for regular water. The fit peak positions can be used for all activities and give an excellent fit of the IR-spectra. The spectra in Figure 8 and its deconvolution show that all peak areas grow with increasing vapor activity. However, it appears that the relative contributions to the total spectrum change with increasing vapor activity. Figure 9 shows the relative contributions.



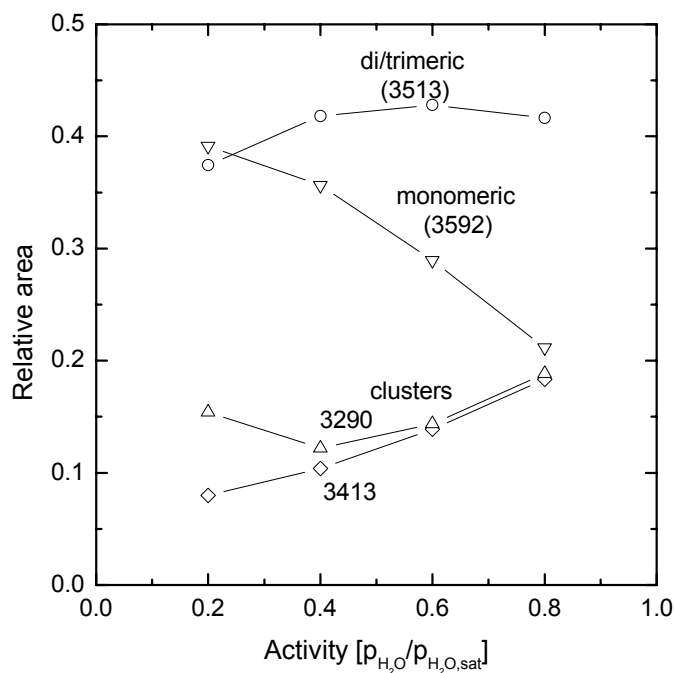


**Figure 9:** The relative peak area obtained from curve fitting as a function of the water vapor activity.

The relative peak area of the monomeric water decreases with an increase of vapor activity. The formation of dimeric/trimeric water increases: in particular, the peak at wave number 3413 increases by a factor 3. A general observation of the spectrum in Figure 8 reveals that the water is stronger bonded to the polymer at low activities (high wave number) and that the average interaction energy of water in the polymer becomes weaker at higher activities (center of the peaks shifts to lower wave numbers). A similar trend also has been observed in a thermodynamic analysis of the sorption isotherms of water vapor in these polymers<sup>14</sup>. It is interesting to observe that dimeric water already forms at low water vapor activities, where it is stronger bound to the polymer than to monomeric water. From an energetic point of view, this lower enthalpic interaction ( $\Delta H_s$ ) must be compensated by a gain in entropy ( $T\Delta S$ ), which lowers the free energy of solvation ( $\Delta G_s$ ) and causes an increase of the amount of water vapor sorbed in the polymer with activity. The increase of the amount of water sorbed in the polymer causes the convex shape of the sorption isotherm (Figure 2). This implies that it is entropically more favorable for water to reside in a water cluster than to be dispersed as a monomer in the polymeric matrix. This also has been observed with molecular dynamic simulations where it was found that the mobility of water molecules is larger if they are surrounded with water than if they

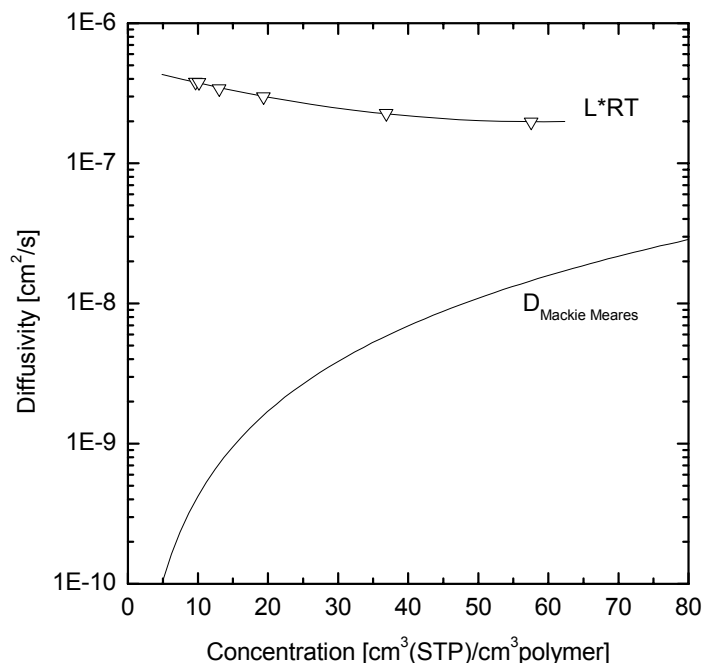
are in contact with the polymer<sup>31</sup>, suggesting a higher entropy for water in the cluster.

#### **6.3.4 Concentration-dependent diffusion coefficient**

The change of the diffusion coefficient with increasing degree of swelling is a complex matter. In some cases a dramatic increase with degree of swelling can be observed. In the case of PEO-PBT, D apparently decreases. An increasing diffusion coefficient with increasing degree of swelling can be predicted by the (simple) macroscopic model of Mackie and Meares<sup>19</sup>:

$$\frac{D}{D_0} = \left( \frac{1-\phi}{1+\phi} \right)^2 \quad (8)$$

where  $\phi$  is the fraction polymer, D the diffusion coefficient through the penetrant sorbed in the polymer, and  $D_0$  the self-diffusion coefficient of water<sup>32</sup>. This model considers the polymer chains as impermeable barriers obstructing the diffusion, and thus diffusion only occurs through water. Recently, molecular dynamic simulations support this model for very different systems such as the diffusion of benzene in polystyrene or water in polyvinylalcohol<sup>33</sup>.



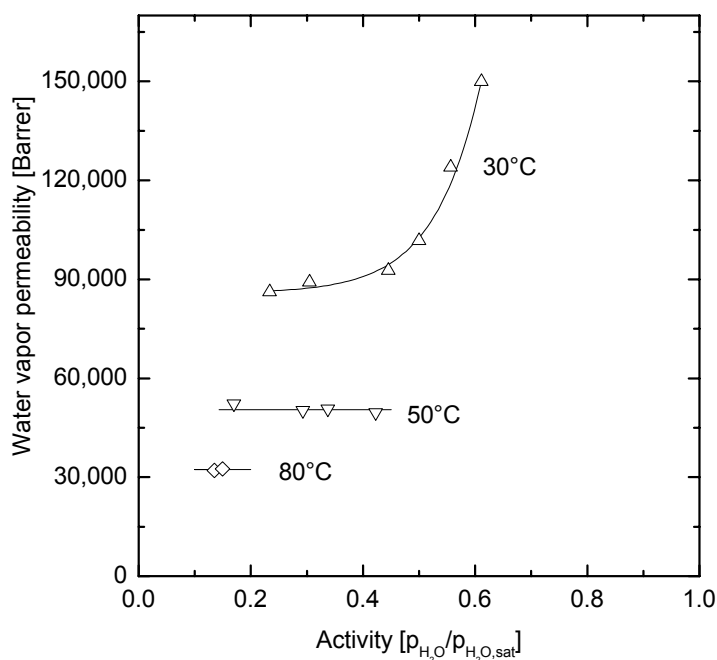
**Figure 10:** Mobility of water in the polymer as a function of the concentration of water in 1000PEO40PBT60 compared with the Mackie-Meares model at 30°C. The self diffusion coefficient of water is obtained from literature<sup>32</sup> ( $2.597 \cdot 10^{-5} \text{ cm}^2/\text{s}$  at 30°C).

Figure 10 compares the mobility of water in 1000PEO40PBT60 with the diffusion coefficient calculated from the Mackie-Meares model. The diffusion coefficient of water in 1000PEO40PBT60 is higher over the entire concentration range. The decreasing trend is in absolute contradiction to the prediction based on the Mackie-Meares model. In fact, the latter model neglects the intrinsic material property completely. It is apparent that a high free volume polymer (at infinite dilution) of the penetrant will have a higher diffusivity than one with a lower free volume. The diffusivity of water in 1000PEO40PBT60 decreases, due to the lower diffusivity of water in water compared to the diffusivity of water in the polymer. This is probably the reason why polymers with a larger free volume, such as PDMS (fraction free volume calculated:  $0.165^{34}$ ), show also a decrease in diffusivity with increasing concentration of water in the polymer. The Mackie-Meares model gives the lower limit of the diffusion of water in water through an inert polymeric matrix.

On the other hand, polymers with a low fractional free volume e.g. polyvinyl alcohol (fraction free volume calculated:  $0.019^{34}$ ), a low diffusion coefficient has at low water concentrations (activity = 0.2  $D = 5.1 \cdot 10^{-11} \text{ cm}^2/\text{s}^1$ ). The diffusion coefficient increases as the polymer sorbs more water, following the Mackie-Mearns prediction<sup>33</sup>. In these systems the diffusion rate of water through water is higher than the diffusivity of water through the polymer: therefore the diffusivity increases with an increase of the amount of water. This is probable the reason why the diffusion coefficient of water in polyvinyl alcohol, nylon, and cellulose increases with an increase of the amount of water vapor in the material.

### 6.3.5 Effect of temperature

Diffusion coefficients and solubilities strongly depend on temperature and activity, the first one increasing with temperature and the later one decreasing. The permeability as a function of temperature and activity hence can reveal complex behavior.



**Figure 11:** Water vapor permeability of 1000PEO56PB44 at (Δ) 30°C, (∇) 50°C, and (◇) 80°C

Figure 11 shows the water vapor permeability of 1000PEO56PB44 at 30, 50, and 80°C as a function the water vapor activity at the feed side of the membrane. The

water vapor permeability decreases with increasing temperature and its dependency on the temperature is often described with the following equation:

$$P = P_0 \exp\left(\frac{-E_p}{RT}\right) \quad (9)$$

where  $P_0$  is a pre-exponential factor, and  $E_p$  the activation energy for permeation.  $E_p$  can be written as the sum of the heat of sorption ( $\Delta H_c$ ) and the activation energy for diffusion ( $E_d$ ):

$$E_p = \Delta H_c + E_d \quad (10)$$

The heat of sorption is the enthalpy difference between the penetrant in the vapor phase and that sorbed in the polymeric matrix, and contains contributions of the isosteric heat of condensation ( $\Delta H_{\text{vap}}$ ) and the isosteric heat of sorption ( $\Delta H_s^*$ ), with ( $\Delta H_s^*$ ) representing the interaction energy between water and the polymer. The enthalpy of sorption is negative causing a lower solubility at higher temperatures. The activation energy for diffusion always has a positive value, which in this case is smaller than the heat of sorption causing the permeance to decrease with temperature. This indicates that the water vapor permeance is mainly determined by the solubility of water vapor.

At 30°C the water vapor permeability isotherm is convex to the activity axis, whereas it is constant at 50°C. This stems from the exothermic heat of sorption, which causes a lower solubility of water vapor at higher temperatures, causing the shape of the isotherm to be more linear towards higher vapor activities.

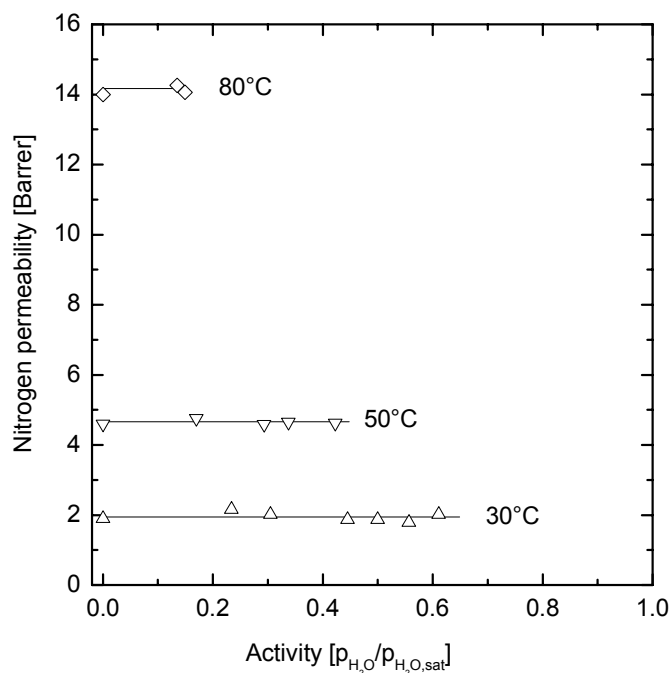


**Figure 12:** Mixed gas nitrogen permeability of 1000PEO56PBT44 at 30°C, 50°C, and 80°C as a function the water vapor activity.

Figure 12 shows the mixed gas nitrogen permeability as a function the water vapor activity in the feed phase. The permeability of nitrogen increases with an increase of temperature due to a larger positive activation energy for diffusion than the negative energy for sorption (Eq. 10). The nitrogen permeability remains constant with an increase of water vapor activity in the feed and is equal to the N<sub>2</sub> permeability in the absence of water vapor (activity 0). This suggests that N<sub>2</sub> explores the dry polymer as well as the swollen polymer. The same phenomena is also observed for the permeation of a acetone/N<sub>2</sub><sup>13</sup>, ethyl benzene/N<sub>2</sub><sup>35</sup> and n-butane/CH<sub>4</sub><sup>36</sup> mixtures through PDMS, where the N<sub>2</sub> permeance remained constant with an increase of acetone or n-butane activity.

One would expect an increase of the N<sub>2</sub> permeability due to the swelling of the polymer, causing an increased diffusivity of N<sub>2</sub>. The diffusivity of N<sub>2</sub> in water is estimated to be  $2 \cdot 10^{-9} \text{ m}^2/\text{s}$  (estimated via the Wilke and Chang method<sup>37</sup>) and the diffusivity of N<sub>2</sub><sup>6</sup> is estimated to be in the order of  $5 \cdot 10^{-11} \text{ m}^2/\text{s}$ . However, the transport of water also is affected by the solubility, which for the PEO-PBT block copolymer is estimated from an analogous Pebax block copolymer containing 57wt. % PEO and polyamide 6. It amounts to  $1.89 \cdot 10^{-4} \text{ cm}^3(\text{STP})/(\text{cm}^3 \text{ polymer cmHg})$  (at 35°C, reproduced from Bondar et. al.<sup>38</sup>), and for the solubility of N<sub>2</sub> in water  $1.77 \cdot 10^{-4} \text{ cm}^3(\text{STP})/(\text{cm}^3 \text{ water cmHg})$  (at 35°C, reproduced from Janssen

and Warmoeskerken<sup>39</sup>). The solubility of N<sub>2</sub> in the polymer and in water is in the same order of magnitude. This means that an increase in N<sub>2</sub> permeance is expected on the bases of an increased diffusion coefficient of N<sub>2</sub> in water.

An increase in the amount of water therefore would increase the nitrogen diffusivity and as a result increases the N<sub>2</sub> permeability. However, due to concentration polarization, the water vapor activity at the feed side of the membrane is lower than the activity in the feed gas mixture. This prevents swelling of the membrane: at a water vapor activity in the feed of 0.84, the activity at the membrane interface is 0.6 and the amount of water vapor sorbed in 1000PEO56PBT44 less than 5 wt%. Moreover, the permeate side of the membrane remains dry, thereby lowering the overall diffusivity of nitrogen through water in the polymer.

To investigate the effect on water vapor activity at the permeate side, the He sweep gas is saturated with water vapor and the N<sub>2</sub> permeability is determined at an 0.6 feed gas activity.

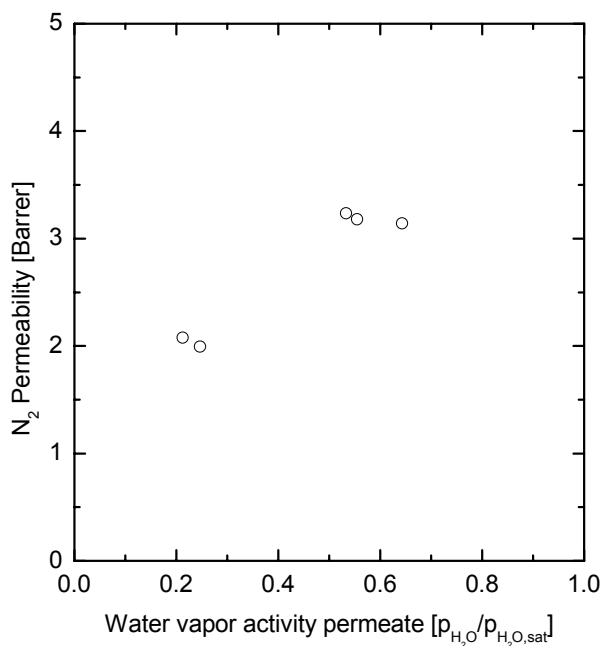


**Figure 13:** Effect of permeate pressure on N<sub>2</sub> permeance in 1000PEO56PBT44 at 30°C.

Figure 13 shows the N<sub>2</sub> permeance at various permeate water vapor activities. The dry sweep gas has an activity of 0.2 since it contains some permeated water, and the N<sub>2</sub> permeability is equal to the pure gas permeability. The N<sub>2</sub> permeability

increases when the sweep gas mixture is saturated with water vapor. This causes an increase of N<sub>2</sub> diffusivity through the complete thickness of the polymeric film and increases the N<sub>2</sub> permeability significantly. The reason that this is not observed in gas mixtures with a “dry” sweep gas is that the material is not completely swollen and that an increase of the N<sub>2</sub> diffusivity on the feed side does not increase the permeability within the experimental error.

The combined effect of decreasing water vapor permeability and an increasing nitrogen permeability with an increase of temperature has an substantial effect on the H<sub>2</sub>O/N<sub>2</sub> selectivity, which is presented in Figure 14. The water vapor/N<sub>2</sub> selectivity at 30°C is a factor 20 times higher than at 80°C. From the previous discussion on the water diffusivity and solubility and the nitrogen permeability, we may conclude that the water solubility overshadows all other parameters with respect to the selectivity.

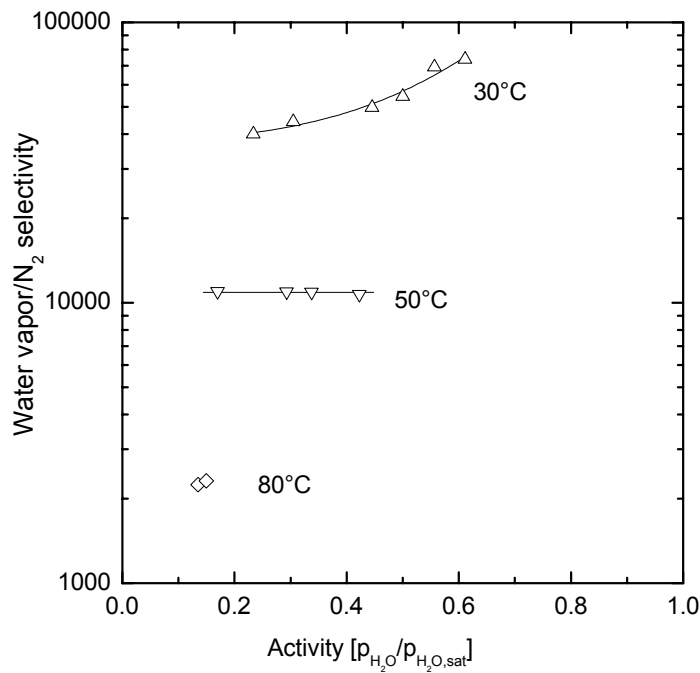


**Figure 14:** Mixed gas H<sub>2</sub>O/N<sub>2</sub> selectivity permeability of 1000PEO56PBT44 at 30°C, 50°C, and 80°C as a function of the water vapor activity.

**6.3.6 Effect of block copolymer composition**

The water vapor/N<sub>2</sub> selectivity of different polymers also depends on the structure of the block copolymer.



**Table 2:** Water vapor and N<sub>2</sub> permeability and selectivity for various PEO-PBT block copolymers with a PEO segment length of 1000 g/mol but with various amounts of PBT at 30°C and activity 0.40.

wt% PEO	P N <sub>2</sub> [Barrer]	P H <sub>2</sub> O [Barrer]	$\alpha$ H <sub>2</sub> O/N <sub>2</sub> [-]
40	0.74	44,650	60,338
56	1.87	92,683	49,563
75	2.77	121,800	43,971

Table 2 shows the water vapor and N<sub>2</sub> permeability for various PEO-PBT block copolymers with a PEO segment length of 1000 g/mol but with various amounts of PBT. The N<sub>2</sub> permeability increases relatively more than the water vapor permeability causing the selectivity to decrease with an increase of the amount of PEO. The diffusive resistance controls the N<sub>2</sub> permeability, whereas the water vapor permeability is controlled by its solubility. The N<sub>2</sub> permeability depends on the amount of impermeable PBT phase and the chain flexibility of the PEO phase<sup>6</sup>. These effects cause a nonlinear increase of the N<sub>2</sub> permeability with the amount of PEO. The water vapor permeability is controlled by the solubility, which increases linearly with the amount of PEO Figure 3.

The water vapor permeability depends strongly on the applied water vapor activity at 30°C. However, at 50°C is this effect of water vapor activity less prominent because the sorption is linear for the activity range studied.

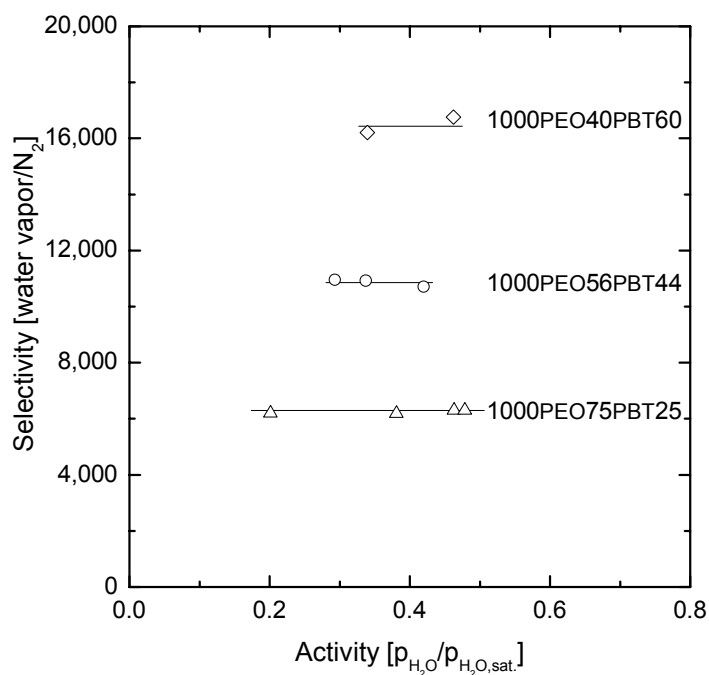


**Figure 15:** Water vapor/N<sub>2</sub> selectivity at 50°C for: 1000PEO40PBT60 (◇), 1000PEO56PBT44 (○), and 1000PEO75PBT25 (△).

Figure 15 shows the water vapor/N<sub>2</sub> at 50°C for 1000PEO40PBT60, 1000PEO56PBT44, and 1000PEO75PBT25. The water vapor/N<sub>2</sub> selectivity decreases with an increase of the PEO content in the block copolymer due to the larger increase of the N<sub>2</sub> permeability compared to the water vapor permeability.

## 6.4 Conclusions

PEO-PBT block copolymers show a high solubility, permeability and selectivity for water vapor, which is completely determined by the PEO segment. The amount of dissolved water vapor depends on the polymeric structure: the larger the PEO weight fraction, the higher the solubility, diffusivity and permeability of water vapor. The diffusion coefficient of water vapor calculated from sorption and permeation isotherms decreases with the amount of water vapor in the polymer. FTIR-ATR analysis of water in the PEO-PBT block copolymers reveals that the interactions between water and the polymer become weaker at higher water contents. This is caused by the formation of water clusters in the material. These clusters develop although the interactions between the water molecules are weaker than the interaction between water and the polymer. Therefore cluster formation is entropically favored, causing a lower free energy for water in the cluster. The diffusion coefficient of water decreases with an increase of the amount of water content due to the lower diffusion rate of water through water. The selectivity of water vapor/N<sub>2</sub> increases with an increase of the amount of PBT due to a relatively higher water vapor permeability compared to N<sub>2</sub>. This is caused by the different permeation mechanisms: the water permeability is controlled by the solubility, whereas the N<sub>2</sub> permeability is controlled by the diffusion.

## 6.5 Acknowledgements

The European Union is kindly acknowledged for supporting this project: Brite Euram III, Contract no. BRPR-CT 98-0804

## 6.6 References

- (1) Barrie, J. A. In *Diffusion in Polymers*; Crank, J.; Park, G. S., Eds.; Academic Press, 1968.
- (2) Barrie, J. A. *Proceeding of the fourth BOC Priestly Conference* **1986**, 89-113.
- (3) Paul, D. R. *Macromol. Symp* **1999**, *138*, 13-20.
- (4) Robeson, L. M. *J. Membr. Sci.* **1991**, *62*, 165-185.
- (5) Nunes, S. P.; Peinemann, K.-V. *Membrane technology in the chemical industry*; Wiley-VCH: Weinheim, 2001.
- (6) Metz, S. J.; Mulder, M. H. V.; Wessling, M. *Chapter 4*.
- (7) Metz, S. J.; Potreck, J.; Mulder, M. H. V.; Wessling, M. *Chapter 2*.
- (8) Boom, J. P.; Punt, I. G. M.; Zwijnenberg, H.; de Boer, R.; Bargeman, D.; Smolders, C. A.; Strathmann, H. *J. Membr. Sci.* **1998**, *138*, 237-258.

- (9) Stamatialis, D.; Wessling, M.; Sanopoulou, M.; Strathmann, H.; Petropoulos, J. *J. Membr. Sci.* **1997**, *125*, 165-175.
- (10) Rezac, M. E.; John, T.; Pfromm, P. H. *J. Appl. Polym. Sci.* **1997**, *65*, 1983-1993.
- (11) Wijmans, J. G.; Baker, R. W. *J. Membr. Sci.* **1995**, *107*, 1-21.
- (12) Favre, A.; Nguyen, Q. T.; Schaetzel, P.; Clement, R.; Neel, J. *J. Chem. Soc. Faraday. Trans.* **1993**, *89*, 4339-4346.
- (13) Singh, A.; Freeman, B. D.; Pinnau, I. *J. Polym. Sci., Polym. Phys. Ed.* **1998**, *36*, 289-301.
- (14) Metz, S. J.; van der Vegt, N. F. A.; Mulder, M. H. V.; Wessling, M. *Chapter 5*.
- (15) Deschamps, A. A.; Grijpma, D. W.; Feijen, J. *Polymer* **2001**, *42*, 9335-9345.
- (16) Bezemer, J. M.; Grijpma, D. W.; Dijkstra, P. J.; van Blitterswijk, C. A.; Feijen, J. *J. Controlled Release* **1999**, *62*, 393-405.
- (17) Merkel, T. C.; Bondar, V. I.; Nagai, K.; Freeman, B. D.; Pinnau, I. *J. Polym. Sci., Polym. Phys. Ed.* **2000**, *38*, 415-434.
- (18) Koros, W. J.; Hellums, M. W. *Fluid Phase Eq.* **1989**, *53*, 339-354.
- (19) Mueller Plathe, F. *journal of membrane science* **1998**, *141*, 147-154.
- (20) Perrin, L.; Nguyen, Q. T.; Clement, R.; Neel, J. *Polymer International* **1996**, *39*, 251-260.
- (21) Rivin, D.; Kendrick, C.; Gibson, P.; Schneider, N. *Polymer* **2001**, *42*, 623-635.
- (22) Barrie, J. A.; Platt, B. *Polymer* **1963**, *4*, 303-313.
- (23) Wellons, J. D.; Stannett, V. *J. Polym. Sci.* **1966**, *4*, 593-602.
- (24) Doghieri, F. B., D. Sarti, G.C. *Ind. Eng. Chem. Res.* **1996**, *35*, 2420-2430.
- (25) Mulder, M. H. V. *Basic principles of membrane technology*, second ed.; Kluwer: Dordrecht, 1996.
- (26) Zimm, B. H.; Lundberg, J. L. *J. Chem. Phys.* **1953**, *21*, 934.
- (27) Zimm, B. H.; Lundberg, J. L. *J. Chem. Phys.* **1956**, *60*, 425.
- (28) Strathmann, H.; Michaels, A. S. *Desalination* **1977**, *21*, 195-202.
- (29) Ide, M. Y., D. Maeda, Y. Kitano, H. *LANGMUIR* **1999**, *15*, 926-929.
- (30) Walrafen, G. E. *Structure of water and Aqueous solutions*; Verlag Chemie: Weinheim, 1974.
- (31) Muller-Plathe, F. *Macromolecules* **1998**, *31*, 6721-6723.
- (32) Holz, M.; Heil, S. R.; Sacco, A. *Phys. Chem. Chem. Phys.* **2000**, *2*, 4740-4742.
- (33) Muller-Plathe, F. *J. Membr. Sci.* **1998**, *141*, 147-154.
- (34) Krevelen, D. W. v. *Properties of polymers*, 3rd ed.; Elsevier: Amsterdam, 1990.

- (35) Dixon-Garrett, S. V.; Nagai, K.; Freeman, B. D. *J. Polym. Sci., Polym. Phys. Ed.* **2000**, *38*, 1078-1089.
- (36) Pinnau, I. T., L.G. *J. Membr. Sci.* **1996**, *116*, 199-209.
- (37) Poling, B. E.; Prausnitz, J. M.; O'Connell, J. P. *The properties of gases and liquids*; McGraw-Hill: New York, 2001.
- (38) Bondar, V. I.; Freeman, B. D.; Pinnau, I. *J. Polym. Sci., Polym. Phys. Ed.* **1999**, *37*, 2463-2475.
- (39) Janssen, L. P. B. M.; Warmoeskerken, M. M. C. G. *Transport phenomena data companion*; Delftse Uitgevers Maatschappij: Delft, 1991.



# Summary

Water vapor transport through polymeric materials plays an important role in a large number of applications such as: food packaging, breathable clothing, roofing membranes, diapers, and the removal of water vapor from gas streams (e.g. dehydration of natural gas or the drying of compressed air). Depending on the application a high or low permeability or selectivity is preferable.

This thesis investigates the transport of water vapor and various gases through polyethylene oxide (PEO) polybutylene terephthalate (PBT) block copolymers and asymmetric polyether sulfone (PES) polyimide (PI) blend hollow fiber membranes.

Chapter 2 describes the permeation set-up, which is used in this thesis for the simultaneous measurement of the transport rate of a water vapor gas mixture, in the pressure range of 1 – 80 bar and the temperature range of 20 – 80°C. This set-up uses a helium sweep gas to remove the water vapor on the permeate side of the membrane in order to determine their transport rates. The resistances for permeation in stagnant boundary layers complicate the exact quantification of the water vapor permeability from the overall transport rate. These resistances are determined and subtracted from the overall resistance for water vapor permeation, resulting in the membrane resistance. Water vapor permeability values of ethyl cellulose and polysulfone films determined and corrected for the resistance in the stagnant boundary layers correspond to those in literature. Permeability values of a highly permeable PEO-PBT block copolymer are presented to illustrate the contribution of the stagnant boundary layers at various process conditions to the overall water vapor permeance.

The influence of water vapor on the gas permeation rates through a PES/PI asymmetric blend hollow fiber is discussed in Chapter 3. An increase of the water vapor concentration in the feed gas mixture lowers the permeation rates of water vapor, carbon dioxide, and nitrogen.

The resistance towards mass transport for water vapor was studied at various feed- and permeate flow rates, enabling the derivation of Sherwood relations, which describe the variation of the overall mass transfer coefficient at various process conditions. This analysis reveals that the main resistance for water vapor transport is situated in the stagnant feed boundary layer.

An increase of the total pressure at constant water vapor activity resulted in a reduction of the water vapor permeance due to a lower diffusivity of water vapor in the stagnant feed boundary layer. The nitrogen permeance remained constant with an increase of total pressure, whereas the carbon dioxide permeance increased due to plasticization of the membrane.

Chapter 4 covers a systematic study of the effect of the PEO-PBT block copolymer composition on the gas permeation properties. The composition of these block copolymers is varied by: (1) the amount of PEO, at constant PEO segment length, (2) the PEO segment length at a constant PEO-PBT weight ratio.

The carbon dioxide/nitrogen selectivity is high ( $\alpha \approx 60$  at  $T = 35^\circ\text{C}$ ), due to the high solubility of carbon dioxide in the PEO phase. The carbon dioxide/nitrogen selectivity shows a different structural dependency than the carbon dioxide/helium selectivity, since carbon dioxide and nitrogen permeate mainly through the amorphous PEO phase whereas helium permeates through both the PEO and PBT phase.

The gas permeability values measured for carbon dioxide and nitrogen are compared with the Maxwell model, which considers the PBT phase as impermeable for carbon dioxide and nitrogen. The difference between the experimental values and the Maxwell model are interpreted on the basis of chain flexibility of the PEO phase. The chain flexibility decreases with increasing amounts of PBT due to a less pronounced phase separation between the PEO and PBT phase. The permeability depends also on the degree of crystallinity and the melting temperature of the PEO phase, which increases with the amount and the PEO segment length.

The influence of the composition of PEO-PBT block copolymers on the solubility of water vapor and the thermodynamic quantities governing the solubility of water vapor in these polymers is studied in Chapter 5.

The sorption isotherms are analyzed with the Flory Huggins model and the interaction parameter ( $\chi$ ) being the fitting parameter, which decreases with the water vapor activity and is lower for block copolymers with a longer PEO segments and higher PEO content.

The solvation Gibbs energies, entropies and enthalpies are extracted from temperature dependent sorption data. They reveal that: (1) water-polymer interactions are stronger than water-water interactions in liquid water, (2) the water-polymer interactions become weaker at higher water vapor activities, (3) the water sorption entropy increases with increasing vapor activity. The latter is responsible for the convex nature of the water sorption isotherm. Moreover, this effect depends on the structure of the polymer: the larger the PEO segment length and the more PEO weight fraction, the higher the solvation entropy and, consequently, the solubility of water vapor in the PEO-PBT block copolymer.

Chapter 6 studies the mass transport properties for water vapor and nitrogen for a series of PEO-PBT block copolymers with a PEO segment of 1000 g/mol, but with various amounts of PBT via: (a) the water vapor sorption, (b) the permeation of water vapor/nitrogen mixtures, (c) the diffusion of water vapor, (d) Zimm and



Lundberg cluster analysis, and (e) the state of water in these polymers via FTIR-ATR analysis.

The water vapor permeability increases with the amount of PEO due to a higher solubility and diffusivity for water vapor. The diffusivity of water vapor decreases significantly with an increase of the amount of water vapor sorbed in the block copolymer. This decrease is caused by the clustering of water vapor, as revealed by a Zimm and Lundberg cluster analysis of the sorption isotherm and by FTIR-ATR.

The mixed gas nitrogen permeability remains constant with an increase of water vapor activity but depends strongly on the polymeric structure, whereas the water vapor permeability depends mainly on the solubility in the block copolymer. This causes a higher water vapor/nitrogen selectivity for block copolymers containing more PBT.



# Samenvatting

*"voor niet-membraantechnologen"*

Dit proefschrift beschrijft het onderzoek dat is verricht om te begrijpen hoe een waterdamp/gasmengsel door een polymeer (plastic) membraan wordt getransporteerd. Met een membraan wordt in dit geval een dunne polymere film bedoeld waar waterdamp sneller doorheen gaat (permeëert) dan andere gassen. De permeatie van waterdamp door polymere materialen is in vele toepassingen belangrijk bijvoorbeeld in: verpakkingsmateriaal (bijvoorbeeld een boterhamzakje), ademende kleding (bijvoorbeeld Goretex®- of Sympatex®jassen), ademend schoeisel, handschoenen, dakbedekkingsmateriaal, luiers en de verwijdering van waterdamp uit gasstromen (bijvoorbeeld de ontwatering van aardgas en het drogen van perslucht).

Afhankelijk van de toepassing kan een hoge (of lage) selectiviteit met een hoge (of lage) transportsnelheid (permeabiliteit) door een membraan gewenst zijn.

In hoofdstuk 2 wordt een nieuwe experimentele opstelling beschreven waarin de transportsnelheid van waterdamp en een gasmengsel door een polymeer materiaal gelijktijdig kunnen worden gemeten. Deze meting is voor waterdamp lastig, omdat waterdamp zo snel door deze membranen permeëert. Hierdoor is de concentratie waterdamp aan het membraanoppervlak lager is dan in de bulk van het gas dat over het membraan stroomt. Daardoor moet waterdamp uit de gasfase naar het membraanoppervlak getransporteerd worden en dit verlaagt de totale transportsnelheid. Hierdoor ontstaat er een extra weerstand voor het transport van waterdamp aan de voedingszijde van het membraan. Ook aan de afvoerszijde (permeaat) bevindt zich een weerstand tegen waterdamptransport. Deze weerstanden zijn bepaald en hierdoor is het mogelijk is om de permeabiliteit van het membraan te bepalen. Dit is getest voor 2 materialen (ethyl cellulose en polysulfone) en deze waarden komen goed overeen met literatuurwaarden.

De bijdrage van de grenslaagweerstand is gevisualiseerd voor een hoog permeabel polyethyle oxide (PEO) polybutylene terephthalate (PBT) blokcopolymeer.

Het effect van waterdamp op de transportsnelheid van kooldioxide (CO<sub>2</sub>) en stikstof (N<sub>2</sub>) door holle membraangasscheidingsvezels is beschreven in hoofdstuk 3. Deze gasscheidingsvezels zijn asymmetrisch (d.w.z. dat deze vezel een heel dun laagje, ongeveer een tienduizendste deel van een millimeter, polymeer heeft dat ondersteund wordt door een poreuze polymere structuur van hetzelfde materiaal). Dit polymeer bestaat uit een mengsel van de volgende polymeren: polyethersulfone en polyimide. Uit metingen van de transportsnelheid door dit membraan met een waterdamp gasmengsel volgt dat wanneer de

waterdampconcentratie in het gasmengsel toeneemt, dat de permeabiliteiten van waterdamp, CO<sub>2</sub> en N<sub>2</sub> door dit membraan afnemen.

De transportsnelheden van waterdamp zijn bepaald voor het transport van: (1) waterdamp uit het gasmengsel naar het membraan, (2) door het membraan en (3) vanuit het membraan naar de binnenzijde van het holle vezelmembraan. Hieruit volgt dat de grootste transportweerstand zich bevindt in het transport van waterdamp uit de gasfase naar het membraanoppervlak.

Een gevolg hiervan is dat wanneer de totale druk van het gasmengsel wordt verhoogd, bij een constante waterdamp concentratie in het gas, de transportsnelheid van waterdamp afneemt door een lagere diffusiecoëfficiënt van waterdamp door het gas aan de voedingszijde van het membraan.

Bij een druktoename blijft de transportsnelheid van N<sub>2</sub> constant, terwijl de transportsnelheid van CO<sub>2</sub> toeneemt. Dit laatste komt door verweking (plastificering) van het membraanmateriaal.

In hoofdstuk 4 is de permeatie van zuivere gassen door PEO-PBT blokcopolymeren beschreven. Dit polymeer bestaat uit 2 afzonderlijke polymere delen die via een chemische binding aan elkaar verbonden zijn. In dit polymeer bevinden zich meerdere delen (blokken) van PEO en PBT. Door de verhouding en de grootte van de afzonderlijke te variëren, kunnen de eigenschappen van dit polymeer worden aangepast.

Het PEO blok is een zeer flexibel polymeer (rubberachtig) dat makkelijk gassen doorlaat. Het PBT blok is star (glasachtig) en laat minder goed gassen door. Door de samenstelling van zo'n blokcopolymeer te veranderen, verandert ook de transportsnelheid door het materiaal. De eigenschappen van dit materiaal zijn gevarieerd door (1) de hoeveelheid PEO, bij constante PEO bloklengte, (2) de PEO bloklengte, bij constante verhouding PEO-PBT. De CO<sub>2</sub>/N<sub>2</sub> selectiviteit is hoog voor deze materialen (CO<sub>2</sub> gaat 60 keer sneller door het materiaal dan N<sub>2</sub> bij 35°C).

Doordat CO<sub>2</sub> en N<sub>2</sub> beide door de PEO fase diffunderen en helium (He) door zowel de PEO en PBT fase, vertonen de CO<sub>2</sub>/N<sub>2</sub> en CO<sub>2</sub>/He selectiviteit een verschillende afhankelijkheid van de samenstelling van het blokcopolymeer.

De CO<sub>2</sub> en N<sub>2</sub> permeabiliteiten zijn vergeleken met het Maxwell model dat de PBT fase als impermeabel veronderstelt. Het verschil tussen het model en de gemeten waarden wordt geïnterpreteerd op basis van ketenflexibiliteit van de PEO fase. Deze neemt af met een toename van de hoeveelheid PBT, door een slechtere fasescheiding tussen de PEO en PBT blokken. Hierdoor bevinden zich tussen de PEO blokken nog delen PBT die de bewegelijkheid van de PEO blokken verlagen.

De permeabiliteit hangt tevens af van de crystalliniteit en de smelttemperatuur van de PEO fase, welke toeneemt met de hoeveelheid PEO en PEO bloklengte.

De invloed van de samenstelling van het PEO-PBT blokcopolymeer op de oplosbaarheid van waterdamp en hun thermodynamische grootheden, zoals de bindingssterkte tussen water en zijn omgeving in het polymeer en het aantal mogelijke manieren hoe water zich in het polymeer kan bevinden wordt bestudeerd in hoofdstuk 5 aan de hand van waterdampsorptie-isothermen. Deze isothermen beschrijven hoeveel water er in het polymeer zit bij een bepaalde waterdamp concentratie in de gasfase. Deze sorptie-isothermen nemen eerst lineair toe bij lage waterdampconcentratie en bij hogere concentratie nemen ze exponentieel toe. Deze sorptie-isothermen zijn gefit met het Flory-Huggins model waarin de interactieparameter ( $\chi$ ) als fitparameter is gebruikt.

De interactieparameter neemt af met toenemende waterdampconcentratie in het polymeer en geeft aan dat het energetisch gunstiger wordt voor waterdamp om zich in het polymeer te bevinden. Of dit nu komt door een sterkere binding tussen water en zijn omgeving of doordat het polymeer zo sterk gezwollen is, zodat er meer water in past, wordt onderzocht met een thermodynamische analyse.

Deze analyse toont aan dat: (1) water-polymeer bindingen sterker zijn dan water-water bindingen, (2) water-polymeer bindingen zwakker worden wanneer de hoeveelheid water toeneemt, (3) het aantal mogelijkheden dat water in het polymeer past toeneemt wanneer er meer water in het polymeer zit. Dit laatste wordt veroorzaakt door zwelling van het polymeer, waardoor er meer watermoleculen in het polymeer passen.

In hoofdstuk 6 wordt het transport van een waterdamp/N<sub>2</sub> mengsel bestudeerd voor PEO-PBT blokcopolymer met een vaste lengte van het PEO blok (1000 g/mol) maar met verschillende hoeveelheden PBT. De polymeren transporteren waterdamp ongeveer 50.000 keer sneller dan N<sub>2</sub> (bij 30°C), wat ontzettend hoog is voor een polymeer. De waterdamp permeatie neemt toe met de hoeveelheid PEO in het blokcopolymeer door een hogere oplosbaarheid van water in dit deel. (Wanneer er zich meer watermoleculen in het polymeer zijn dan bewegen er ook meer doorheen). Echter de diffusie van water neemt af wanneer er zich meer watermoleculen in het polymeer bevinden. Deze afname vindt gelijktijdig plaats met de clustering van water in het polymeer (d.w.z. in het polymeer bevinden zich gebiedjes waarin zich 2, 3 of meer watermoleculen bevinden). Waarschijnlijk vinden de watermoleculen het energetisch gunstiger om zich in een cluster te bevinden dan zich door het polymeer te diffunderen.

# Dankwoord

Vier jaar promoveren lijkt veel als je eraan begint, maar eenmaal begonnen vloog de tijd voorbij en zit ik dit dankwoord te schrijven. Dat deze periode zo snel voorbij is gegaan komt door de speciale omgeving waarin ik mij bevind. Door het hoge aantal sociale activiteiten in de membraangroep zoals: koffiepauzes, borrels, karten, zeilweekend, kroamschudparties, Geusavonden, BBQ's, batavierenraces, promotiefeesten, bruiloften, fietstochten enz., voelde ik mij snel thuis en werd ik al snel een echte "membrane lover". Hiervoor wil ik de hele membraantechnologiegroep en iedereen die op wat voor wijze dan ook aan dit proefschrift hebben bijgedragen bedanken. Een aantal mensen wil ik in het bijzonder bedanken.

Allereerst natuurlijk Marcel Mulder. Marcel nam mij als AIO aan en heeft mij, op een voor mij ideale manier, 3 jaar kunnen begeleiden. Marcel gaf mij alle vrijheid en heeft mij nooit zijn ideeën laten uitvoeren, maar probeerde mij via hints en het stellen van veel vragen een eigen beeld te laten vormen. Hiervan heb ik veel geleerd. Ik vind het ontzettend jammer dat ik Marcel nu niet meer bedanken kan.

Nico, jou enthousiasme voor de wetenschap stak vele andere mensen aan, ook mensen die jij niet direct begeleidt. Van jou heb ik veel geleerd en ik vind het ontzettend leuk om samen met jou aan hoofdstuk 5 te hebben gewerkt.

Matthias wil ik bedanken voor het corrigeren van mijn proefschrift en het stellen van een schijnbaar oneindig aantal vragen, waardoor ik vaak diep moest nadenken en dingen anders moest schrijven.

Betty, jou wil ik bedanken voor de eerste 2 maanden toen jij in mijn project werkte. Van jou heb ik geleerd hoe je een membraan moest maken, een sorptie-experiment deed, hoe de gaspermeatie opstelling werkt enz.

Veel werk dat in dit proefschrift is beschreven is uitgevoerd door een aantal studenten waaronder: Jens Potreck (Semesterpraktikum), Wilbert van de Ven en Cari van Rood (afstudeeropdracht) en Joris Smit en Stefan van Osch (literatuuropdracht).

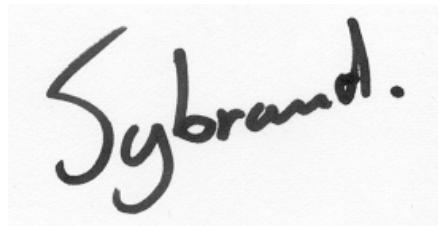
Uiteraard mijn kamergenoten Magda, Kitty, John Kroll, Dimitris, Nela, Jonathan en Laura voor de talloze discussies, roddels, hulp en adviezen.

George Kapantaidakis, I want to thank you for the collaboration and all the measurements we performed during the weekends for the work described in chapter 3. You also taught me some Greek words, which were very helpful to impress the Greek people whenever I was for a holiday in Greece.

Een aantal mensen hebben mij enorm geholpen zoals: Klaus Ohlrogge, Torsten Brinkmann, Bernd Keil en Thomas Loewe van GKSS voor hun samenwerking in het Brite Euram III project, Arie Pleiter voor het bouwen van de waterdamp permeatieopstelling, Antoine voor het kritisch doorlezen van dit proefschrift, Bastiaan voor het vangen van de labtopdief, Greet voor al het papierwerk, Peter voor de vele schaakpartijen via het internet, iedereen van de werkplaats en inkoop, de mevrouw van de bieb die mijn naam wel weet maar ik de hare niet, Sandy te Poele, Jelle Roorda, Herman Evenblij en Jasper Verkerk voor het samen organiseren van NYM-3 en natuurlijk Wytse Wijbenga voor het ontwerpen van de voor- en achterkant van dit proefschrift.

Heit en mem, al is het misschien moeilijk voor te stellen wat ik nu allemaal doe op de universiteit jullie hebben me altijd gesteund. Tige Tank!

Marijje, jij hebt mij deze hele periode gesteund en de laatste 1,5 jaar wel van heel dichtbij dat was en is bjusterbaarlik!

A handwritten signature in black ink on a white background. The signature reads 'Sybrand.' with a period at the end. The letters are cursive and somewhat slanted.